Synthesis of small molecules via click chemistry for positron emission tomography (PET) imaging of tumor integrin αvβ3 and/or α5β1 expression

Monaco, Alessandra

UNIVERSITÉ DE GENÈVE
Section de Sciences Pharmaceutiques

Laboratoire de Biochimie Pharmaceutique

FACULTÉ DES SCIENCES
Professeur Leonardo Scapozza
FACULTÉ DE MÉDECINE
Prof. Assistant Yann Seimbille

Synthesis of Small Molecules via Click Chemistry for Positron Emission Tomography (PET) Imaging of Tumor Integrin $\alpha_v\beta_3$ and/or $\alpha_5\beta_1$ Expression

THÈSE

présentée à la Faculté des sciences de l'Université de Genève
pour obtenir le grade de Docteur ès sciences, mention sciences pharmaceutiques

par

Alessandra Monaco
de
Foggia (Italie)

Thèse N°: 4583

Genève
Atelier de reproduction Repromail
2012

UNIVERSITÉ
DE GENÈVE

FACULTÉ DES SCIENCES

Doctorat ès sciences
Mention sciences pharmaceutiques

Thèse de *Madame Alessandra MONACO*

intitulée :

" Synthesis of Small Molecules via Click Chemistry for Positron Emission Tomography (PET) Imaging of Tumor Integrin $\alpha_v\beta_3$ and/or $\alpha_5\beta_1$ Expression "

La Faculté des sciences, sur le préavis de Messieurs L. SCAPOZZA, professeur ordinaire et directeur de thèse (Section des sciences pharmaceutiques) et Y. SEIMBILLE, professeur assistant et codirecteur de thèse (Faculté de médecine, Département de radiologie), N. LANGE, docteur (Section des sciences pharmaceutiques), B. WINDHORST, professeur (University Medical Center, Department Radiology & Nuclear Medicine, Location Radionuclide Center, Amsterdam, The Netherlands), Y. P. AUBERSON, docteur (Novartis Institutes for BioMedical Research, Global Discovery Chemistry Group, Basel, Switzerland) et A. ZAMBON, docteur (The Institute of Cancer Research, Cancer Research UK, Sutton, United Kingdom), autorise l'impression de la présente thèse, sans exprimer d'opinion sur les propositions qui y sont énoncées.

Genève, le 30 juillet 2013

Thèse - 4583 -

Le Décanat

N.B. - La thèse doit porter la déclaration précédente et remplir les conditions énumérées dans les "Informations relatives aux thèses de doctorat à l'Université de Genève".

Table of Contents

Summary of the thesis

Integrins is a large family of cell surface receptors, which mediate cell-to-cell and cell-to extracellular matrix interactions during the focal adhesion. They play an important role in angiogenesis process and their expression in several diseases makes them an interesting target. In the last years, several integrin antagonists were developed for antiangiogenic therapies.

Accordingly, the interest in noninvasive techniques to visualize angiogenesis in growing tumors has increased. The most sensitive imaging technology among the clinical imaging modalities is positron emission tomography (PET). It is a technique which requires a positron emitting (β^+) radiopharmaceutical and a tomograph for the detection of the gamma ray emissions coming from positron anhylation. The most common radionuclides for the production of radiopharmaceuticals are ^{11}C, ^{13}N, ^{15}O and ^{18}F, which are easily introduced in biomolecules. Among them ^{18}F is the most used positron emitting radionuclide because of its half-life of 110 min which makes it compatible with more complexes synthetic strategies. As a matter of fact, the development of appropriate synthetic methods is one of the challenges in radiochemistry, and many novel approaches have been developed to improve the reproducibility and efficiency of radiolabeling reactions.

The majority of the radiolabeled molecules evaluated for imaging angiogenesis are peptides developed from the natural binding sequence RGD (Arg-Gly-Asp). The sequence usually consists of cyclic pentapeptides and promising results in preclinical and clinical studies have been obtained. Many synthetic non-click chemistry based procedures have been investigated for RGD peptides labeling. Only more recently, the introduction of the Cu(I) catalysed Huisgen's 1,3-dipolar cycloaddition made click chemistry of great interest for radiochemistry.

To address the above mentioned challenge in radiochemistry, the aims set for this thesis were: 1) to develop prosthetic groups, which can be conjugated with RGD peptides by the use of azido-alkyne Huisgen's cycloaddition; 2) to develop a selective radioligand for $\alpha_v\beta_3$ integrin receptor; 3) to develop a selective non-peptidic radoligand for $\alpha_5\beta_1$ integrin receptor. Because of its specificity and short time of reaction, the azido-alkyne cycloaddition has been selected as principal reaction for the development of our molecular probes.

Seven azide and seven alkyne small molecules have been synthetised to be evaluated as prosthetic groups for ^{18}F-labeling via click chemistry reaction. Two of them, 3-azido-*N*-(4-fluorophenyl)propanamide and 6-azido-*N*-(4-fluorophenyl) hexanamide were selected as standard to test the reaction conditions with the modified amino acids. The amino acid selected were glycine, valine, proline, phenylalanine, tyrosine, glutamic acid and lysine because of their different chemical properties. The alkynyl moiety was easily incorporated in all the amino acids (yield 60-90%) and the reaction between the prosthetic groups and all the amino acids was reproducible and provided good yields (54-98%). The time of reaction was significantly shorter than similar reactions described in literature; indeed it was between 1 and 3.5h instead of 24h. Our results suggest that the prosthetic groups synthesized can be easily incorporated into peptides by the Huisgen's cycloaddition.

These conditions were used for the conjugation of the *N*-(4-fluorophenyl)pent-4-ynamide (**FPPA**) with the cyclic pentapeptide [RGDfK]. The reaction gave the conjugated peptide in quantitative yield after 1h. The selectivity of FPPA-[RGDfK] for $\alpha_v\beta_3$ integrin receptor was confirmed by a new validated ELISA protocol.
To obtain the ^{18}F-prosthetic group (**FPPA**), several precursors have been used and two synthetic strategies have been developed. The first one was a one step strategy and *N*-(4-trimethylammoniun)phenyl)pent-4-ynamide•trifluoromethanesulfonate was selected as precursor. The fluorination was tested in CH_3CN and DMSO with temperature between 60 and 165°C from 10 to 15 min, but the best radiochemical yield obtained was around 5% (decay non-corrected). For that reason another strategy was considered having 4-trimethylammonium-nitrobenzene trifluoromethanesulfonate as precursor. The precursor was fluorinated and then the nitro group was reduced to obtain the ^{18}F-aniline with 69% radiochemical yield (decay non-corrected). The aniline was coupled with 2,5-dioxopyrrolidin-1-ylpent-4-ynoate to obtain the ^{18}F-prosthetic group with 48% yield (decay non-corrected) in 90 min. In the last step, the ^{18}F-prosthetic group (**FPPA**) was conjugated with the peptide by Huisgen's cycloaddition, to have the final ^{18}F-labeled c[RGDfK] in 140 min with 8% radiochemical yield (decay corrected).

The non-peptidic ligand has been selected by *in silico* screening of different $\alpha_5\beta_1$ antagonists. The molecule selected (**4PMt** or (S)-tert-butyl 3-(2-((3R,5S)-1-pent-4-

ynoyl-5-((pyridin-2-ylamino)methyl)pyrrolidin-3-yloxy)acetamido)-2-(2,4,6-trimethylbenzamido)propanoate) mimics the 3D conformation of the cyclo-[Arg-Gly-Asp-D-Phe-NMe-Val]. The synthesis of the molecule was planned by dividing it in 3 moieties. The first moiety (**4YPTt** or tert-butyl 2-((3R,5S)-5-((tert-butyldimethylsilyloxy)methyl)-1-pent-4-ynoylpyrrolidin-3-yloxy)acetate) was synthesized in four step with a final yield of 82%. The second moiety (**A3MeBP** or (S)-tert-butyl 3-amino-2-(2,4,6-trimethylbenzamido)propanoate) was obtained in two steps with a yield of 64% and treated with **4YPTt** to obtain **4Y3MeOH** ((S)-tert-butyl 3-(2-((3R,5S)-5-(hydroxymethyl)-1-pent-4-ynoylpyrrolidin-3-yloxy)acetamido)-2-(2,4,6-trimethylbenzamido)propanoate) with 40% yield. The final molecule was obtained with 67% yield by an aldol condensation between the 2-aminopyridine and the oxidized **4Y3MeOH**. **4PMt** was then clicked with two prosthetic groups: 3-(5-azidopentyloxy)-2-fluoropyridine and 1-azido-2-fluoroethane. Only the cycloaddition between the 1-azido-2-fluoroethane and **4PMt** gave the final compound, and this prosthetic group was then selected for the development of the radiosynthesis. The selected precursor was the 2-azidoethyl-4-methylbenzenesulfonate, which was successfully fluorinated and clicked with **4PMt** to give the ^{18}F-ligand in 70 min with 25% radiochemical yield (decay corrected).

In conclusion, in this work we evaluated the use of the Huisgen's cycloaddition for the development of novel PET tracers to selectively image the expression of $\alpha_v\beta_3$ and $\alpha_5\beta_1$ integrin receptors with a cyclic RGD peptide and a non-peptide ligand (**4PMt**) respectively.

The click reaction has been evaluated between the prosthetic groups and several non-natural amino acids. The results of this study was that the reaction conditions are perfectly suited to c[RGDfK] for the synthesis of FPPA-c[RGDfK]. The [^{18}F]FPPA-c[RGDfK] was synthesized in four steps with an acceptable radiochemical yield.

The non-peptidic ligand (**4PMt**) was obtained in six steps and the ^{18}F-labeled **4PMt** was obtained in good radiochemical yield and purity in a reasonable time.

Résumé de la Thèse

Les intégrines sont une grande famille de récepteurs de surface cellulaire qui sont responsable des interactions entre les cellules ou de cellules à matrice extracellulaire pendant l'adhésion focale. Elles jouent un rôle important dans l'angiogenèse et leur expression dans plusieurs maladies en font une cible intéressante. Au cours des dernières années, plusieurs antagonistes d'intégrine ont été développés pour des thérapies antiangiogéniques. En conséquence, l'intérêt pour visualiser l'angiogenèse dans les tumeurs avec des techniques non invasives a grandi. La technologie la plus sensible dans l'imagerie médicale clinique est la tomographie par émission de positrons (PET). Cette technique requiert des radiomédicaments émetteur de positrons (β^+) ainsi qu'un tomographe pour détecter les rayons gamma issus de l'annihilation des positrons. Les radionucléides les plus courants pour la production de radiopharmaceutiques sont ^{11}C, ^{13}N, ^{15}O et ^{18}F et ont l'avantage d'être facilement intégrable dans les biomolécules. Parmi eux, le ^{18}F est l'émetteur de positrons le plus utilisé car il bénéficie d'une demi-vie de 110 minutes, ce qui en fait un candidat idéal pour des synthèses plus longues et plus complexes. Le développement de méthodes de synthèse appropriées est un des plus grands défi en radiochimie et beaucoup de nouvelles approches ont été développées afin d'améliorer la reproductibilité et l'efficacité des réactions de marquages radioactifs.

La majeure partie des radiomolécules évaluée pour l'imagerie d'angiogenèse sont des peptides développés à partir de la séquence d'un ligand naturel, le RGD. Ladite séquence consiste en pentapeptides cycliques et des résultats prometteurs ont été obtenus lors d'essais précliniques et cliniques. Plusieurs voies de synthèses basées sur la chimie classique ont été essayées pour le marquage de peptides RGD. Ce n'est que récemment, grâce à l'introduction de la cycloaddition 1,3-dipolaire de Huisgen catalysée par du Cu(I), que la « click-chemistry » est devenue importante pour la radiochimie.

En réponse à tous les défis mentionnés en radiochimie, les objectifs ciblés pour la thèse étaient les suivants: 1) développer des groupes prosthétiques qui peuvent être conjugués avec des peptides RGD grâce à la cycloaddition azido-alcyne de Huisgen; 2) développer un radio-ligand sélectif pour des récepteurs d'intégrines $\alpha_v\beta_3$; 3) développer un radio-ligand non-peptidique sélectif pour récepteurs d'intégrines $\alpha_5\beta_1$.

Étant donné la spécificité et la courte durée de la réaction, la cycloaddition azido-alcyne a été sélectionnée comme principale voie de synthèse pour le développement de nos molécules sondes.

Sept azides et sept alcynes ont été synthétisés pour être évalué en tant que groupe prosthétique pour le marquage au ^{18}F via la «click reaction».
Le 3-azido-*N*-(4-fluorophenyl)propanamide et le 6-azido-*N*-(4-fluorophenyl) hexanamide ont été sélectionnés comme standard afin de tester les conditions de réaction avec les acides aminés modifiés. Les acides aminés qui ont été choisis sont la glycine, la valine, la proline, le phénylalanine, la tyrosine, l'acide glutamique et la lysine car elles ont différentes propriétés. La partie alcyne a été facilement incorporée à tous les acides aminés avec un rendement entre 60 et 90%. La réaction entre les groupes prosthétiques et les acides aminés sont reproductibles et ont de bons rendements, entre 54 et 98%. Le temps de réaction était significativement plus courts que ceux décrits dans la littérature. En effet, elles duraient entre 1h et 3h30 au lieu de 24h. Les résultats suggèrent que les groupes prosthétiques synthétisés peuvent être aisément incorporés aux peptides par la cycloaddition de Huisgen.

En effet, les conditions identifiées précédemment ont été utilisées pour la conjugaison du *N*-(4-fluorophenyl)pent-4-ynamide (FPPA) avec le pentapeptide cyclique [RGDfK]. La synthèse a donné le peptide conjugué avec un rendement conséquent après 1 heure. La sélectivité du FPPA-[RGDfK] pour le récepteur d'intégrine $\alpha_v\beta_3$ a été confirmée par un nouveau protocole ELISA validé.
Plusieurs précurseurs ont été utilisés et deux voies de synthèse ont été développées afin d'obtenir le groupe prosthétique marqué au ^{18}F. La première est une synthèse en une étape, faite avec le précurseur *N*-(4-trimethylammoniun)phenyl)pent-4-ynamide trifluoromethanesulfonate. La fluorisation a été testée dans CH_3CN et dans DMSO avec des températures variant entre 60 et 165°C et de 10 à 15 minutes, mais le meilleur rendement radiochimique a été obtenu était de 5% sans correction de décroissance. Ainsi, une autre stratégie a été considérée en utilisant le 4-trimetyl.....
Le précurseur a été fluoré puis le groupe nitro a été réduit pour obtenir du ^{18}F-aniline avec un rendement radiochimique (décroissance non corrigée) de 69%. L'aniline a ensuite été couplée avec le 2,5-dioxopyrrolidin-1-ylpent-4-ynoate pour obtenir le groupe prosthétique marqué au ^{18}F en 90 minutes pour un rendement (décroissance

non corrigé) de 48%. Dans la dernière étape, le groupe prosthétique marqué au ^{18}F a été conjugué avec le peptide via la cycloaddition de Huisgen pour obtenir finalement le c[RGDfK] marqué au ^{18}F en 140 minutes avec un rendement radiochimique de 8% (décroissance non-corrigé).

Le ligand non-peptidique a été sélectionné par in silico screening de différents antagonistes $\alpha_5\beta_1$. La molécule sélectionnée (4PMt or (S)-tert-butyl 3-(2-((3R,5S)-1-pent-4-ynoyl-5-((pyridin-2-ylamino)methyl)pyrrolidin-3-yloxy)acetamido)-2-(2,4,6-trimethylbenzamido)propanoate) ressemble à la conformation 3D du cyclo-[Arg-Gly-Asp-D-Phe-NMe-Val]. La synthèse de la molécule a été pensée en trois parties. La première (4YPTt or tert-butyl 2-((3R,5S)-5-((tert-butyldimethylsilyloxy)methyl)-1-pent-4-ynoylpyrrolidin-3-yloxy)acetate) a été synthétisée en quatre étapes avec un rendement final de 82%. La seconde partie (A3MeBP or (S)-tert-butyl 3-amino-2-(2,4,6-trimethylbenzamido)propanoate) a été obtenue à partir de deux étapes avec un rendement de 64% et traitée avec le 4YPTt pour obtenir le 4Y3MeOH ((S)-tert-butyl 3-(2-((3R,5S)-5-(hydroxymethyl)-1-pent-4-ynoylpyrrolidin-3-yloxy)acetamido)-2-(2,4,6-trimethylbenzamido)propanoate)avec un rendement de 40%. La molécule finale a été obtenue avec un rendement de 67% grâce à un condensation aldolique entre la 2-aminopyridine et le 4Y3MeOH oxydé. Le 4PMt a ensuite été clické avec deux groupes prosthétiques: le 3-(5-azidopentyloxy)-2-fluoropyridine et le 1-azido-2-fluoroethane. Seule la cycloaddition avec le 1-azido-2-fluoroethane avec le 4PMt a donné le produit final, qui a ensuite été sélectionné pour le développement de la radiosynthèse. Le précurseur sélectionné, le 2-azidoethyl-4-methylbenzenesulfonate, a été fluoré avec succès et clickée avec le 4PMt pour donner le ligand ^{18}F en 70 minutes avec un rendement radiochimique corrigé de 25%.

En conclusion, l'utilisation de la cycloaddition de Huisgen pour le développement de nouveaux traceurs PET dans le but d'imager sélectivement l'expression des récepteurs d'intégrines $\alpha_v\beta_3$ et $\alpha_5\beta_1$ avec respectivement le peptide cyclique RGD et le ligand non-peptidique (4PMt) a été évaluée dans ce travail. La réaction "click" entre les groupes prosthétiques et plusieurs acides aminés non-naturels a été évaluée. Les résultats de cette étude montrent que les conditions de réactions conviennent parfaitement au c[RGDfK] pour la synthèse du FPPA-c[RGDfK] Le [^{18}F]FPPA-c[RGDfK] a été synthétisé en quatre étapes avec un rendement

radiochimique acceptable. Le ligand non-peptidique (4PMt) a été obtenu en six étapes et le 4PMt marqué au ^{18}F a été obtenu à un bon rendement radiochimique et à bonne une pureté dans un temps raisonnable.

Abbreviations

A3MeBP	(S)-*tert*-Butyl-3-amino-2-(2,4,6-trimethylbenzamido)propanoate
Aca	Aminocaproic Acid
BAVN	Brain Arteriovenous Malformation
BBN	Bombesin
ANGPTL	Angioprotein-like
API	Analytical Profile Index
ATSM	Diacetyl-bis (N4-methylthiosemicarbazone)
BAVM	Brain Arteriovenous Malformation
Cn	Collagen
CNS	Central Nervous System
CRC	Colorectal Cancer
CuAAC	Copper catalyzed Azide-Alkyne Cycloaddition
DCM	Dichloromethane
Del	Developmental Endothelial Local
DMF	Dimethylformammide
DNA	Deoxyribonucleic Acid
DOTA	1,4,7,10-Tetraazacyclododecane-1,4,7,10-tetraacetic acid
ECM	Extracellular Matrix
EDC	*N*-(3-Dimethylaminopropyl)-*N*′-ethylcarbodiimide
ELISA	Enzyme-Linked Immunosorbent Assay
EOB	End of the Beam
Et_2O	Diethylether
EtOAc	Ethyl acetate
ERK	Mitogen-Activated protein Kinases
ES	Electro Spray
ESI	Electro Spray Ionization
Fab	Agent-Binding Fragment
FACS	Flow Cytometry
FAK	Focal Adhesion Kinase
FBA	Fluorobenzaldehyde
FBBO	Fluorobenzaldehyde-butylmaleimide oxime

FBEM	Fluorobenzamido-ethylmaleimide
FBzA	Fluorobenzoic acid
FDG	2-deoxy-2-fluoro-D-glucose
FGF	Fibroblast Growth Factor
Fg	Fibrinogen
Fn	Fibronectin
FLT	fms-like Tyrosine Kinase
FPA	Fluoropropionic acid
FP-PRGD	Fluoropropionate-Proline, Arginine, Glycine,Asparagine
FPPA	N-(4-Fluorophenyl)pent-4-ynamide
FP-SRGD	Fluoropropionate-Serine, Arginine, Glycine,Asparagine
FPyME	Fluoropyridinyloxypropylmaleimide
hfRPE	Human Fetal Retinal Pigment Epithelia
HEK	Human Embryonic Kidney
HER	Human Epidermal Growth Factor
Hex	Hexane
HOBT	1-Hydroxybenzotriazole hydrate
HOXD	Homeboxyn Transcription Factor
HPLC	High Pressure Liquid Chromatography
HRMS	High Resolution Mass Spectrometry
HUVEC	Human Umbilical Vascular Endothelial Cells
ICAM	Intracellular Adhesion Molecules
IgG-Fc	Immunoglobulin G-fragment Crystallizable
ITH	Intratumoral Hemorrage
K_{222}	Kryptofix
KPQVTRGDVFTEG	Lysine, Proline, Glutamine, Valine, Threonine, Arginine, Glycine, Asparagine, Valine, Phenylalanine, Threonine, Glutamic acid, Glycine
IL	Interleukin
LAD	Leukocyte Adhesion Deficiency
LIBS	Ligand Induced Binding Site
Ln	Laminin
mAb	Monoclonal antibody
MAPK	Mitogen Activated-Protein Kinases

MIDAS	Metal Ion-Dependent Adhesion Sites
MS	Mass Spectrometry
MSC	Mesenchymal Stem Cells
NHS	*N*-Hydroxysuccinimide
NMR	Nuclear Magnetic Resonance
NOTA	1,4,7-Triazacyclononane-1,4,7-triacetic acid, 8-Aoc-8-aminooctanoic acid
NPFP	Nitrophenyl fluoropropanoate
Opn	Osteopontin
PDGFR	Platelet-Derived Growth factor
PEG	Polyethylene glicol
PET	Positron Emission Tomography
PHSCN	Proline, Hitidine, Serine, Cysteine, Aparagine
PHSRN	Proline, Hitidine, Serine, Arginine, Aparagine
PIFA	[Bis(trifluoroacetoxy)iodo]benzene
4PMt	(S)-tert-Butyl 3-(2-((3R,5S)-1-pent-4-ynoyl-5-((pyridin-2-ylamino)methyl)pyrrolidin-3-yloxy
PSI	Plexins, Semaphorins, Integrins
PTH	Paratyroid Hormone
PTSM	Pyruvaldehyde-bis(N4-methylthiosemicarbazone)
RGD	Arginine, Glycine,Asparagine
RGDfV	Arginine, Glycine,Asparagine, d-Phenylalanine, Valine
RGDyK	Arginine, Glycine,Asparagine, d-Tyrosine, Valine
RGDfK	Arginine, Glycine,Asparagine, d-Phenylalanine, Lysine
RGDSCRGDSY	Arginine, Glycine, Asparagine, Serine, Cysteine, Arginine, Glycine, Asparagine, Serine, Tyrosine
RT	Radiation Theraphy
SAR	Structure-activity relationship
SFB	Succinimidyl fluorobenzoate
TBTA	Tris[(1-benzyl-1*H*-1,2,3-triazol-4-yl)methyl]amine
TETA	Tri-*tert*-butyl 1,4,7,10-tetraazacyclododecane-1,4,7,10-tetraacetate
TGF	Transforming Growth Factor
THF	Tetrahydrofurane

TK	Tyrosine Kinase
TLC	Thin Layer Chromatography
TMZ	Metronomic Temozolomide
Tn	Tenascin
TNF	Tumor Necrosis Factor
TPTX	Thyroparathyroidectomized
Tsp	Trombospondin
βTD	β Tail Domain
Tsp	Trombospondin
VCAM	Vascular Intracellular Adhesion Molecules
VEGF	Vascular Endothelial Growth Factor
VEGFR	Vascular Endothelial Growth Factor Receprot
Vn	Vitronectin
vWF	von Willebrand Factor
4Y3MeOH	(S)-*tert*-Butyl 3-(2-((3R,5S)-5-(hydroxymethyl)-1-pent-4-ynoylpyrrolidin-3-yloxy)acetamido)-2-(2,4,6-trimethylbenzamido)propanoate
4YPTt	*tert*-Butyl 2-((3R,5S)-5-((tert-butyldimethylsilyloxy)methyl)-1-pent-4-ynoylpyrrolidin-3-yloxy)acetate

Chapter 1: INTRODUCTION

1.1 Positron Emission Tomography (PET)

1.1.1 PET radioisotopes

Positron emission tomography (PET) is the most sensitive method in nuclear medicine to measure biological and physiological processes *in vivo* with an imaging technology. PET is a radionuclide imaging technique introduced in 1970, which requires a positron emitting (β^+) radiopharmaceutical and a tomograph to detect the positron emission. The radiopharmaceutical administered to the patient by injection or inhalation and the choice of the radionuclides is dependent on the biological process of interest (**table 1**).[1]

The most common radionuclides used in PET are ^{11}C, ^{13}N, ^{15}O and ^{18}F, since they can be produced with high yields with biomedical cyclotrons, they can be easily introduced in biomolecules and their decay is close to 100% positron emission. Moreover ^{11}C, ^{13}N and ^{15}O are isotopes of the most abundant elements in organic compounds allowing the labeling of biological molecules without alterations of biochemical properties of the native compound. Those radionuclides have a short half-life (2 minutes for ^{15}O, 10 minutes for ^{13}N and 20 minutes for ^{11}C) and on-site production is necessary.

^{18}F is the most used positron emitting radionuclide. It can be incorporated in a large number of molecules. It usually substitutes hydrogen or hydroxyl groups creating labeled analogs of the original compound. ^{18}F half-life of 110 min makes it suitable for more complexes synthetic strategies and on-site production is no longer required.[2]

With PET becoming more and more widespread, other radionuclides, such as radiometals, have been investigated. ^{64}Cu is the most versatile copper radionuclide, because of its peculiar decay scheme which combine the electron capture (41%), β^- (40%) and β^+ (19%) decay. Moreover it is characterized by Auger electron emission that has therapeutic potential. It has 12.7 hours half-life and is in current use for labeling antibodies and compounds such as ATSM and PTSM.[3] ^{64}Cu is not directly bound to the molecule but is carried by chelators such as DOTA, TETA or NOTA.[4]

PET is broadly used in three important areas of clinical diagnosis: cancer diagnosis and management; neuropsychiatric disorders and neurology; cardiology and cardiac surgery.[5]

Radionuclide	Target/Reaction	Half life	PET tracers	Applications
^{11}C	^{12}C(p,pn) **^{14}N(p,α)** ^{14}N(d,n α) ^{12}C(3He, α) ^{10}B(d,n) ^{11}B(p,n)	20.3 min	^{11}CO ^{11}C-Acetate ^{11}C-Leu, ^{11}C-Met, and ^{11}C-Tyr ^{11}C-deprenyl ^{11}C-raclopride,^{11}C-carfentanyl (etc) ^{11}C-cocaine	Blood volume Substrate metabolism Protein synthesis Enzyme activity Receptor ligand Drug distribution
^{13}N	^{13}C(p,n) ^{12}C(d,n) **^{16}O(p, α)** ^{14}N(p,pn)	10 min	$^{13}NH_3$	Blood flow
^{15}O	^{16}O(p,pn) ^{15}N(p,n) **^{14}N(d, n)** ^{12}C(4He,n)	2.07 min	^{15}O-water and ^{15}O-butanol C^{15}O $^{15}O_2$	Blood flow Blood volume Substrate metabolism
^{18}F	**^{18}O(p,n)** **^{16}O(3He,p)** ^{20}Ne(d,α)	109.8 min	^{18}F-fluorodeoxyglucose ^{18}F-misonidazole ^{18}F-deoxyfluorotymidine ^{18}F-deoxyuracil ^{18}F-fluorouracyl, ^{18}F-fluconazole ^{18}F-fluoroethylspiperone, ^{18}F-Fluorodopa ^{18}F-fluoropencyclovir	Substrate metabolism Hypoxia DNA synthesis Enzyme activity Drug distribution Receptor ligands Receptor gene expression
^{64}Cu	**^{64}Ni(p, n)**	12.7 h	^{64}Cu-PTSM ^{64}Cu-ATSM ^{64}Cu-Ab	Blood flow Hypoxia Receptor binding

Table 1 | PET isotopes and their applications

1.1.2 PET isotopes production and detection

The positron emitting radionuclides are usually produced by accelerators. A cyclotron is a circular accelerator, the space required for the accelerator to produce isotopes is much reduced compared to a linear accelerator. It is hence the most common and appropriate particle accelerator used to produce PET radionuclides.[6] Cyclotrons can accelerate protons or deuterons with energy of 18MeV and 9 MeV respectively. The principle of the acceleration is to provide an electric field placed in a perpendicular static magnetic field, which gives the circular trajectory to the particles by Lorentz Force. A cyclotron consists of two D-shaped regions (dees) separated by a gap (**figure 1**).[6] A magnetic field perpendicular to the plane is applied and in the gap there is a uniform electric field generated by the application of an electric potential difference to two electrodes (called dees and counter-dees), which are connected to the alternating current source (radiofrequency generator). The negative ion source (H^- or D^-) is situated at the center and the high voltage applied to the gas (hydrogen or deuterium) generates the ions.[6] Once the negative ion is generated it is extracted from the source by the electrical field from the dees, and then accelerated towards

them. When the dee has a positive charge, the counter dee has a negative charge and vice versa.[6] The positively charged dee attracts the ion and the switch on negative charge accelerates the ion to the counter dee. The same happens in the second dee guarantying a continuous increase of the ion speed. Such process "drives" the ion in a spiral movement. When the trajectory reaches certain radius the ion hits the stripper (graphite foil), which block the electrons and transforms the negative ion in a positive ion (H^+ or D^+). The positive ion is directed to an external target, containing the substance to be enriched, from which the isotope is generated.[6]

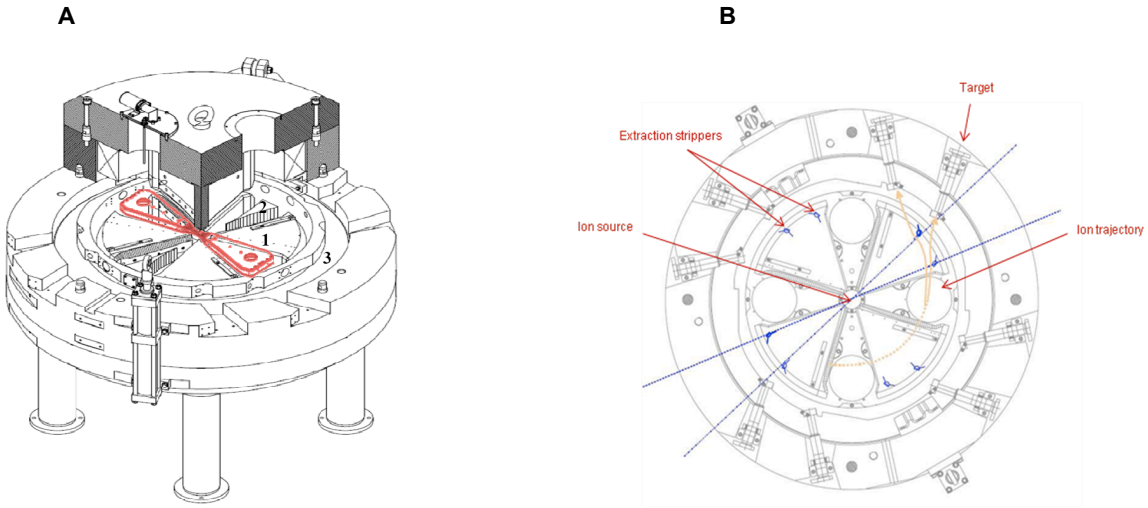

Figure 1 | Cyclotron and the accelerating plane (adapted from IBA manual user)
IBA Cyclone 18/9 cyclotron (**A**), the two dees (**1**) are in red. The magnetic field is created by coils (**3**) and flaps (**2**) adapted the magnetic field depending on the particle accelerated (H^- or D^-).
In the accelerating plane (**B**) is possible to see the ion source in the middle. The spiral ion trajectory drives the ions to the stripper and then into the selected target.

Subsequently the isotope is transported (as solution or gas) to the appropriate synthesis module to produce PET tracers.

The spontaneous decay of the positron-emitting radioisotopes produces a positron (β^+) that travels shortly before colliding with an electron of a surrounding atom and annihilates. The process produces two γ-rays with an energy of 511 keV and which are emitted at 180° to each other. The γ-rays escape from the body and are recorded by the ring detector of the PET scanner, providing the tomographic images (**figure 2**).[5, 7]

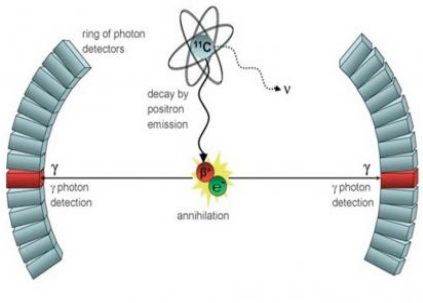

Figure 2 | Radioisotope annihilation and detection
When the two γ-rays at 180° are emitted, there is a simultaneous detection on the ring detector. The opposite simultaneous detection is named coincidence lines. Sometimes the γ-rays can be deviated creating a scattered coincidence. During a PET, only the coincidence lines are recorded to form the image.[7]

1.1.3 PET in oncology

The use of PET in oncology has widely increased with the development of the whole-body scan in 1980s. By the use of PET, it is actually possible to differentiate benign and malignant tumors, to define the extension of the disease, to monitor the response to the treatment and to identify the site of the primary disease (**figure 3**). Moreover, PET allows quantifying tumor perfusion, evaluating tumor metabolism and tracing radiolabeled cytostatic agents. Such information can be used for planning of chemotherapy and radiotherapy.[5]

In a standard whole-body scan, the tracer is injected intravenously to the patient and the acquisition starts after the uptake time. The patient is placed in the scanner and the period of time of data acquisition depends on the tracer. The data are reconstructed to obtain 2D or 3D images. If kinetic information is needed, the acquisition starts prior to the injection and dynamic acquisition is recorded during the uptake time.[5, 7]

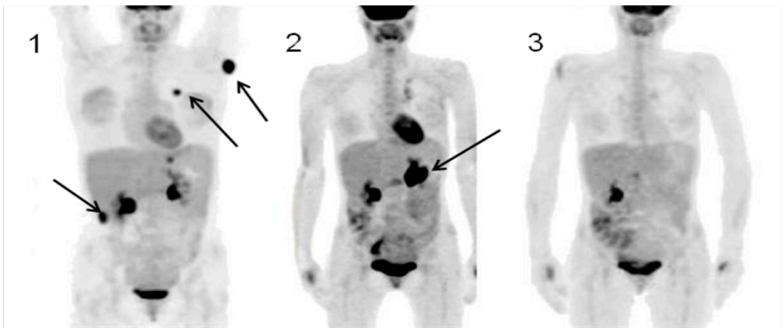

Figure 3 | PET/CT scan (adapted from Ridolfi et al[8])
Periodical PET/CT scans of the patient show the good answer to the therapy. Metastasis in picture 1 and 2 are not any more present in picture 3.

A common tracer used in the clinics is ^{18}F-FDG (^{18}F-2-deoxy-2-fluoro-D-glucose). For the clinical standard ^{18}F-FDG whole body scan, 370 MBq of the tracer are injected and the uptake time is between 20 and 30 min.[7]

^{18}F-FDG is used for soft tissues. Its uptake is proportional to glycolysis activity of the tissue, thus getting mainly concentrated in brain, kidneys, heart and tumors. ^{18}F-FDG has the same metabolic pathway as glucose, but it cannot be catabolized until total decay of ^{18}F in ^{18}O.[7, 9]

Other interesting tracers for tumor imaging are ^{18}F-choline and ^{18}F-FLT.

Choline is a substrate for the synthesis of phosphatidylcholine, and is an essential component of the cell membrane. As well as ^{18}F-FDG, ^{18}F-choline uptake is due to the high metabolic activity of tumoral cells. It can be ^{11}C or ^{18}F labeled and ^{18}F-choline is considered an excellent tracer for prostate and renal cancer.[10]

^{18}F-FLT is a fluorine-modified thymidine analogue, its accumulation in tissues is linked to the expression of cytosolic thymidine kinase-1 (TK-1) expressed in pathway of DNA synthesis in the S-phase of the cell cycle. Results of clinical trials studies suggest that ^{18}F-FLT is a promising tracer to monitor the tumor response to treatment.[11]

PET scan has revolutionized the medical diagnostics by increasing accuracy in identification of the cancer primary tumor and by detecting the distal sites of tumor spread. Nevertheless, it is still not possible to recognize cancer deposits smaller than 1 cm and pinpoints a specific site of tumor. In order to deal with that, many novel probes and tracer agents for specific targets are in development.[12]

Lately, angiogenesis has been proposed as a PET target to overcome the issues in the detection of small tumors and several multimolecular probes have been developed having as target the integrin receptors, which are the primary mediators of such process.[13]

1.2 Integrin receptors

Integrins are a large family of transmembrane cell adhesion receptors, which mediate cell-to-cell and cell-to-extracellular matrix interactions. They are heterodimers composed by non-covalently linked α and β subunits that are interdependent for correct processing and encoded by independent genes. In mammals, 18 α subunits and 8 β subunits have been identified, combining in 24 αβ receptors (**table 2**).[14] The

two subunits have an extensive N-terminal extracellular domain with about 1000 amino acids for α and about 750 amino acids for β.[15] The α chain has a short cytoplasmic domain and a transmembrane domain that is attached to two calf domains (Calf-1 and Calf-2), which form a flexible “knee” with the thigh domain. The upper moiety is formed by a repetition of β-propeller domains. The interactive domain (α-I domain) has an important role in ligand binding and is situated between the α-subunits 2 and 3 of the β-propeller domain. The β chain has a longer cytoplasmic domain and the transmembrane domain makes up the “leg region” starting with a β-tail domain (βTD), which consists of a PSI (plexins, semaphorins and integrins) domain, and four epidermal growth factor domains (EGF). The head is formed by a βA domain connected to the leg by a hybrid domain.[16] (**figure 3**)

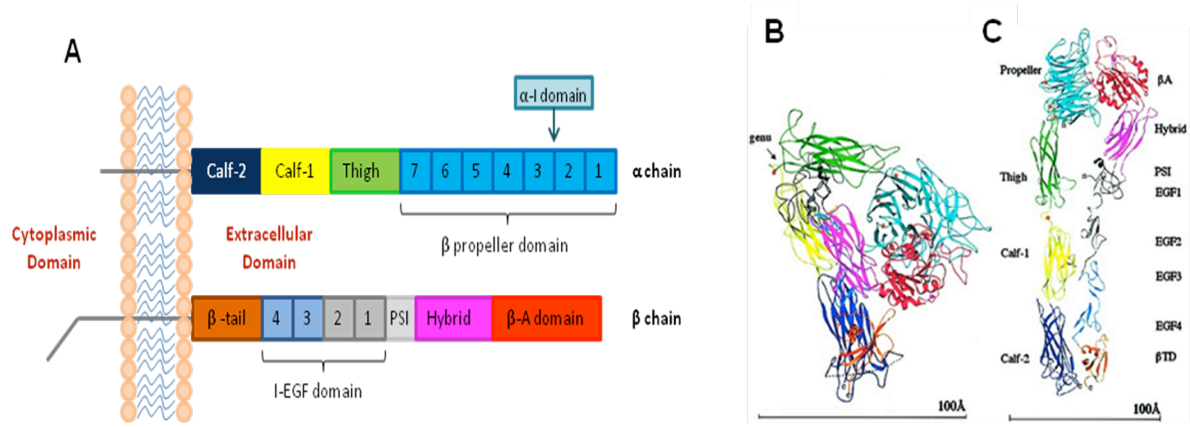

Figure 3 | Diagram of integrin structure
The image is based on the crystal structure of the integrin $\alpha_v\beta_3$ adapted form Xiong et al[16]. **A** is a simplification of sequence structure of the extracellular domain of α and β chain. In its inactive form (**B**) the receptor is bent in a flexible region (genu), which is between the calf-1 (yellow) and thigh (green) domains for α chain. On β chain the PSI, EGF-1 and EGF-2 regions (grey) are responsible for flexibility. In this close conformation, the receptor has a low affinity for the ligand. The active form (**C**) has linear α and β chain.[17]

The binding site is situated in a pocket between the β-propeller and the βA domain and includes metal ion-dependent adhesion sites (MIDAS), situated on both the α-I and βA domains. MIDAS bind divalent metal ions which influence the interaction with the ligand.[18] The bound cations (Ca^{2+}, Mn^{2+} and Mg^{2+}), determine the conformation of the integrin and its binding properties.[19] However the substitution of Ca^{2+} with Mn^{2+} does not correspond to important structural rearrangements of the receptor.[20]
Integrins have three distinct conformations: a low affinity conformation (bent conformer) with the closed head-moiety, a partially active conformation and a high affinity ligand-binding conformation with open head-moiety (**figure 4**). The bent

conformer is stabilized in Ca^{2+} solution but destabilized in Mn^{2+} solution. Furthermore presence of cyclo-RGDfV highly destabilizes the bent conformer and shifts the combination among the several conformations almost totally to the highly active one, independently from the cation solution. The partially active conformer is an intermediate between the inactive and active forms, since it has the closed head moiety of the bent conformers and the “extended legs” of the highly active conformer.[21]

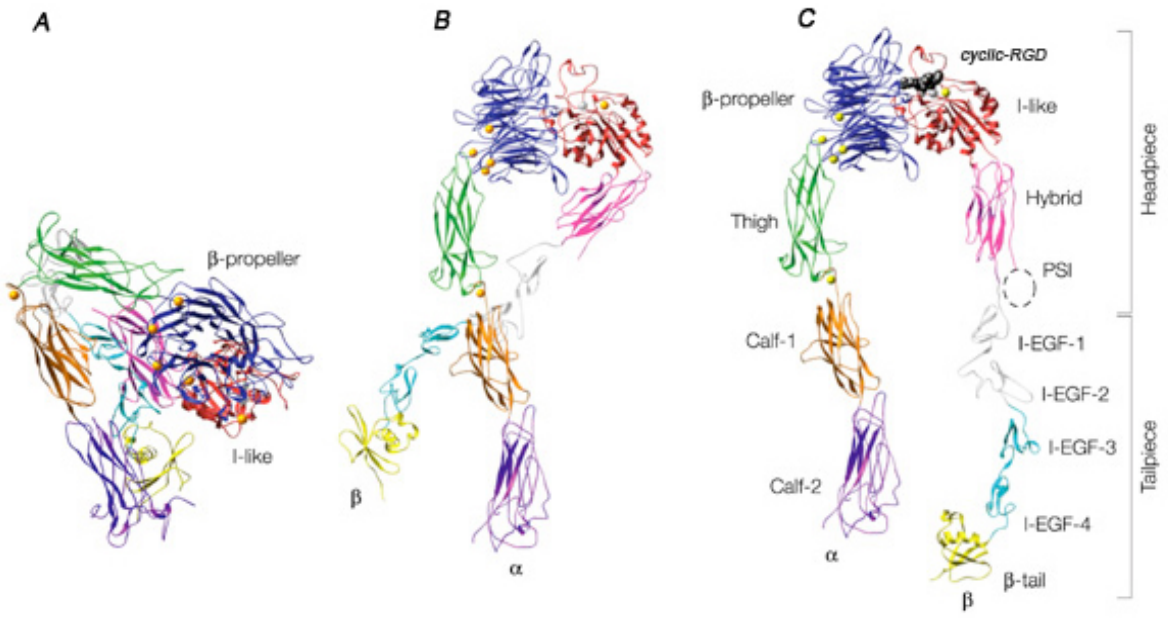

Figure 4 | Conformation states of integrins
The three distinct conformation states are based on crystal magnetic resonance and electron microscopy of integrin $\alpha_v\beta_3$ adapted from Shimaoca et al[22]. The three conformers are present at the same time only in Mn^{2+} solution.[21] In **A** there is the bent form adopted in Ca^{2+} solution with closed headpiece. **B** is the intermediate form with closed headpiece and extended tailpiece. The highly active form (**C**) with open headpiece is the states adopted in presence of RGD ligands. The cyclic-RGD (black) binds into the binding pocket between the β-propeller (α-I domain) and the βA domain (I-like).[22]

Integrins bind many structural extracellular matrix (ECM) proteins like Fibronectin (Fn) and collagens (Cn), as well as temporary ECM proteins produced in trombotic events or during tissue remodeling like Vitronectin (Vn), fibrinogen (Fg), trombospondin (Tsp), entactin, intracellular adhesion molecules (ICAM) and vascular cell adhesion molecules (VCAM). Many ligands are characterized by the tripeptide sequence Arg-Gly-Asp (RGD) which is the recognition motif for several different integrins.[23]

Integrin	Ligands	Physiological distribution	Roles
α1β1	Cn-VI, Cn-I, Ln, semaphorin7A	Chondrocytes, endothelial cells	Introduction of laminin-1 expression
α2β1	Cn-I, Cn-IV, Ln, Echovirus 1, Tn	Keratinocytes, chondrocytes, platelets, endothelial cells	Wound healing
α3β1	Ln, VEFG-A, Tsp	Keratinocytes	Branching morphogenesis in mammary epithelia, tumorigenesis and metastasis
α4β1	Fn, VCAM-1, MadCAM-1	Leukocytes, endothelial cells	Adhesion and extravasation of lymphocytes, monocytes and progenitor cells tumor homing
α5β1	Fn, Fibrillin-1, Tsp	Chondrocytes, endothelial cells	Angiogenesis
α6β1	Ln, Tsp, CYR61	Chondrocytes, endothelial cells	Angiogenesis
α7β1	Ln	Differentiated muscle cells	Unclear
α8β1	Fn, LAP-TGFβ	Smooth muscle cells	Fibrotic response
α9β1	Tn, VCAM-1, VEFG-A-C-D, HGF	Keratynocytes, endothelial cells	Lymphangiogenesis
α10β1	Cn	Chondrocytes	Unclear
α11β1	Cn	Mesenchymal non-muscle cells	Embryonic development
αvβ1	Ln, Fn, Opn, Vn	SMCs, fibroblast, osteoclast, tumor cells	Vascular disorders
αvβ3	Fg, Vn, Tn, Opn, Tsp, Fn, PECM, MMP2, VEFG-A, Fibrillin-1, vWF	Endothelial cells, SMCs, osteoclast, platelets, fibroblast, tumor cells, epithelial cells, chondrocytes	Angiogenesis, vascular disorders, restenosis, osteoporosis
αvβ5	Opn, F, Vn, Fn, Tsp	Endothelial cells, SMCs, osteoclast, platelets, epithelial cells, chondrocytes, leukocytes	Angiogenesis, vascular disorders
αvβ6	Fn, Fg, Vn, Tn, LAP-TGFβ, Fibrillin-1	Epithelial cells, carcinoma cells	Promotion of cell migration, control cell proliferation, activation of TGFbs, suppression of apoptosis, modulation of protease activity and mediating invasion of carcinoma cells.
αvβ8	Vn	Melanoma, kidney, brain ovary uterus, placenta	Proper brain blood vessel development
αDβ2	VCAM-I, Vn, Plasmogen	Leukocytes	LAD
αLβ2	ICAM-2, Fg, Fn	Leukocytes	LAD
αMβ2	iC3b, factor X, heparin	Leukocytes	LAD
αxβ2	ICAM-2, Fg, iC3b, factor X, heparin	Leukocytes	LAD
αIIbβ3	Fg, Fn, vWF	Platelets	Stable clot formation and homestasis
α6β4	Ln	Endothelial cells	Keratinocyte migration and survival, carcinoma invasion
α4β7	MAdCAM-I	Leukocytes	Multiple sceloris and psoriasis
αEβ7	ICAM-1, Fg, iC3b, factor X, heparin	Leukocytes	

Table 2 | Integrins, ligands, distribution and roles (adapted from Niu et al[24])
The type of integrin receptor(s) expressed depends on the ECM ligands present in the local environment and on the cell type. All the essential tissues express integrins, but each tissue only expresses only a limited subset.[25]
Ln (laminin), Tn (temascin), Opn (osteopontin), vWF (von Willebrand factor).

The role of the integrins is to mediate the cell migration by connecting the ECM with the intracellular cytoskeleton during the focal adhesion. Bidirectional signaling (inside-out and outside-in) is used to integrate the extracellular and cytoplasmic environment.[21] On cell surfaces, the integrins are not fixed in a single conformation but there is an equilibrium among the different conformers, which can be modified depending on the presence of the activating intracellular factors or extracellular ligands.[22] The binding of the ligands induces integrins activation and stabilizes the highly active conformation inducing the clustering of several integrin receptors and the formation of multiprotein complexes.[26] Such a process triggers a cytoplasmic signaling pathway, which involves Src-family kinases and FAK. They activate the mitogen activated-protein kinases (MAPK) cascade by small GTPases which in turn has effects on the cytoskeleton[27] and activates some transcription events in the cell nucleus.[28]

While activation of the integrins by ligand binding promotes cell proliferation, migration and survival, unligated or antagonized integrin receptors may activate the process of apoptosis. ECM behaves as a trophic factor and the alteration of its microenvironment, with the absence of integrin ligands as well as the presence of proteases or antagonists, compromise cell survival.[25, 29] The “integrin-mediated death” is induced by the presence of unligated integrins which recruit caspase-8 to the membrane and promote the caspase cascade that leads to apoptosis.[30]

1.3 Angiogenesis

Integrins are of crucial support for the formation of capillaries and angiogenesis. As a matter of fact integrins $\alpha_2\beta_1$, $\alpha_3\beta_3$, $\alpha_5\beta_1$ and $\alpha_v\beta_3$ are expressed in large vessels, while other integrins such as $\alpha_1\beta_1$, $\alpha_6\beta_1$, $\alpha_6\beta_4$ and $\alpha_v\beta_3$ are expressed in microvascular endothelial cells. The expression of integrins in large and small vessels is modulated by the transforming growth factor (TGF),[31] and the vascular endothelial growth factor (VEGF).[32] Angiogenesis has physiological importance in embryonic development and tissue repair, but also plays an important role in the progression or status of inflammatory processes, diabetic retinopathy, macular degeneration and cancer.[29]

Physiological angiogenesis is known to be a self-limiting process, regulated by a balance between pro and antiangiogenetic factors. The control of the signals during the process is mediated by specific interactions among ligands, receptors, ECM and

antiangiogenic factors. Proangiogenic factors are initially produced to allow the endotelial proliferation, invasion and survival; their effect is subsequently reduced by the production of antiangiogenic factors.[33] Angiogenesis ends with the induction of apoptosisis of the endothelial cells by proapoptotic factors and/or growth factors withdrawal.[34]

Angiogenic endothelial cells are quite sensitive to alteration of the microenvironment: the lack of growth factors or protein fragments on the ECM induce stop of angiogenesis and vascular regression via apoptosis.[35] In pathological conditions, the balance between proangiogenic and antiangiogenic factors is deregulated, with an excess of stimulus and an abnormal angiogenesis.[36]

Several integrins are required for angiogenesis, but three integrins have prominent roles: $\alpha_v\beta_3$, $\alpha_v\beta_5$ and $\alpha_5\beta_1$.[37] Integrins $\alpha_v\beta_3$ and $\alpha_5\beta_1$ participate in the same angiogenic pathway, which is different for integrin $\alpha_v\beta_5$.[38]

1.3.1 Integrin $\alpha_v\beta_3$

Integrin $\alpha_v\beta_3$ expression in angiogenesis is induced by basic fibroblast growth factor (bFGF), interleukin 8 (IL8) and tumor necrosis factor α (TNF-α) in tumor cells.[39].

Integrin $\alpha_v\beta_3$ was the first α_v integrin to be identified as upregulated during angiogenesis and to be implicated in cancer growth and invasion. It can bind different EC ligands having the RGD tripeptide sequence such as fibronectin (Fn), vitronectin, fibrinogen, collagen, laminin and osteopontin. Integrin $\alpha_v\beta_3$ has a limited tissue distribution; it has a limited expression in quiescent or normal blood vessels and the higher expression have been observed on blood vessels in granulation tissue and tumors.[40]

Expression of $\alpha_v\beta_3$ is associated to tumor growth, lymph nods and metastasis in melanoma, prostate, ovarian, pancreatic and breast cancer as well as decreasing of patient survival in cervical cancer.[41]

Integrin $\alpha_v\beta_3$ is linked to cell migration and invasion, but it appears to have also a crucial role in mediating cell survival.[42]

In vivo studies demonstrate that the α_v subunit is important for the physiological process of angiogenesis. Indeed, α_v knockout mice have a short life after birth because of extensive brain and intestinal hemorrhaging.[40] On the other hand experiments on $\alpha_v\beta_3$ deficient mice showed that this integrin is not essential for

physiological development of blood vessels.[43] In chronic pathologies such as tumor growth, the expression of $\alpha_v\beta_3$ increases angiogenesis.[44]

The signaling pathways activated by integrins tumor cells by the integrins are similar to those observed in physiological endothelial cells during the angiogenesis. They mediate the migration, invasion, survival and proliferation of tumor cells, facilitating tumor growth and formation of metastasis. The overexpression of $\alpha_v\beta_3$ in tumor cells contributes to enhancing the invasive potential of the transendothelial migration and it is positively correlated to metastasis.[45] Inhibition of $\alpha_v\beta_3$ in endothelial cells induces the activation of caspase 8-dependent cell death[30] and increases the activity of the tumor suppressor p53 after 48h of treatment.[46]

$\alpha_v\beta_3$ integrin cooperate with vascular endothelial growth factor receptor 2 (VEGFR-2) and platelet-derived growth factor receptor β (PDGFR-β) to promote cellular proliferation and migration.[47] Indeed, complexes between β_3 subunit and VEGFR-2 are observed in angiogenic blood vessels[48] and they play a pro-angiogenic role.[49] The extracellular domain of β_3-subunit is essential for the interaction with the two growth factors, whereas α_v subunit increases the interaction with VEGFR-2.[49] The complex VEGFR-2/$\alpha_v\beta_3$ is stimulated by the VEGFR-A and stabilized by the transglutaminase and tyrosine kinase enzymatic activities of coagulation factor III (FXIII).[50] VEGFR-2 interact with $\alpha_v\beta_3$ only in its active form, and the formation of such complex is essential for the activation of the endothelial cells and the stimulation of the VEGF-induced angiogenesis.[51]

Studies on mice β_3 null suggest that integrin $\alpha_v\beta_3$ has both a positive and negative role during angiogenesis. In facts, $\alpha_v\beta_3$ can bind pro-angiogenic (i.g. VEGFR2, vitonectin, fibronectin, Del1, ANGPTL3 and thrombin) as well as anti-angiogenic factors (i.g. tumstatin, trombosondin and angiostatin). In this way it works as a regulator of angiogenesis by balancing the ECM signals.[24]

1.3.2 Integrin $\alpha_5\beta_1$

Integrin $\alpha_5\beta_1$ expression is activated by transforming growth factor-β (TGF-β)[52], bFGF, IL8 and the ECM protein DEL1. In endothelial cells expression is regulated by the homeobox family transcription factor 3 (HOXD3), which is also induced by bFGF.[52] In vivo studies showed that mutation of the α_5 integrin gene is a recessive

embryonic lethal mutation. Indeed, α_5-knockout mice die around days 10.5 of gestation because of disorders on notochords, somites and heart.[53]

Integrin $\alpha_5\beta_1$ is a major receptor for Fn, and the interaction occurs via the RGD sequence on the $FnIII_{10}$ domain and the PHSRN synergy site on the adjacent $FnIII_9$ domain. Mutation on the $FnIII_9$ domain reduces the binding activity for integrin $\alpha_5\beta_1$ due to a loss of conformational stability.[54] The PHSRN synergy site stabilizes the binding of $\alpha_5\beta_1$ and RGD site, but it is no longer required if the integrin is in its high-affinity state. There are evidences that the integrin $\alpha_5\beta_1$ has three distinct activation states that produce distinct strengths of binding with Fn. The different states of $\alpha_5\beta_1$ interact with many sites of Fn, including RGD and PHSRN.[55]

Fn is fundamental for the development of angiogenesis. It is expressed specifically in new formed blood vessels and the ECM is fibronectin-rich during angiogenesis.[56] In the absence of growth factor stimulation, mesenchymal stem cells (MSC) specifically induce the adhesion of integrin $\alpha_5\beta_1$ to fibronectin, by the activation of PDGFR-β which induces MSC migration for vascular remodeling.[57]

Integrin $\alpha_5\beta_1$ is poorly expressed in quiescent endothelial cells but it is highly expressed in angiogenic endothelial cells. In the central nervous system (CNS), $\alpha_5\beta_1$ has an important role in stimulating the endothelial cell proliferation in the phases of the early angiogenic process and for endothelial cells response in hypoxia-induced angiogenesis.[58] Integrin $\alpha_5\beta_1$ also plays a fundamental role in brain angiogenesis. In disorders like brain arteriovenous malformation (BAVM), upregulation of $\alpha_5\beta_1$ integrin increases the VEGF and TGF-β levels to create proangiogenic conditions.[59] The same mechanism is observed in the brain after ischemic stroke.[60]

$\alpha_5\beta_1$ is expressed in several types of tumors, sometimes associated with an aggressive phenotype, such as in brain tumor or non-small cell lung carcinoma, and decreased survival in patient.[41, 61]

Upregulation of integrin $\alpha_5\beta_1$ and Fn has been observed in blood vessels in mouse and human tumors and evidence suggest that the p53-mediate response to genotoxic damage is compromised in tumors with overexpression of the α_5 subunit.[61]

The β_1 subunit has a role in mediating resistance to chemotherapy and radiation therapy as well as in the regulation of tumor dormancy and transition to proliferation and metastasis formation.[62]

Antagonists of $\alpha_5\beta_1$ inhibit growth factor-stimulated endothelial cell survival and proliferation,[63] tumor angiogenesis and tumor proliferation.[52]

1.4 Integrins as therapeutic targets

The overexpression of the integrins in several diseases such as tumor, thrombosis, cardiovascular diseases, inflammatory diseases,[64] multiple sclerosis, osteoporosis and immune system disorders,[65] makes them an appealing target. Several integrin antagonists are in preclinical and clinical evaluation; these compounds can be classified in monoclonal antibodies (mAb), peptides and small molecules (or peptidomimetics).

1.4.1 Monoclonal antibodies

Function-blocking monoclonal antibodies were the first integrin antagonists developed having a good anti-angiogenic activity in cell cultures.[66]

Bevacizumab (Avastin) is an anti-angiogenic humanized monoclonal antibody which is indirectly active on integrin $\alpha_v\beta_3$. It has anti-VEGF activity and blocks the co-operation between $\alpha_v\beta_3$ and VEGF2 that promote endothelial cell migration.[67] It was the first antiangiogenic monoclonal antibody to receive the approval from FDA. It is used as a first line agent, in combination with 5-fluorouracil or carboplatin/paclitaxel, for metastatic colorectal cancer and for metastatic HER-2 negative breast cancer. Avastin is currently in clinical trials for several kinds of tumors,[68] having the advantage of well tolerated at therapeutic doses and high survival of the patients. The efficacy of the antibody was evaluated in combination with chemotherapy (5-fluorouracil 500 mg/m^2 plus leucovorin 500 mg/m^2 weekly from 6 to 8 weeks cycle), with a low dose of bevacizumab (5 mg/kg every 2 weeks), or the same chemotherapy in combination with a high dose of bevacizumab (10 mg/kg every 2 weeks).[69] Common side effects are thrombosis, reduced wound healing, proteinuria, hypertension and gastrointestinal perforation.[70]

MEDI-522 (Vitaxin or Abegrin) is a humanized monoclonal antibody, which was derived from LM609, selective for integrin $\alpha_v\beta_3$. Its anti-angiogenic effects induce suppression of tumor growth[71] and inhibition of osteoclast attachment with reduction of bone metastasis.[72] In phase I study in patients with solid tumor metastasis the

treatment was well tolerated with a low-grade toxicity.[73] Evidence suggests that the optimal biological dose is 8 mg/kg, but such dosage has stable disease as best treatment outcome.[74, 75] Vitaxin is currently in phase I/II for different type of tumors, metastatic tumors and rheumatoid arthritis.[76]

CNTO 95 (Intetumumab) is a human monoclonal antibody which has both $\alpha_v\beta_3$ and $\alpha_5\beta_1$ integrins as targets. It is phase I trials for solid tumors and prostate cancer, in phase II for advanced melanoma.[77] In nude rats, the combination with fractionated radiation therapy increases the inhibition of tumor growth, and the tumor response rate is significantly better than single therapy alone.[78]

Volociximab (M200) was the first chimeric monoclonal antibody selective for $\alpha_5\beta_1$; it is an inhibitor of the $\alpha_5\beta_1$/Fn interaction and causes consequent inhibition of neoangiogenesis. It is well tolerated in monotherapy or in combination with chemotherapy in several tumor types. The pharmacokinetic evaluation suggests that Volociximab has a bi-exponential decline with an initial distribution phase followed by the elimination phase. In phase II clinical trials, patients were treated with 10 mg/kg per week for pancreatic cancer (cohort 1), kidney cancer and non-small cell lung cancer and 10 mg/kg every 3 weeks for melanoma. 15mg/kg per week were administered in case of pancreatic cancer (cohort 2) and ovarian cancer, or every 3 weeks for malignant melanoma. Stable disease was documented for all the treatments, and for ovarian cancer reduction of metastasis and increasing of patients survival were observed.[79] Volociximab is in clinical trials also for other diseases such as Alzheimer's diseases and age-related macular degeneration.[80]

Chimeric 7E3 Fab (Abciximab) is an $\alpha_v\beta_3$ and $\alpha_{IIb}\beta_3$ antagonist. It is a chimeric antigen-binding fragment (Fab) of a monoclonal antibody which binds GPIIb/IIIa receptors. It is active in preventing the fibrinogen-mediated platelet aggregation and it is under investigation for different coronary and cardiac diseases.[81] Patient treated with Abciximab after ischemic stroke show high survival but several events of bleeding complications during hospitalization were also observed.[82, 83]

1.4.2 Peptides

The majority of the anti-angiogenic peptides have been designed based on the RGD structure of natural ligands for $\alpha_v\beta_3$ and $\alpha_5\beta_1$ integrins.

Cilengitide, a cyclic RGD-based peptide, was the first peptidic small molecule with anti-angiogenic activity to become candidate as drug. It efficiently inhibits $\alpha_V\beta_3$-mediated cell adhesion and induces endothelial cell detachment-mediated death.[84] In preclinical studies it showed high selectivity for vascularized tumors and increased efficacy in non-small-cell lung cancer and endothelial cells. In phase I clinical trials, cilengitide showed activity in glioblastoma with low toxicity at doses up to 2.4 mg/m^2. In children with brain tumor, 1.8 mg/m^2 of cilengitide were administered, associated with low risk of ITH (intratumoral hemorrhage). Moreover, its antitumor activity is enhanced in combination with chemotherapeutic agents. Clinical trials combining Cilengitide (200 or 500 mg) with radiation therapy (RT) or metronomic temozolomide (TMZ) solved good tolerance with positive effects.[85] Thanks to these results cilengitide is currently in phase II for many tumors and metastatic tumors.[86]

ATN-161 (Ac-PHSCN-NH_2) is a small peptide selective for $\alpha_5\beta_1$. It inhibits the interaction Fn/$\alpha_5\beta_1$ since its basic sequence, PHSCN, derives from the PHSRN $FnIII_9$ domain.[87] Pharmacokinetic studies showed that it has rapid clearance and high tissue distribution. The half-life is short but, despite that, preclinical models evidenced a durable effect of tumor growth suppression. In phase I, patients were treated with eight different dose levels (0.1, 0.25, 0.5, 1.0, 2.0, 4.0, 8.0, and 16.0 mg/kg) 3 times per week, with cycles of treatment running from 1 to 14 weeks. The resulting data demonstrate its tolerability, non-immunogenicity and preliminary anti-angiogenic and anti-metastatic activities[88, 89] ATN-161 is in phase II for advanced renal cancer and malignant glioma in monotherapy or in combination with chemotherapies.[89, 90]

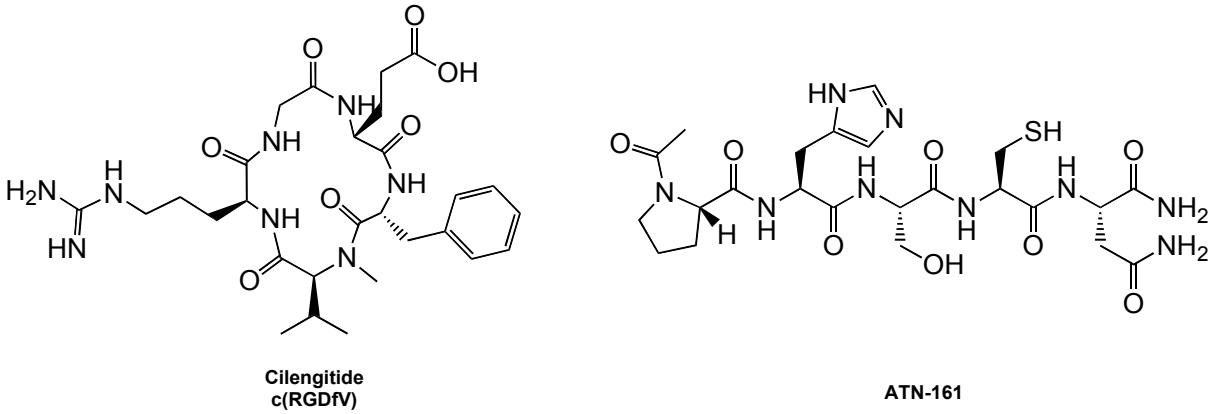

Figure 5 | Chemical structure of Cilengitide and ATN 161

1.4.3 Small molecules

Resveratrol is a natural compound found in grapes, berries, peanuts and medicinal plants. It showed anticancer and cardioprotective activities and among its targets[91] we can find $\alpha_v\beta_3$ integrin receptor.[92]

The binding site for resveratrol is close to the RGD recognition site and it is situated on the β_3 monomer. The binding with the integrin initiates transduction via mitogen-activated protein kinases (ERK1/2), which in turn promote p53-dependent apoptosis.[93] In several studies resveratrol showed a very low bioavailability, but the beneficial effects observed were considerable. It has an evident dose-dependent response, clinical trials for colon cancer 0.5 up to 80 g/day are administered to patients.[86] Resveratrol is in phase I for colon cancer, colorectal cancer (CRC) hepatic metastasis and it is under investigation for cardiovascular, Alzheimer's and inflammatory diseases.[94]

JSM6427 is a designed molecule having cyclo-(Arg-Gly-Asp-D-Phe-NMe-Val) as template.[95] It is a potent, highly specific $\alpha_5\beta_1$ antagonist (IC_{50} 3.5 nM) with IC_{50} value for other integrins ($\alpha_v\beta_3$, $\alpha_v\beta_5$, $\alpha_{IIb}\beta_3$, and $\alpha_3\beta_1$) as high as >300000 nM in a competitive integrin binding assay.[96] Inhibition of $\alpha_5\beta_1$ by JSM6427 induces significant reduction of glioma in a mouse model, where a consistent reduction of microglial migration was observed together with a reduction in proliferation of approximately 70% at 20 μM and 60% at 50 μM.[97]

In hypoxia-induced neurovascularization, systemic administration of JSM6427 suppressed laser-induced choroidal neovascularization in monkey and rabbit models. In vitro tests on hfRPE (human fetal RPE cell line) demonstrate that the inhibition of the serum-induced proliferation is dose-dependent, while PDGF-BB and bFGF-dependent cell migration is significantly inhibited at 50 μM JSM6427 and the effect on quiescent cells is null.[98] JSM6427 is in phase I for age-related macular degeneration but the results are not published yet.[99]

S137 and S247 are peptidomimetics with selectivity for $\alpha_V\beta_3$, they have IC_{50} on $\alpha_V\beta_3$ of 1.6 ± 1.3 nM (S137) and 0.4 ± 0.24 nM (S247). Despite S137 having a better plasmatic half-life than S247 for oral administration, the in vivo activity is similar for both at the same dose. They showed a significant anti-metastatic and anti-angiogenic activity in a mouse model on breast tumor cells and colon cancer hepatic metastasis.[100, 101]

In vivo studies on hepatic metastasis demonstrate that S247 has high anti-angiogenic activity and increases cell apoptosis and mice survival. Its anti-angiogenic effect is limited to metastasis, and it did not show any activity on the primary tumor in vivo.[102, 103]

SB265123 is an inhibitor of $\alpha_V\beta_3$-mediated cell adhesion and osteoclast-mediated bone resorption. In an *in vitro* assay on human osteoclast mediated bone resorption, it showed an IC_{50} of 48 ± 3 nM while a total inhibition was obtained at 500 nM. SB265123 activity was evaluated in vivo in the TPTX rat model and an inhibition of 85% was observed on PTH-induced bone resorption after 6h from administration.

Considering its activity, SB265123 can be considered for the treatment of postmenopausal osteoporosis, moreover it has the advantage to be an orally bioavailable molecule.[104]

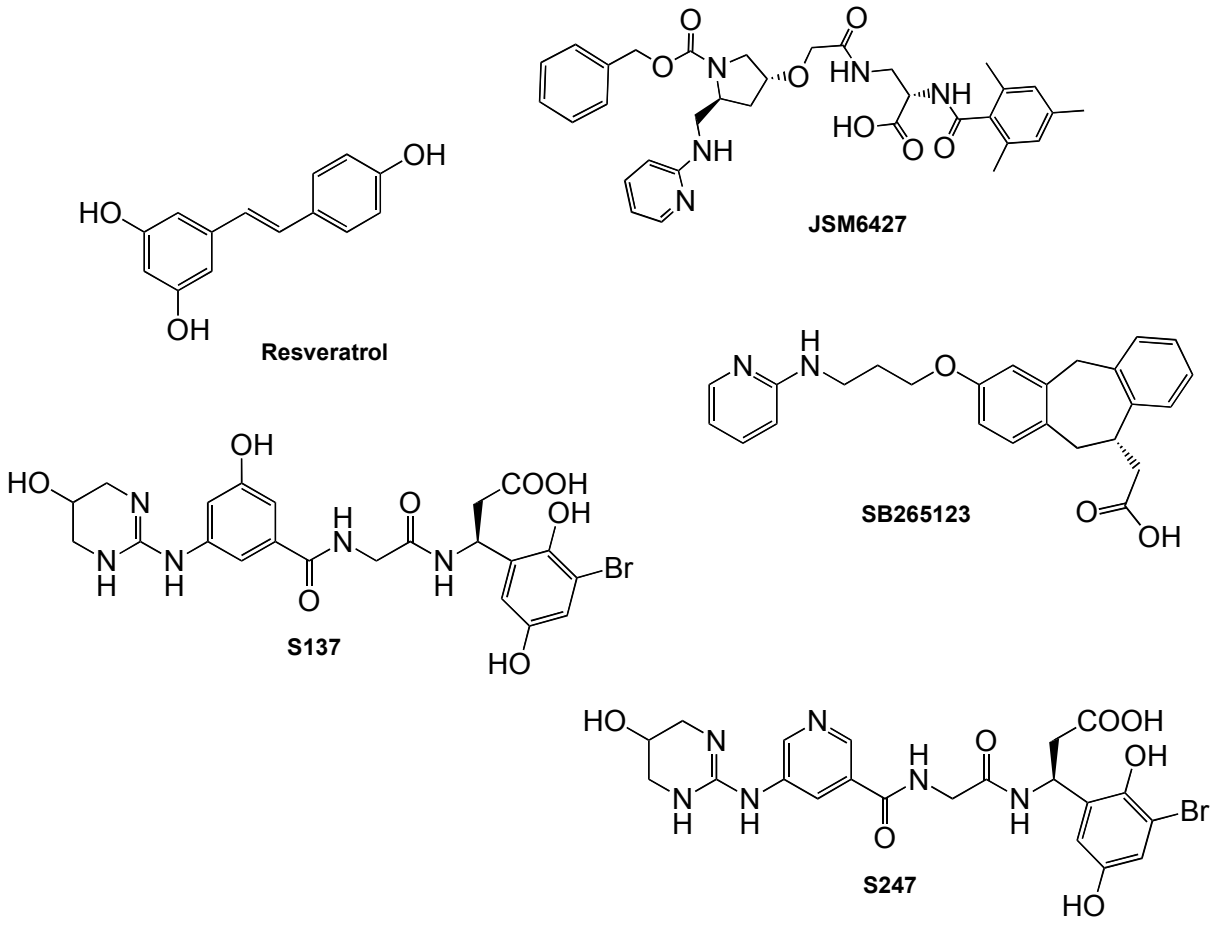

Figure 6 | Chemical structure of resveratrol, JSM6427,[95] SB265123, S137 and S247.[100]

Integrin target	Drug	Company	Disease	Clinical phase	Reference
VEGF-αvβ3	Bevacizumab (Avastin)	Genentech/Roche	Metastatic colorectal cancer Metastatic negative breast cancer Solid tumors Brain tumors Lung cancer Non-small-cell lung cancer Metastatic breast cancer	FDA app. FDA app. I II I/II II II	[86, 105]
αvβ3	MEDI-522 (Vitaxin, Abegrin)	Medimmune	Metastatic melanoma Metastatic prostate cancer Colorectal carcinoma Kidney cancer Rheumatoid arthritis Prostate cancer Refractory solid tumors	II II II I/II II II I	[71, 106]
α5β1	M200 (Volociximab)	Protein Design Labs Biopharma Inc	Metastatic melanoma Renal cell carcinoma Non-small-cell lung cancer Advanced ovarian cancer Hematologic cancer Moderate Alzheimer's disease Age-related macular degeneration	II II II II II III I	[52, 64]
α5β1 **αvβ3**	CNTO 95 (Intetumumab)	Centocor	Advanced refr. prostate cancer Solid tumors Advanced melanoma	I I I/II	[107]
αvβ3 **αIIbβ3**	Chimeric 7E3 Fab (Abciximab)	Centocor	Myocardial infarction Angina Adverse hemorrhaging events Acute coronary syndrome Chock cardiogenic Carotid stenosis Stroke	IV IV II IV IV I/II III	[64, 86]
αvβ3 **αvβ5**	EMD 121974 (Cilengitide)	Merck KGaA	Metastatic melanoma Metastatic prostate cancer Pancreatic cancer Non-small-cell lung cancer Glioblastoma multiforme Glioblastoma	II II II I/II III II	[108, 109]
α5β1	ATN 161 (Endostatin)	Attenuon LLC	Advanced renal cancer Malignant glioma	II I/II	[89]
αvβ3	Resveratrol	N/A	Colon cancer Prev. cardiovascular diseases Alzheimer's disease Inflammations CRC hepatic metastasis Multiple myeloma	I II II III I II	[64]
α5β1	JSM6427	Jerini	Age-related macular degeneration	I	[65, 86]
αvβ3	S137 S247	N/A	Brest and hepatic metastasis	N/A	[102, 103]
αvβ3	SB265123	SmithKline Beecham	Osteoporosis	N/A	[104]

Table 3 | Integrin antagonists
Monoclonal antibodies: Bevacizumab (Avastin), MEDI-522 (Vitaxin,Abegrin), M200 (Volociximab), CNTO 95 (intetumumab), Chimeric 7E3 Fab (Abciximab).
Peptides: EMD 121974 (Cilengitide), ATN 161 (Endostatin).
Small molecules: Resveratrol, JSM6427, S137 – S247, SB255123

1.5 Integrin as target for cancer imaging

With the rise of anti-angiogenic therapies there is a great interest in noninvasive techniques to visualize angiogenesis in growing tumors. In the last decades several anti-angiogenic RGD peptides have been developed for integrin targeted radiotracers.[110] There are several advantages in using RGD peptides and among them the two principal one are: firstly RGD is a natural binding unit that interacts with integrin receptors; secondly small RGD peptides tolerate chemical modifications and harsh conditions for radiochemistry and they have the adequate T/B (tumor/blood) ratio to be used as radiotracers.[111]

Radiolabeled linear peptides containing mono or double RGD-sequence, such as ^{18}F-labeled KPQVT**RGD**VFTEG-NH2[112] and ^{99m}Tc-labeled **RGD**SC**RGD**SY,[113] have been evaluated as radioligands for PET and SPECT respectively. *In vitro* and *in vivo* studies showed high affinity and good selectivity for integrin $\alpha_v\beta_3$ with receptor-specific tumor and metastasis uptake. However, high activity in liver and kidneys is observed 10 min post injection due to the rapid degradation by serum proteases and fast elimination.[112, 113]

In order to avoid the side accumulations and improve the pharmacokinetic profile, several modifications were proposed directly on the peptide or on the linker. Evidence suggests that changing from a linear structure to a cyclic one increases selectivity, improves binding affinity and the metabolic stability. Such an effect is due to the fact that a rigid scaffold adopts only one conformation, which is the correct one to have specific interaction with the receptor.[114] Structure-activity relationship (SAR) studies of cyclic peptides suggest that the best results of affinity and selectivity are obtained including the RGD sequence in a cyclic pentapeptide, moreover the amino acid in position 4 can increase the binding while the amino acid in position 5 has no influence.[115] Good results were obtained cyclizing RGD with d-Phe and Val in cyclo(Arg-Gly-Asp-D-Phe-Val), also called c(RGDfV). Preclinical studies with ^{125}I-c(RGDfV) showed good binding properties and high affinity for $\alpha_v\beta_3$. Moreover, it demonstrates positive tumor targeting capacity and high stability against enzymatic cleavage. Despite that, the high lipophilicity of the molecule and its metabolism caused high accumulation in liver, bile and intestine decreasing the quality of the image.[116] To increase the hydrophilicity, cyclic peptides were coupled with sugars:

this is the case of Gluco-RGD, obtained coupling c(RGDyK) with glucose or Galacto-RGD (c(RGDfK) coupled with galactose).

^{125}I-gluco-RGD has high affinity for $\alpha_v\beta_3$ *in vitro* and *in vivo* shows good affinity for $\alpha_v\beta_3$-expressing tumors. Because of its hydrophilicity (log $P_{[^{125}I]Gluco\text{-}RGD}$ = -2.45 vs log $P_{c[RGDfV]}$ = -1.2) ,[117, 118] it stays longer than c(RGDfV) in the circulatory system, but this causes accumulation in muscles, myocardium and lungs. In melanoma and osteosarcoma models, the uptake remains constant 1h and 3h post injection.[119]

The selectivity of ^{18}F-galacto-RGD for $\alpha_v\beta_3$ was demonstrated by blocking experiments, injecting c(RGDfV) 10 min prior tracer injection. In clinical studies, the tracer showed a good accumulation in primary tumors while the accumulation in metastases has large intraindividual variations. ^{18}F-galacto-RGD has predominant renal excretion with rapid blood clearance, the accumulation in muscles and other tissues is very low, with an exception for the liver and the bladder.[120]

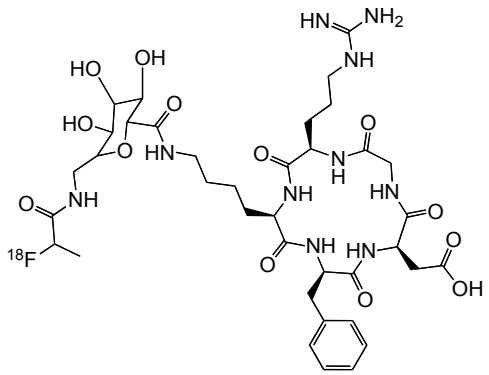

^{18}F-GALACTO-RGD

Figure 7 | Chemical structure of ^{18}Fgalacto-RGD

The idea of multimeric RGD peptides came from the consideration that the integrin may have multivalent binding sites, as it is the case for $\alpha_5\beta_1$ which interacts with both $FnIII_9$ and $FnIII_{10}$ domains.[54] Moreover, after the activation integrins start a process of clustering and in that case the ligand may interact with more than one receptor. Consequently, cyclic RGD dimers and tetramers were developed, in order to improve the tumor targeting efficacy, and thus could be labeled with ^{18}F and ^{64}Cu.[121] Dimers as $E[c(RGDfK)]_2$ and $E[c(RGDyK)]_2$ were labeled with ^{18}F, ^{64}Cu, ^{111}In, ^{90}Y and ^{99m}Tc.

^{18}F-FB-E[c(RGDyK)]$_2$ showed a higher tumor uptake when compared to the ^{18}F-FB-c(RGDyK). The dimer peptide has renal elimination, whereas the monomeric analog has higher hydrophobicity and it is eliminated by bile. *In vivo* studies showed side accumulation 1h post injection but that did not affect the quality of the image which was very high.[122] As a matter of fact, ^{18}F-FB-E[c(RGDyK)]$_2$ is a promising candidate for translation to the clinic.

^{64}Cu-DOTA-E[c(RGDyK)]$_2$ and ^{64}Cu-DOTA-E[c(RGDfK)]$_2$ have been investigated for breast cancer in preclinical studies. ^{64}Cu-DOTA-E[c(RGDyK)]$_2$ showed a slightly higher initial activity concentration and slightly better tumor targeting and visualization than ^{64}Cu-DOTA-E[c(RGDfK)]$_2$. The biodistribution was similar for both of them, with a low side accumulation in blood and liver, but a significant accumulation in kidneys. Compare to the monomers, the two dimers had almost double tumor uptake.[123]

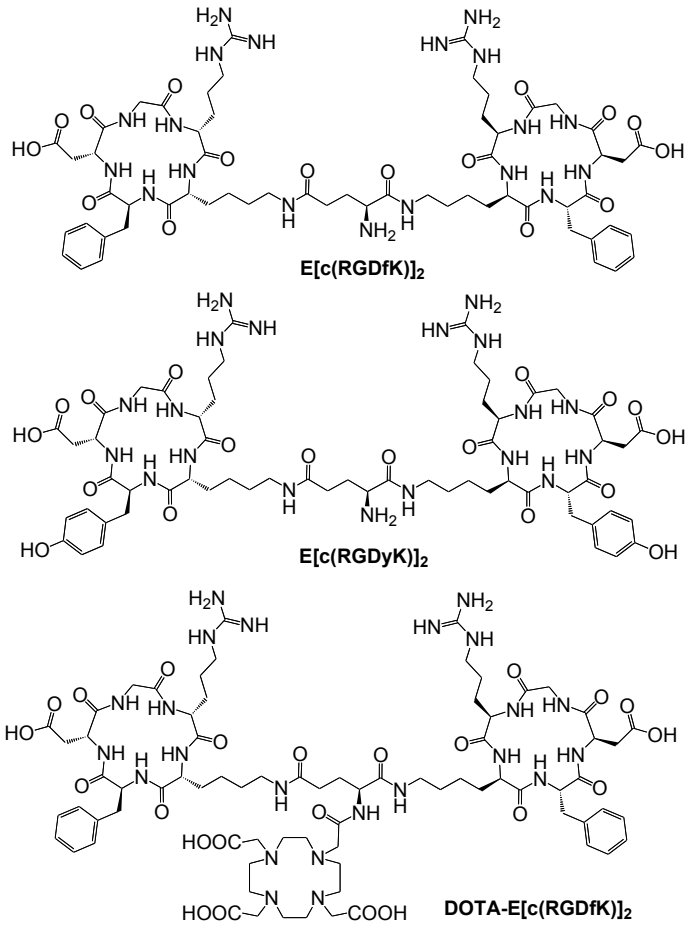

Figure 8 | structure of E[c(RGDfK)]$_2$, E[c(RGDyK)]$_2$ and DOTA-E[c(RGDfK)]$_2$

Galacto dimers, such as ^{18}F-FP-SRGD2 and ^{18}F-FP-PRGD2, were evaluated in U87-MG tumor-bearing nude mice. They had high tumor uptake, the initial kidney accumulation was consistent, very low accumulation was observed on liver and intestine and biodistribution data showed a background accumulation levels in other organs.[124]

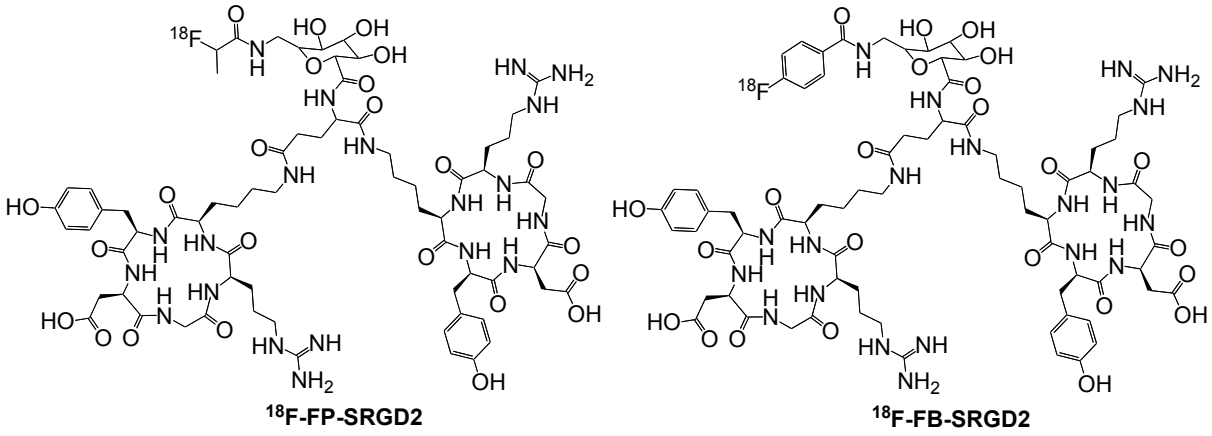

Figure 9 | structure of ^{18}F-FP-SRGD2 and ^{18}F-FP-PRGD2

The results obtained with dimers encouraged several research groups in studying tetramers. Evaluation on CHO3a (Chinese hamster ovary) cells showed an enhanced binding affinity for $\alpha_v\beta_3$ compared to the correspondent monomer and dimer peptides. ^{64}Cu-DOTA-E{E[c(RGDfK)]$_2$}$_2$ was also evaluated as radiotracer for human glioma. It showed a high tumor uptake with rapid blood clearance at 30 min post injection and long tumor retention time that starts to decrease 2h post injection. Kidneys uptake of tetramers was higher than the dimer but the accumulation in liver was considerably lower.[125]

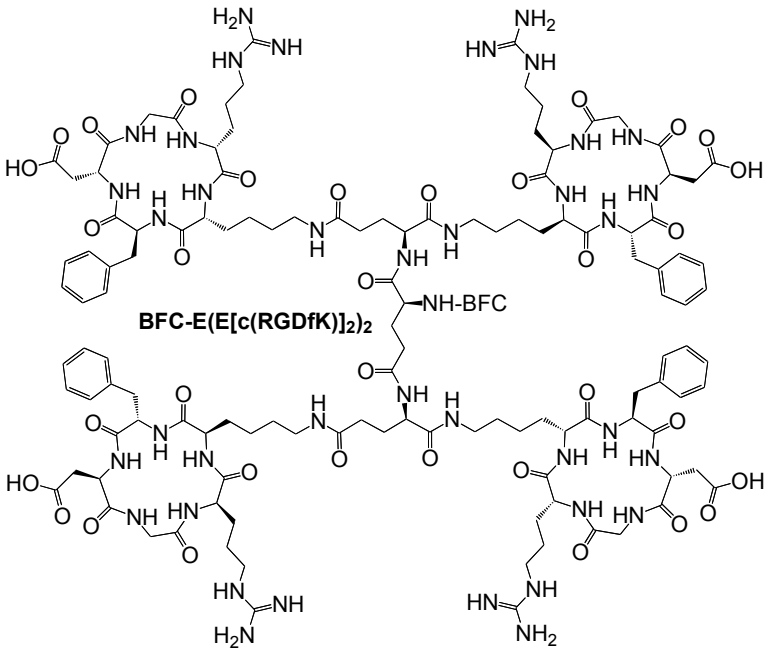

Figure 10 | structure of E[c(RGDfK)]$_2$

PEGylated dimers and tetramers were also developed, using PEG as linker. [^{18}F]PEG-E[c(RGDyK)]$_2$ and [^{18}F]PEG-E{E[c(RGDyK)]$_2$}$_2$ were both tested in mouse model using U87-MG cell line, with absolute tumor uptake. As well as in non PEGylated peptides, the uptake is higher for tetramer than dimer.[116] Clinical tests on healthy volunteers were performed with PEG3-E[c(RGDyk)]$_2$ or ^{18}F-FPPRGD2, and no adverse symptoms were registered. The tracers were mainly distributed in bladder, kidneys, liver, spleen and bowel; this suggests elimination by bile and kidneys. The plasma clearance curve showed a constant blood level of tracer after 30 min, in fact 25% of the tracer remained in circulation after 30 min, 20% after 60 min and only 10% at 90 min.[126]

In vivo assays to compare ^{64}Cu-labeled DOTA-PEG-E[c(RGDyK)]$_2$ with ^{64}Cu-DOTA-E[c(RGDyK)]$_2$ suggest that the two tracers have the same activity, but 4h after injection the accumulation in liver, muscles and kidneys was significantly lower for the PEGylated derivative, which was also excreted faster than ^{64}Cu-DOTA-E[c(RGDyK)]$_2$. In lung cancer, the images obtained with ^{64}Cu-DOTA-PEG-E[c(RGDyK)]$_2$ were superior than those with ^{18}F-FDG.[127]

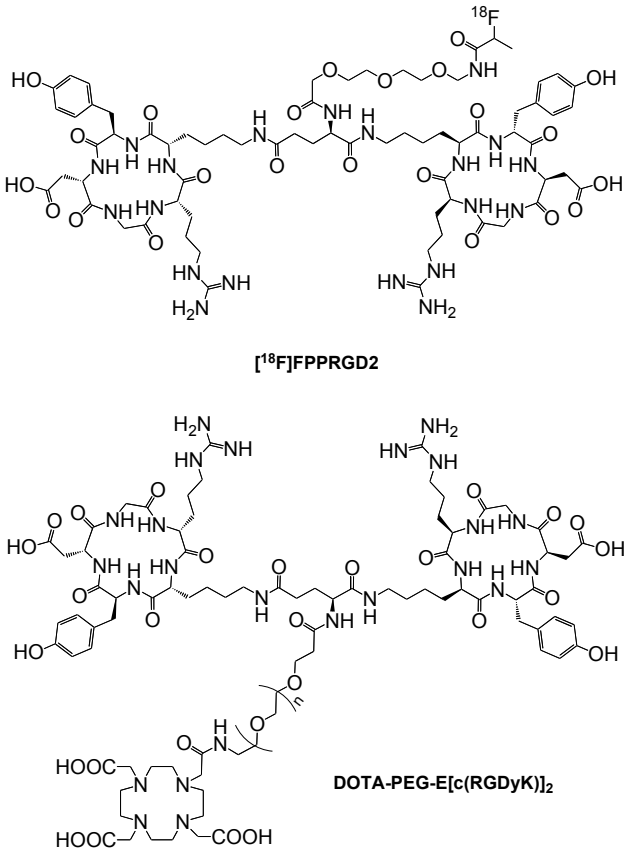

Figure 11 | Structure of ^{18}F-FPPRGD2 and DOTA-PEG-E[c(RGDyK)]$_2$

As well as the other molecules, PEGylated tracers were modified to implement the radiotracer characteristics. As a matter of fact, heterodimers and galacto-PEGylated dimers were evaluated *in vitro* and *in vivo*.

Glu-RGD-BBN, is an heterodimeric peptide with c(RGDyK) connected with Aca-BBN (aminocaproic acid-bombesin(7-14)) through a glutamate linker. ^{18}F-FB-PEG3-Glu-RGD-BBN was evaluated in the PC-3 tumor model and microPET imaging shows a good tumor uptake with high contrast to background accumulation (acquisition 30, 60 and 120 min). It is eliminated by kidneys where there is high activity accumulation. The clearance is rapid and the tumor/non tumor ratio increases with the time.[128]

Evaluation of the potential interference with activity of the galacto-PEG spacer were performed *in vitro* and showed a negligible effect on receptor binding. In vivo evaluation of galacto-PEGylated dimers, such as^{18}F-FP-PEG3-SRGD2, showed predominant kidneys elimination. The tumor uptake was higher than for ^{18}F-galacto-RGD.[124]

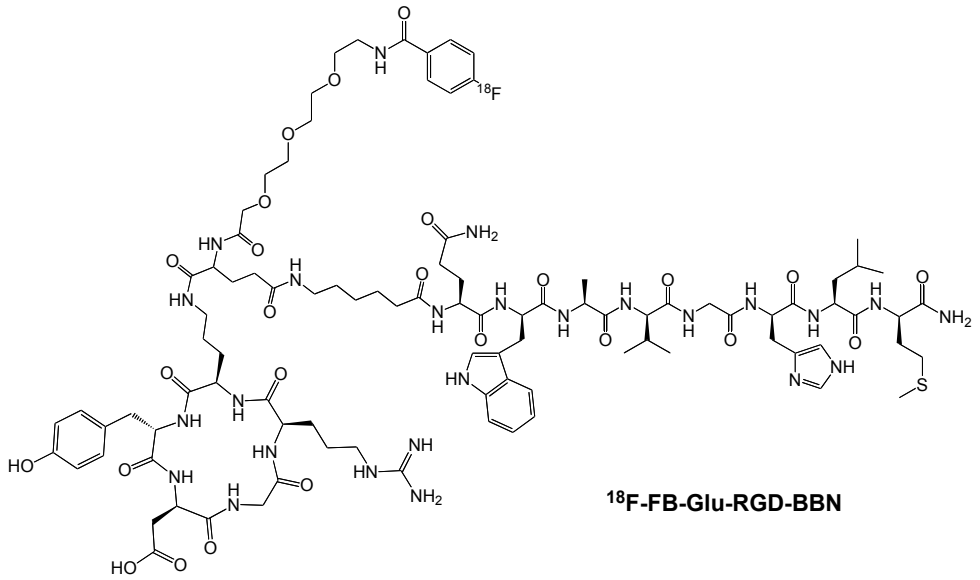

Figure 12| structure of ^{18}F-FB-Glu-RGD-BBN

1.6 Radiolabeling strategies

The development of appropriate synthetic methods is one of the biggest challenges in radiochemistry. Nevertheless, several synthetic strategies and technologies such as microwaves, microfluidic, ultrasound and solid phase extraction are investigated to improve the reproducibility and the efficiency of radiolabeling synthesis.

One of the most used radionuclide in PET is ^{18}F, and there are two main synthetic strategies to introduce it into molecules: direct fluorination or conjugation with a prosthetic group.

The direct fluorination is a single step reaction: the molecules are fluorinated with a ^{18}F-fluoride by electrophilic or nucleophilic substitution. The ^{18}F-fluoride for the electrophilic substitution is obtained from [^{18}F]F_2-gas which is highly reactive. The ^{18}F-fluorination is unspecific and the presence of a second ^{19}F-fluoride limited the substitution with the radioactive isotope to 50% (theoretical max yield). To decrease the reactivity of the fluoride and increase the selectivity of the ^{18}F-fluorination, the transfer of [^{18}F]F_2 on carriers such as acetyl hypofluorite ([^{18}F]CH_3COOF) or xenon difluoride ([^{18}F]XeF_2) is sometimes used.[129]

The [^{18}F]-fluoride for the nucleophilic substitution is generated from [^{18}O]-enriched water and it is used for the reaction without addition of carrier. The [^{18}F]-fluorine is obtained as a negative ion in K_2CO_3 aqueous solution, and its nucleophilicity is

increased by the presence of Kriptofix K_{222}.[130] At the moment, the radiopharmaceuticals are produced by non-carrier-added [^{18}F]-fluoride since it is the only synthetic strategy that allows obtaining high radiochemical molar yield. This reaction generally requires polar organic solvents, strong bases and high temperature.[131] Such harsh conditions limit its application to a restricted number of compounds and it is not applicable to large molecules such as oligonucleotides[132] and limited application to peptides.[133]

The majority of the peptides are indirectly labeled with a ^{18}F-containing prosthetic group. It is a small molecule which is first ^{18}F-labeled and then conjugated with a second molecule such as peptides, oligonucleotides, proteins or mAb under mild reaction conditions. The most common reactions adopted for the coupling to the large molecules are ^{18}F-fluoroalkylation, ^{18}F-fluoroamidation or ^{18}F-fluoroacylation since the reactions are carried out under aqueous conditions.[122, 134, 135]

Several prosthetic groups, especially molecules with the ^{18}F-fluoride in a stable aromatic position, have been investigated for peptide labeling (**figure 13)**, such as ^{18}F-fluorobenzaldhyeide ([^{18}F]-FBA), ^{18}F-fluoropropionic acid ([^{18}F]-FPA), ^{18}F-fluoropyriddinyloxypropylmaleimide ([^{18}F]-FPyME).

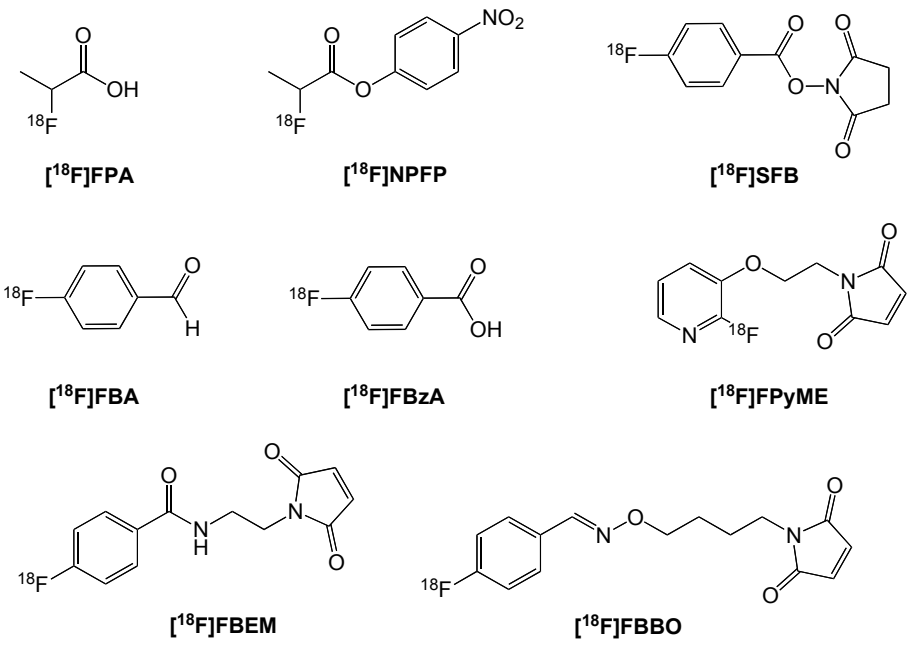

Figure 13 | Prosthetic groups for ^{18}F-labeling peptides (adapted K. Chen, P.S. Conti[132])
FPA = fluoropropionic acid; NPFP = nitrophenyl fluoropropanoate; SFB = succinimidyl fluorobenzoate; FBA = fluorobenzaldehyde; FBzA = florobenzoic acid; FPyME = fluoropyridinyloxypropylmaleimide; FBEM = fluorobenzamido-ethylmaleimide and FBBO = fluorobenzaldehyde-butylmaleimide oxime.

Unfortunately, some of them are not amenable to direct fluorination with no-carried-added ^{18}F-fluoride and the synthesis of the ^{18}F-prosthetic group requires an elaborated multi step procedure (**table 4**).[136] Moreover, the coupling between the prosthetic group and the peptide often involves amine or carboxyl groups with scarce selectivity.[136] One of the options adopted to improve the chemoselectivity is the conjugation of the prosthetic group with thiol groups, which are less copious than amines and carboxyl groups. However, this strategy is not always applicable.[137]

Reaction with Peptides	^{18}F-Prosthetic Group	Steps	Time (min)	Radiochemical Yield %	Referene
Alkylation	4-[^{18}F]fluorophenacylbromide	3	75	28-40	[138]
Alkylation	N-(p-[^{18}F]fluorophenyl)maleimide	4	100	15	[139]
Amidation	1-[4-(-[^{18}F]fluoromethyl)benzoyl]-aminobutane-4-amine	2	80	52	[140]
Acylation	2-[^{18}F]fluoroacetic acid	2	80	50	[141]
Acylation	N-Succinimidyl-8-[(4'[^{18}F]fluoro-benzyl)-amino]suberate	3	55-60	25-40	[142]
Acylation	N-Succinimidyl-[^{18}F]fluorobenzoate	3	100	25	[143]
Acylation	4-Nitrophenyl2--[^{18}F]fluoroprprionate	3	90	60	[144]

Table 4| Synthetic strategies for ^{18}F-labeled prosthetic groups (adapted from H.J. Wester et al.[136])

The need to reduce the time of reaction and to increase the chemoselectivity has induced the application of new radiosynthetic strategies with simple ^{18}F-labeled procedures for the application on macromolecules.[145]

One of the synthetic approaches adopted is the "click chemistry". The principle of this approach is to have quick, powerful, selective and highly reliable reaction, by the combination of small entities. Indeed, the criteria of the click chemistry are to have reactions with high yields, mild reaction conditions, selective with the formation of a single product, simple product isolation and stereospecific (but not necessarily enantioselective).[146]

The most popular and exploited click chemistry reaction is the Huisgen's 1,3-dipolar cycloaddition, which has been widely adopted in radiochemistry since its Cu(I)-catalysed improvement was published.[145] This reaction occurs between an azide and alkyne moiety and provides a versatile tool for coupling drug-like fragments in

high yields and under mild conditions (usually water with a polar solvent such as THF or acetonitrile at room temperature) with a simple work-up and high specificity.[147] Cu(I)-catalysed azide-alkyne 1,3-dipolar cycloaddition reaction (CuAAC) is one of the most used technique for combinatorial libraries in organic chemistry[148] and is getting increasingly common in radiochemistry thanks to its characteristics that fulfill the synthetic requirements for ^{18}F-labeled macromolecules.[149] As a matter of fact, alkynes are relatively inert, and the majority of the organic azides are stable in solution and room temperature. Moreover they can easily be incorporated into a wide range of molecules and the reaction can be completed in a range of time between 5 and 30 minutes under optimized conditions and the purification step of the ^{18}F-prosthetic group is not always required.[150]

The reaction between azide and alkyne moieties results in a triazole, which can be 1,4-disubstituted or 1,5-disubstituted (**figure 14**).[151]

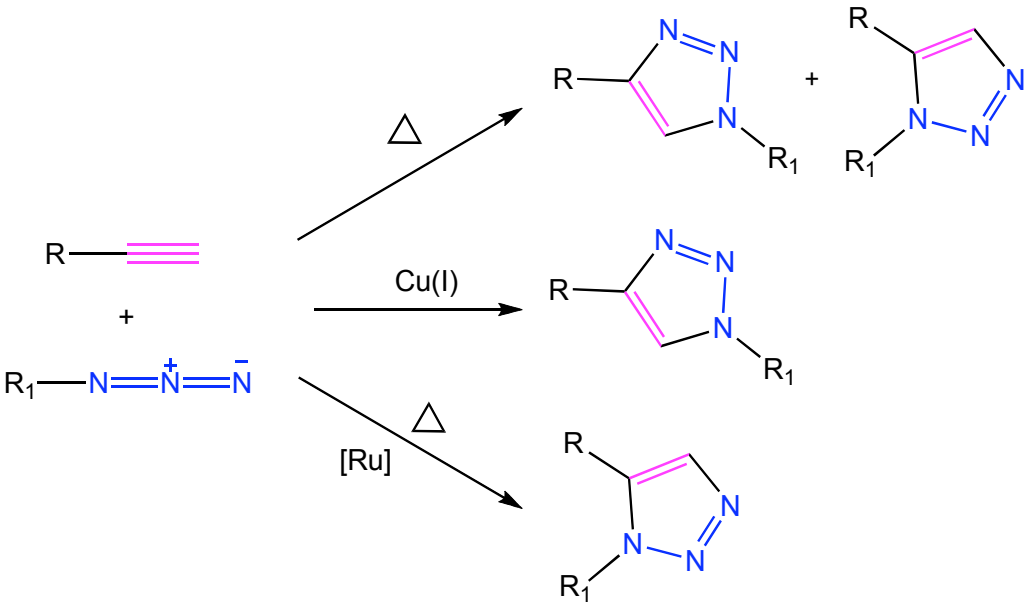

Figure 14 | Condition of reactions for azide-alkyne 1,3-dipolar cycloaddition. (Adapted form Tron et al[151])
The use of high temperature as reaction conditions for azide-alkyne 1,3-dipolar cycloaddition gave as product a mix of 1,4-disubstituted triazole and 1,5-disubstituted triazole. 1,4-disubstituted triazole is obtained using Cu(I or II) as catalyst, and 1,5-disubstituted triazole is obtained warming the reaction in presence of [Ru].

The 1,2,3-triazole formed has polarity and size similar to amide bonds indeed since the introduction of the CuAAC it has been used as peptide bond isostere[152]. Specifically, a 1,4-disubstituted triazole is similar to a *Z*-amide bond, and a 1,5-

disubstituted triazole is similar to an *E*-amide bond, giving two different geometries of the molecule. The formation of 1,4-disubstituted triazole or 1,5-disubstituted triazole depends on the reaction conditions adopted for the cycloaddition as showed in **figure 14**.[151]

The substitution of an amide bond with a 1,4-disubstituted triazole is quite common in medicinal chemistry, as such modification has been introduced in a large number of molecules because of its stability in acidic and basic conditions and resistance to metabolic degradation.[153] Considering all the advantages of the click reaction, several aliphatic, aromatic and sugar prosthetic groups have been developed. The majority of them have a fast ^{18}F-fluorination affording in a ^{18}F-labeled prosthetic group in high yield. Some examples are reported in **table 5**.[150]

18F-prosthetic group	Precursor	Reaction Comditions	Purification	RCY%
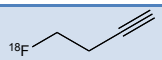	Tosylate	[^{18}F]KF/K_{222}/K_2CO_3 CH_3CN, 100°C, 10–15 min, distillation	distillation	36
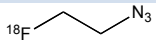	Tosylate	[^{18}F]KF/K_{222}/K_2CO_3 CH_3CN, 80°C, 15 min, distillation	distillation	55
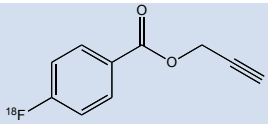	2-trimethylammonium	[^{18}F]KF/K_{222}/K_2CO_3 CH_3CN, 130°C, 15 min		58
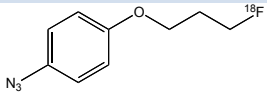	Mesylate	**t**BuNHCO$_3$, **t**BuOH, 100°C, 20 min		95
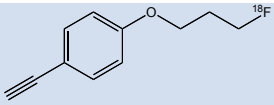	Mesylate	[^{18}F]KF/K_{222}/K_2CO_3 **t**BuNHCO$_3$, **t**BuOH, 100°C, 20 min		94
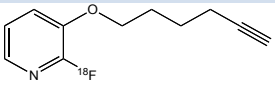	2-Nitro or 2-trimethylammonium	[^{18}F]KF/K_{222}/K_2CO_3 DMSO, 110°C, 15 min,	HPLC tC18-SepPak	42-50
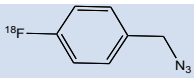	2-trimethylammonium	1) [^{18}F]KF/K_{222}/K_2CO_3 2) $NaBH_4$; 3) HBr; 4) azido resin; 75 min		34
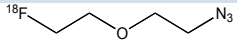	Mesylate	[^{18}F]KF/K_{222}/K_2CO_3 **t**BuNHCO3, **t**BuOH, 100°C, 20 min		92
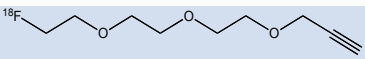	Tosylate	[^{18}F]KF/K_{222}/K_2CO_3 DMSO, 110°C, 30 min	HPLC	84
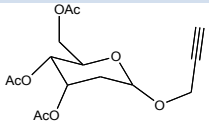	Triflate	[^{18}F]KF/K_{222}/K_2CO_3 KH_2PO_4, CH_3CN, 85°C, 5 min		7

Table 5│**Click chemistry prosthetic groups and reaction conditions** Adapted form Galaser et al[150]

Clickable prosthetic groups have been largely investigated for the ^{18}F-labeling of small molecules and peptides, in the wake of the promising results obtained in preclinical studies for imaging of angiogenesis.

Several linear as well as cyclic peptides have been chemically modified to introduce azido or alkyne functions, in order to make them suitable for click chemistry (**figure 15**).[154, 155] This synthetic approach simplified the protocols and allowed the synthesis of radiolabeled peptides in one-pot procedures.[155]

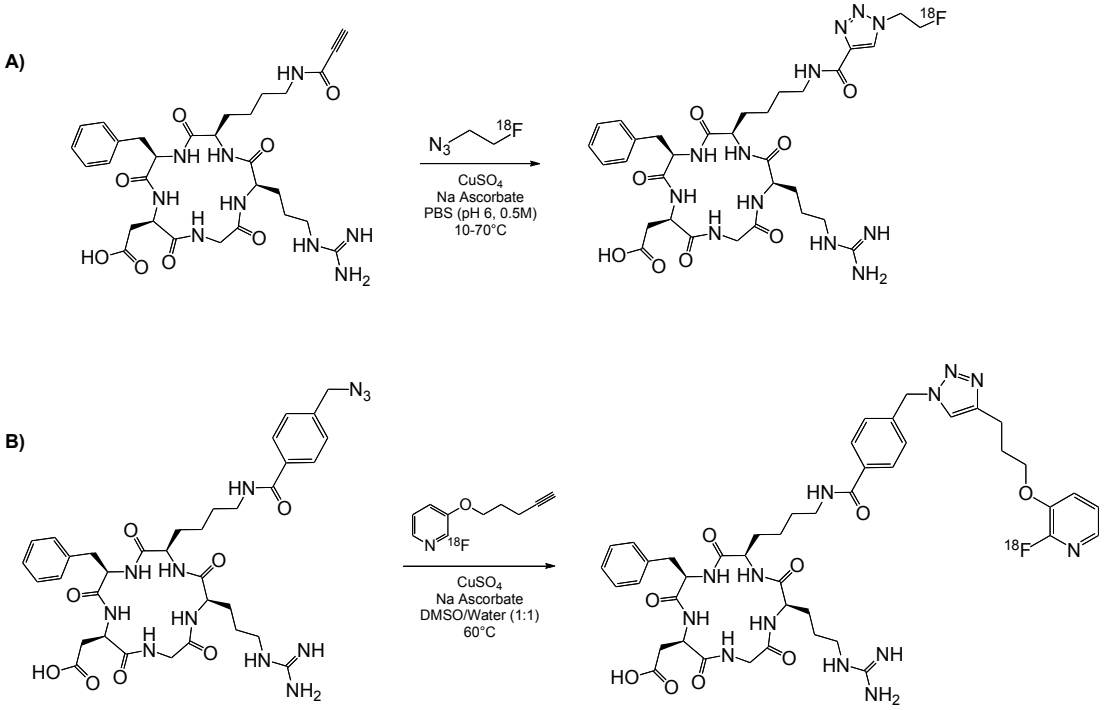

Figure 15 | Click chemistry of RGD peptides

Two examples of click chemistry for ^{18}F-labelled RGD peptides. c(RGDfK)-alkyne (**A**) is coupled with an azide prosthetic group,[149] while c(RGDyK)-azido (**B**) is clicked with an alkyne prosthetic group.[156] The two reactions are Cu(II)-catalyzed.

Nevertheless, some limitations were observed. The two principal disadvantages are the alkyne homocoupling as side reaction, and the instability of some azide derivatives that are highly unstable and explosive in presence of heavy metals and high temperature.[147]

However, the use of click chemistry has largely enhanced the development of radiolabeled peptides, undoubtedly the development of radiolabeled macromolecules will continue to benefit from it.

1.7 References

1. Robert, G. and R. Milne, *Positron emission tomography: establishing priorities for health technology assesment.* Health Technology Assesment 1999. **3**(16).
2. Cherry, S., *Fundamentals of positron emission tomography and applications in preclinical drug development.* The Journal of Clinical Pharmacology, 2001. **41**(5): p. 482-491.
3. Blower, P.J., J.S. Lewis, and J. Zweit, *Copper radionuclides and radiopharmaceuticals in nuclear medicine.* Nuclear Medicine and Biology, 1996. **23**(8): p. 957-980.
4. Zhou, Y. and S. Liu, *64Cu-Labeled Phosphonium Cations as PET Radiotracers for Tumor Imaging.* Bioconjugate Chemistry, 2011. **22**(8): p. 1459-1472.
5. Bailey, D.L., D.W. Townsend, and P.E.M. Valk, eds. *Positron Emission Tomography*. ed. Springler2003.
6. IBA, ed. *Cyclotron Produced Radionuclides: Principe and Practice*. 2008.
7. http://www.crump.ucla.edu.
8. Ridolfi, L., et al., *Unexpected High Response Rate to Traditional Therapy after Dendritic Cell-Based Vaccine in Advanced Melanoma: Update of Clinical Outcome and Subgroup Analysis.* Clinical and Developmental Immunology, 2010. **2010**.
9. Jaini, S. and E. Dadachova, *FDG for Therapy of Metabolically Active Tumors.* Seminars in nuclear medicine, 2012. **42**(3): p. 185-189.
10. Gulyás, B. and H. C., *New PET radiopharmaceuticals beyond FDG for brain tumor imaging.* Minerva Medica 2012. **56**(2): p. 156 - 190.
11. Soloviev, D., et al., *[18F]FLT: An imaging biomarker of tumour proliferation for assessment of tumour response to treatment.* European Journal of Cancer, 2012. **48**(4): p. 416-424.
12. Strong, V., et al., *Portable PET probes are a novel tool for intraoperative localization of tumor deposits.* Annals of Surgical Innovation and Research, 2009. **3**(1): p. 2.

13. Stacy, M., M. MW, and S. AJ., *Targeted molecular imaging of angiogenesis in PET and SPECT: a review.* Yale J. Biol. Med, 2012. **85**(1): p. 75 - 86.
14. Humphries, J.D., A. Byron, and M.J. Humphries, *Integrin ligands at a glance.* Journal of Cell Science, 2006. **119**(19): p. 3901-3903.
15. Loftus, J.C., J.W. Smith, and M.H. Ginsberg, *Integrin-mediated cell adhesion: the extracellular face.* Journal of Biological Chemistry, 1994. **269**(41): p. 25235-8.
16. Xiong, J.-P., et al., *Crystal Structure of the Extracellular Segment of Integrin αVβ3.* Science, 2001. **294**(5541): p. 339-345.
17. Xiong, J.-P., et al., *New insights into the structural basis of integrin activation.* Blood, 2003. **102**(4): p. 1155-1159.
18. Humphries, M.J., *Insights into integrin-ligand binding and activation from the first crystal structure.* Arthritis Res, 2002. **4**(Suppl 3): p. S69 - S78.
19. Gailit, J. and E. Ruoslahti, *Regulation of the fibronectin receptor affinity by divalent cations.* Journal of Biological Chemistry, 1988. **263**(26): p. 12927-12932.
20. Xiong, J.-P., et al., *Crystal Structure of the Extracellular Segment of Integrin αVβ3 in Complex with an Arg-Gly-Asp Ligand.* Science, 2002. **296**(5565): p. 151-155.
21. Takagi, J., et al., *Global Conformational Rearrangements in Integrin Extracellular Domains in Outside-In and Inside-Out Signaling.* Cell, 2002. **110**(5): p. 599-611.
22. Shimaoka, M. and T.A. Springer, *Therapeutic antagonists and conformational regulation of integrin function.* Nat Rev Drug Discov, 2003. **2**(9): p. 703-716.
23. Plow, E.F., et al., *Ligand Binding to Integrins.* Journal of Biological Chemistry, 2000. **275**(29): p. 21785-21788.
24. Niu, G. and C. X., *Why Integrin as a Primary Target for Imaging and Therapy.* Theranostics, 2011. **1**: p. 30-47.
25. Stupack, D.G., *Integrins as a distinct subtype of dependence receptors.* Cell Death Differ, 2005. **12**(8): p. 1021-1030.

26. Wehrle-Haller, B., *Structure and function of focal adhesions.* Current Opinion in Cell Biology, 2012. **24**(1): p. 116-124.
27. Kornberg, L., et al., *Cell adhesion or integrin clustering increases phosphorylation of a focal adhesion-associated tyrosine kinase.* Journal of Biological Chemistry, 1992. **267**(33): p. 23439-42.
28. Aplin, A.E., et al., *Integrin-Mediated Adhesion Regulates ERK Nuclear Translocation and Phosphorylation of Elk-1.* The Journal of Cell Biology, 2001. **153**(2): p. 273-282.
29. Stupack, D.G. and D.A. Cheresh, *Apoptotic cues from the extracellular matrix: regulators of angiogenesis.* Oncogene, 2003. **22**(56): p. 9022-9029.
30. Stupack, D.G., et al., *Apoptosis of adherent cells by recruitment of caspase-8 to unligated integrins.* The Journal of Cell Biology, 2001. **155**(3): p. 459-470.
31. Luscinskas, F.W. and J. Lawler, *Integrins as dynamic regulators of vascular function.* The FASEB Journal, 1994. **8**(12): p. 929-38.
32. Soldi, R., et al., *Role of [alpha]v[beta]3 integrin in the activation of vascular endothelial growth factor receptor-2.* EMBO J, 1999. **18**(4): p. 882-892.
33. Keshet, E. and S.A. Ben-Sasson, *Anticancer drug targets: approaching angiogenesis.* The Journal of Clinical Investigation, 1999. **104**(11): p. 1497-1501.
34. Taverna, D. and R.O. Hynes, *Reduced Blood Vessel Formation and Tumor Growth in β5-Integrin-negative Teratocarcinomas and Embryoid Bodies.* Cancer Research, 2001. **61**(13): p. 5255-5261.
35. Dickson, S.E., R. Bicknell, and H.M. Fraser, *Mid-luteal angiogenesis and function in the primate is dependent on vascular endothelial growth factor.* Journal of Endocrinology, 2001. **168**(3): p. 409-416.
36. Carmeliet, P., *Angiogenesis in life, disease and medicine.* Nature, 2005. **438**(7070): p. 932-936.
37. Albelda, S.M. and C.A. Buck, *Integrins and other cell adhesion molecules.* The FASEB Journal, 1990. **4**(11): p. 2868-80.

38. Kim, S., et al., *Regulation of Angiogenesis in Vivo by Ligation of Integrin α5β1 with the Central Cell-Binding Domain of Fibronectin.* The American Journal of Pathology, 2000. **156**(4): p. 1345-1362.
39. Brooks, P.C., R.A. Clark, and D.A. Cheresh, *Requirement of vascular integrin alpha v beta 3 for angiogenesis.* Science, 1994. **264**(5158): p. 569-571.
40. Eliceri, B.P. and D.A. Cheresh, *The role of alphav integrins during angiogenesis.* Mol. Med., 1998. **4**(12): p. 741-750.
41. Desgrosellier, J.S. and D.A. Cheresh, *Integrins in cancer: biological implications and therapeutic opportunities.* Nat Rev Cancer, 2010. **10**(1): p. 9-22.
42. Malyankar, U.M., et al., *Osteoprotegerin Is an αvβ3-induced, NF-kB-dependent Survival Factor for Endothelial Cells.* Journal of Biological Chemistry, 2000. **275**(28): p. 20959-20962.
43. Hodivala-Dilke, K.M., et al., *β3-integrin–deficient mice are a model for Glanzmann thrombasthenia showing placental defects and reduced survival.* The Journal of Clinical Investigation, 1999. **103**(2): p. 229-238.
44. Reynolds, L.E., et al., *Enhanced pathological angiogenesis in mice lacking [beta]3 integrin or [beta]3 and [beta]5 integrins.* Nat Med, 2002. **8**(1): p. 27-34.
45. Mahabeleshwar, G.H., et al., *Integrin signaling is critical for pathological angiogenesis.* The Journal of Experimental Medicine, 2006. **203**(11): p. 2495-2507.
46. Strömblad, S., et al., *Suppression of p53 activity and p21WAF1/CIP1 expression by vascular cell integrin alphaVbeta3 during angiogenesis.* The Journal of Clinical Investigation, 1996. **98**(2): p. 426-433.
47. Gaertner, F.C., et al., *Radiolabelled RGD peptides for imaging and therapy.* European Journal of Nuclear Medicine and Molecular Imaging, 2012. **39**(1): p. 126-138.
48. Mahabeleshwar, G.H., et al., *Mechanisms of Integrin-Vascular Endothelial Growth Factor Receptor Cross-Activation in Angiogenesis.* Circulation Research, 2007. **101**(6): p. 570-580.

49. Robinson, S.D. and K.M. Hodivala-Dilke, *The role of β3-integrins in tumor angiogenesis: context is everything.* Current Opinion in Cell Biology, 2011. **23**(5): p. 630-637.
50. Serini, G., et al., *Besides adhesion: new perspectives of integrin functions in angiogenesis.* Cardiovascular Research, 2008. **78**(2): p. 213-222.
51. Somanath, P., N. Malinin, and T. Byzova, *Cooperation between integrin α_vβ₃ and VEGFR2 in angiogenesis.* Angiogenesis, 2009. **12**(2): p. 177-185.
52. Avraamides, C.J., B. Garmy-Susini, and J.A. Varner, *Integrins in angiogenesis and lymphangiogenesis.* Nat Rev Cancer, 2008. **8**(8): p. 604-617.
53. Yang, J.T., H. Rayburn, and R.O. Hynes, *Embryonic mesodermal defects in alpha 5 integrin-deficient mice.* Development, 1993. **119**(4): p. 1093-1105.
54. Altroff, H., et al., *The Eight FIII Domain of Human Fibronectin Promotes Integrin α5β1 Binding via Stabilization of the Ninth FIII Domain.* J. Biol. Chem., 2001. **276**(42): p. 38885-38892.
55. García, A.J., J.E. Schwarzbauer, and D. Boettiger, *Distinct Activation States of α5β1 Integrin Show Differential Binding to RGD and Synergy Domains of Fibronectin†.* Biochemistry, 2002. **41**(29): p. 9063-9069.
56. Khan, Z., et al., *EDB fibronectin and angiogenesis – a novel mechanistic pathway.* Angiogenesis, 2005. **8**(3): p. 183-196.
57. Veevers-Lowe, J., et al., *Mesenchymal stem cell migration is regulated by fibronectin through α5β1-integrin-mediated activation of PDGFR-β and potentiation of growth factor signals.* Journal of Cell Science, 2011. **124**(8): p. 1288-1300.
58. Li, L., et al., *An angiogenic role for the α5β1 integrin in promoting endothelial cell proliferation during cerebral hypoxia.* Experimental Neurology, 2012. **237**(1): p. 46-54.
59. Kahle, M.P., et al., *Perlecan domain V is upregulated in human brain arteriovenous malformation and could mediate the vascular endothelial growth factor effect in lesional tissue.* NeuroReport, 2012. **23**(10): p. 627-630 10.1097/WNR.0b013e3283554c5c.

60. Lee, B., et al., *Perlecan domain V is neuroprotective and proangiogenic following ischemic stroke in rodents.* The Journal of Clinical Investigation, 2011. **121**(8): p. 3005-3023.
61. Janouskova, H., et al., *Integrin α5β1 Plays a Critical Role in Resistance to Temozolomide by Interfering with the p53 Pathway in High-Grade Glioma.* Cancer Research, 2012. **72**(14): p. 3463-3470.
62. Barkan, D. and A.F. Chambers, *β1-Integrin: A Potential Therapeutic Target in the Battle against Cancer Recurrence.* Clinical Cancer Research, 2011. **17**(23): p. 7219-7223.
63. Kim, S., M. Harris, and J.A. Varner, *Regulation of Integrin αvβ3-mediated Endothelial Cell Migration and Angiogenesis by Integrin Î±5Î²1 and Protein Kinase A.* Journal of Biological Chemistry, 2000. **275**(43): p. 33920-33928.
64. Huveneers, S., H. Truong, and E.H.J. Danen, *Integrins: Signaling, disease, and therapy.* International Journal of Radiation Biology, 2007. **83**(11-12): p. 743-751.
65. Cox, D., M. Brennan, and N. Moran, *Integrins as therapeutic targets: lessons and opportunities.* Nat Rev Drug Discov, 2008. **9**(10): p. 804-820.
66. Brooks, P.C., et al., *Antiintegrin alpha v beta 3 blocks human breast cancer growth and angiogenesis in human skin.* The Journal of Clinical Investigation, 1995. **96**(4): p. 1815-1822.
67. Tae Jin Kim, et al., *Combined anti-angiogenic therapy against VEGF and integrin aVb3 in an orthotopic model of ovarian cancer.* Cancer Biology & Therapy, 2009. **8**(23): p. 2261-2270.
68. clinicaltrialsfeeds.org/clinical-trials/results/term=Avastin.
69. Rosen, L.S., *Clinical Experience With Angiogenesis Signaling Inhibitors: Focus on Vascular Endothelial Growth Factor (VEGF) Blockers.* Cancer control, 2002. **9**(2): p. 36-44.
70. Gordon, C.R., et al., *A Review on Bevacizumab and Surgical Wound Healing: An Important Warning to All Surgeons.* Annals of Plastic Surgery, 2009. **62**(6): p. 707-9.

71. Gutheil, J.C., et al., *Targeted Antiangiogenic Therapy for Cancer Using Vitaxin: A Humanized Monoclonal Antibody to the Integrin αvβ3.* Clinical Cancer Research, 2000. **6**(8): p. 3056-3061.
72. Mulgrew K, et al., *Direct targeting of alphavbeta3 integrin on tumor cells with a monoclonal antibody, Abegrin.* Mol Cancer Ther, 2006. **5**(12): p. 3122-9.
73. McNeel, D.G., et al., *Phase I Trial of a Monoclonal Antibody Specific for αvβ3 Integrin (MEDI-522) in Patients with Advanced Malignancies, Including an Assessment of Effect on Tumor Perfusion.* Clinical Cancer Research, 2005. **11**(21): p. 7851-7860.
74. Moschos, S.J., et al., *Pharmacodynamic (Phase 0) Study Using Etaracizumab in Advanced Melanoma.* Journal of Immunotherapy, 2010. **33**(3): p. 316-325 10.1097/CJI.0b013e3181c1f216.
75. Hersey, P., et al., *A randomized phase 2 study of etaracizumab, a monoclonal antibody against integrin αvβ3, ± dacarbazine in patients with stage IV metastatic melanoma.* Cancer, 2010. **116**(6): p. 1526-1534.
76. clinicaltrialsfeeds.org/clinical-trials/results/term=Vitaxin.
77. clinicaltrialsfeeds.org/clinical-trials/results/term=CNTO95.
78. Ning, S., et al., *Anti–αv Integrin Monoclonal Antibody Intetumumab Enhances the Efficacy of Radiation Therapy and Reduces Metastasis of Human Cancer Xenografts in Nude Rats.* Cancer Research, 2010. **70**(19): p. 7591-7599.
79. Almokadem, S. and C.P. Belani, *Volociximab in cancer.* Expert Opinion on Biological Therapy, 2012. **12**(2): p. 251-257.
80. clinicaltrialsfeeds.org/clinical-trials/results/term=volociximab.
81. Angiolillo, D.J., *The Evolution of Antiplatelet Therapy in the Treatment of Acute Coronary Syndromes: From Aspirin to the Present Day.* Drugs, 2012. **72**(16): p. 2087-2116 10.2165/11640880-000000000-00000.
82. Diener, H.C., et al., *Secondary prevention in the acute and early chronic phase after ischaemic stroke and transient ischaemic attacks with antiplatelet drugs – is antiplatelet monotherapy still reasonable?* International Journal of Clinical Practice, 2011. **65**(5): p. 531-535.

83. Brener, S.J., et al., *Abciximab-facilitated percutaneous coronary intervention and long-term survival—a prospective single-center registry.* European Heart Journal, 2003. **24**(7): p. 630-638.
84. Alghisi, G.C., L. Ponsonnet, and C. Rüegg, *The Integrin Antagonist Cilengitide Activates αVβ3, Disrupts VE-Cadherin Localization at Cell Junctions and Enhances Permeability in Endothelial Cells.* PLoS ONE, 2009. **4**(2): p. e4449.
85. Mas-Moruno C., Florian Rechenmacher, and H. Kessler*, *Cilengitide: The First Anti-Angiogenic Small Molecule Drug Candidate. Design, Synthesis and Clinical Evaluation.* Anticancer Agents Med. Chem., 2010. **10**(10): p. 753-768.
86. clinicaltrialsfeeds.org/clinical-trials/results/term=cilengitide.
87. Livant, D.L., et al., *Anti-invasive, Antitumorigenic, and Antimetastatic Activities of the PHSCN Sequence in Prostate Carcinoma.* Cancer Research, 2000. **60**(2): p. 309-320.
88. Khalili, P., et al., *A non–RGD-based integrin binding peptide (ATN-161) blocks breast cancer growth and metastasis in vivo.* Molecular Cancer Therapeutics, 2006. **5**(9): p. 2271-2280.
89. Cianfrocca, M.E., et al., *Phase 1 trial of the antiangiogenic peptide ATN-161 (Ac-PHSCN-NH2), a beta integrin antagonist, in patients with solid tumours.* Br J Cancer, 2006. **94**(11): p. 1621-1626.
90. clinicaltrialsfeeds.org/clinical-trials/results/term=ATN161.
91. Pirola, L. and S. Fröjdö, *Resveratrol: One molecule, many targets.* IUBMB Life, 2008. **60**(5): p. 323-332.
92. Lin, H.-Y., et al., *Integrin αVβ3 contains a receptor site for resveratrol.* The FASEB Journal, 2006. **20**(10): p. 1742-1744.
93. Lin, H.-Y., et al., *Resveratrol and apoptosis.* Annals of the New York Academy of Sciences, 2011. **1215**(1): p. 79-88.
94. clinicaltrialsfeeds.org/clinical-trials/results/term=resveratrol.
95. Stragies, R., et al., *Design and Synthesis of a New Class of Selective Integrin α5β1 Antagonists.* Journal of Medicinal Chemistry, 2007. **50**(16): p. 3786-3794.

96. Maier, A.-K.B., et al., *Modulation of Hypoxia-Induced Neovascularization by JSM6427, an Integrin α5β 1 Inhibiting Molecule.* Current Eye Research, 2007. **32**(9): p. 801-812.
97. Färber, K., et al., *An α5β1 integrin inhibitor attenuates glioma growth.* Molecular and Cellular Neuroscience, 2008. **39**(4): p. 579-585.
98. Li, R., et al., *Integrin α5β1 Mediates Attachment, Migration, and Proliferation in Human Retinal Pigment Epithelium: Relevance for Proliferative Retinal Disease.* Investigative Ophthalmology & Visual Science, 2009. **50**(12): p. 5988-5996.
99. clinicaltrialsfeeds.org/clinical-trials/results/term=JSM6427.
100. Shannon, K., et al., *Anti-metastatic properties of RGD-peptidomimetic agents S137 and S247.* Clin Exp Metastasis, 2004. **21**: p. 129 - 138.
101. Kaspar, M., L. Zardi, and D. Neri, *Fibronectin as target for tumor therapy.* International Journal of Cancer, 2006. **118**(6): p. 1331-1339.
102. Sloan, E., et al., *Tumor-specific expression of alphavbeta3 integrin promotes spontaneous metastasis of breast cancer to bone.* Breast Cancer Research, 2006. **8**(2): p. R20.
103. Reinmuth, et al., *αVβ3 Integrin antagonist S247 decreases colon cancer metastasis and angiogenesis and improves survival in mice.* 2003. **63**(9): p. 9.
104. Lark, M.W., et al., *Design and Characterization of Orally Active Arg-Gly-Asp Peptidomimetic Vitronectin Receptor Antagonist SB 265123 for Prevention of Bone Loss in Osteoporosis.* Journal of Pharmacology and Experimental Therapeutics, 1999. **291**(2): p. 612-617.
105. Sun, W., *Angiogenesis in metastatic colorectal cancer and the benefits of targeted therapy.* Journal of Hematology & Oncology, 2012. **5**(1): p. 63.
106. Trikha, M., et al., *CNTO 95, a fully human monoclonal antibody that inhibits αv integrins, has antitumor and antiangiogenic activity in vivo.* International Journal of Cancer, 2004. **110**(3): p. 326-335.
107. Mullamitha, S.A., et al., *Phase I Evaluation of a Fully Human Anti–αv Integrin Monoclonal Antibody (CNTO 95) in Patients with Advanced Solid Tumors.* Clinical Cancer Research, 2007. **13**(7): p. 2128-2135.

108. Nabors, L.B., et al., *Phase I and Correlative Biology Study of Cilengitide in Patients With Recurrent Malignant Glioma.* Journal of Clinical Oncology, 2007. **25**(13): p. 1651-1657.
109. Bradley, D.A. and e. al, *EMD121974 (NSC 707544, cilengitide) in asymptomatic metastatic androgen independent prostate cancer (AIPCa) patients (pts): A randomized trial by the Prostate Cancer Clinical Trials Consortium (NCI 6372).* J. Clin. Oncol. 2007 ASCO Annu. Meeting Proc., 2007. **25**: p. 5137.
110. Dijkgraaf, I. and O.C. Boerman, *Radionuclide Imaging of Tumor Angiogenesis.* Cancer Biotherapy & Radiopharmaceuticals, 2009. **24**(6): p. 637 - 647.
111. Liu, S., *Radiolabeled Multimeric Cyclic RGD Peptides as Integrin αvβ3 Targeted Radiotracers for Tumor Imaging.* Molecular Pharmaceutics, 2006. **3**(5): p. 472-487.
112. Sutcliffe-Goulden, J., et al., *Rapid solid phase synthesis and biodistribution of 18F-labelled linear peptides.* European Journal of Nuclear Medicine and Molecular Imaging, 2002. **29**(6): p. 754-759.
113. Sivolapenko, G.B., et al., *Imaging of metastatic melanoma utilising a technetium-99m labelled RGD-containing synthetic peptide.* European Journal of Nuclear Medicine, 1998. **25**(10): p. 1383-1389.
114. Gottschalk, K.-E. and H. Kessler, *The Structures of Integrins and Integrin–Ligand Complexes: Implications for Drug Design and Signal Transduction.* Angewandte Chemie International Edition, 2002. **41**(20): p. 3767-3774.
115. Haubner, R., et al., *Structural and Functional Aspects of RGD-Containing Cyclic Pentapeptides as Highly Potent and Selective Integrin αVβ3 Antagonists.* Journal of the American Chemical Society, 1996. **118**(32): p. 7461-7472.
116. Gaertner, F., et al., *Radiolabelled RGD peptides for imaging and therapy.* European Journal of Nuclear Medicine and Molecular Imaging, 2012. **39**(0): p. 126-138.
117. Haubner, R., et al., *[18F]Galacto-RGD: Synthesis, Radiolabeling, Metabolic Stability, and Radiation Dose Estimates.* Bioconjugate Chemistry, 2003. **15**(1): p. 61-69.

118. pubchem.ncbi.nlm.nih.gov/summary/summary.cgi?cid=21932600#x27.
119. Haubner, R., et al., *Glycosylated RGD-Containing Peptides: Tracer for Tumor Targeting and Angiogenesis Imaging with Improved Biokinetics.* Journal of Nuclear Medicine, 2001. **42**(2): p. 326-336.
120. Beer, A.J., et al., *Biodistribution and Pharmacokinetics of the αvβ3-Selective Tracer 18F-Galacto-RGD in Cancer Patients.* Journal of Nuclear Medicine, 2005. **46**(8): p. 1333-1341.
121. Niu, G. and D. Valdembri, *PET Imaging of Angiogenesis.* PET Clin., 2010. **4**(1): p. 17 - 38.
122. Chen X, et al., *Micro-PET imaging of alphavbeta3-integrin expression with 18F-labeled dimeric RGD peptide.* Mol. Imaging, 2004. **3**(2): p. 96 - 104.
123. Chen, X., et al., *MicroPET imaging of breast cancer alphav-integrin expression with 64Cu-labeled dimeric RGD peptides.* Mol. Imaging Biol, 2004. **6**(5): p. 350 - 359.
124. Liu, S., et al., *18F-labeled galacto and PEGylated RGD dimers for PET imaging of αvβ3 integrin expression.* Molecular imaging and biology : MIB : the official publication of the Academy of Molecular Imaging, 2010. **12**(5): p. 530-538.
125. Wu, Y., et al., *microPET Imaging of Glioma Integrin αvβ3 Expression Using 64Cu-Labeled Tetrameric RGD Peptide.* Journal of Nuclear Medicine, 2005. **46**(10): p. 1707-1718.
126. Mittra, E.S., et al., *Pilot Pharmacokinetic and Dosimetric Studies of 18F-FPPRGD2: A PET Radiopharmaceutical Agent for Imaging αvβ3 Integrin Levels.* Radiology, 2011. **260**(1): p. 182-191.
127. Chen, X., et al., *Integrin αvβ3-Targeted Imaging of Lung Cancer.* Neoplasia, 2005. **7**(3): p. 271 - 279.
128. Liu, Z., et al., *Dual Integrin and Gastrin-Releasing Peptide Receptor Targeted Tumor Imaging Using 18F-labeled PEGylated RGD-Bombesin Heterodimer 18F-FB-PEG3-Glu-RGD-BBN.* Journal of Medicinal Chemistry, 2008. **52**(2): p. 425-432.
129. Constantinou, M., et al., *Xenon Difluoride Exchanges Fluoride under Mild Conditions: A Simple Preparation of [18F]Xenon Difluoride for PET*

and Mechanistic Studies. Journal of the American Chemical Society, 2001. **123**(8): p. 1780-1781.

130. Pretze, M., P. Große-Gehling, and C. Mamat, *Cross-Coupling Reactions as Valuable Tool for the Preparation of PET Radiotracers.* Molecules, 2011. **16**(2): p. 1129-1165.
131. Schubiger, P.A.L. and M. L. and Friebe, Eds, *in PET chemistry - the driving force in molecular imaging* 2007, Berlin: Springer-verlag.
132. Chen, K. and P.S. Conti, *Target-specific delivery of peptide-based probes for PET imaging.* Advanced Drug Delivery Reviews, 2010. **62**(11): p. 1005-1022.
133. Jacobson, O., et al., *Rapid and Simple One-Step F-18 Labeling of Peptides.* Bioconjugate Chemistry, 2011. **22**(3): p. 422-428.
134. Chen, X., et al., *18F-labeled RGD peptide: initial evaluation for imaging brain tumor angiogenesis.* Nuclear Medicine and Biology, 2004. **31**(2): p. 179-189.
135. Wuest, F., et al., *Synthesis and Application of [18F]FDG-Maleimidehexyloxime ([18F]FDG-MHO): A [18F]FDG-Based Prosthetic Group for the Chemoselective 18F-Labeling of Peptides and Proteins†.* Bioconjugate Chemistry, 2008. **19**(6): p. 1202-1210.
136. Wester, H.-J., K. Hamacher, and G. Stöcklin, *A comparative study of N.C.A. Fluorine-18 labeling of proteins via acylation and photochemical conjugation.* Nuclear Medicine and Biology, 1996. **23**(3): p. 365-372.
137. Becaud, J., et al., *Direct One-Step18F-Labeling of Peptides via Nucleophilic Aromatic Substitution.* Bioconjugate Chemistry, 2009. **20**(12): p. 2254-2261.
138. Kilbourn, M.R., et al., *Fluorine-18 Labeling of Proteins.* Journal of Nuclear Medicine, 1987. **28**(4): p. 462-470.
139. Shiue, C.Y., A.P. Wolf, and J.F. Hainfeld, *Synthesis of 18F-labelled N-(p-[18F]fluorophenyl)maleimide and its derivatives for labelling monoclonal antibody with 18F.* Journal of Labelled Compounds and Radiopharmaceuticals, 1989. **26**(1-12): p. 287-289.
140. Shai, Y., et al., *Fluorine-18 labeled insulin: a prosthetic group methodology for incorporation of a positron emitter into peptides and proteins.* Biochemistry, 1989. **28**(11): p. 4801-4806.

141. Müller-Platz, C.M., et al., *18F-Fluoroacetate: An agent for introducing n.c.a. fluorine-18 into urokinase without loss of biological activity.* J. Lab. Compds. Radoppharm., 1982. **19**: p. 1645.
142. Garg, P.K., S. Garg, and M.R. Zalutsky, *Fluorine-18 labeling of monoclonal antibodies and fragments with preservation of immunoreactivity.* Bioconjugate Chemistry, 1991. **2**: p. 44.
143. Vaidyanathan, G. and M.R. Zalutsky, *Labeling proteins with fluorine-18 using N-succinimidyl 4-[18F]fluorobenzoate.* International Journal of Radiation Applications and Instrumentation. Part B. Nuclear Medicine and Biology, 1992. **19**(3): p. 275-281.
144. Guhlke, S., H.H. Coenen, and G. Stöcklin, *Fluoroacylation agents based on small n.c.a. [18F]fluorocarboxylic acids.* Applied Radiation and Isotopes, 1994. **45**(6): p. 715-727.
145. Kolb, H.C. and K.B. Sharpless, *The growing impact of click chemistry on drug discovery.* Drug Discovery Today, 2003. **8**(24): p. 1128-1137.
146. Kolb, H.C., M.G. Finn, and K.B. Sharpless, *Click Chemistry: Diverse Chemical Function from a Few Good Reactions.* Angewandte Chemie International Edition, 2001. **40**(11): p. 2004-2021.
147. Nwe, K. and M.W. Brechbiel, *Growing Applications of "Click Chemistry" for Bioconjugation in Contemporary Biomedical Research* Cancer Biotherapy & Radiopharmaceuticals, 2009. **24**(3): p. 298 - 302.
148. He, X.-P., et al., *CuAAC Click Chemistry Accelerates the Discovery of Novel Chemical Scaffolds as Promising Protein Tyrosine Phosphatases Inhibitors.* Curr Med Chem, 2012. **19**(15): p. 2399–2405.
149. Li, J., et al., *Radiolabeling of RGD peptide and preliminary biological evaluation in mice bearing U87MG tumors.* Bioorganic & Medicinal Chemistry, 2012. **20**(12): p. 3850-3855.
150. Glaser, M. and E.G. Robins, *'Click labelling' in PET radiochemistry.* Journal of Labelled Compounds and Radiopharmaceuticals, 2009. **52**(10): p. 407-414.
151. Tron, G.C., et al., *Click chemistry reactions in medicinal chemistry: Applications of the 1,3-dipolar cycloaddition between azides and alkynes.* Medicinal Research Reviews, 2008. **28**(2): p. 278-308.

152. Bock, V.D., et al., *1,2,3-Triazoles as peptide bond isosteres: synthesis and biological evaluation of cyclotetrapeptide mimics.* Organic & Biomolecular Chemistry, 2007. **5**(6): p. 971-975.
153. Glaser, M. and E. Arstad, *"Click Labeling" with 2-[18F]Fluoroethylazide for Positron Emission Tomography.* Bioconjugate Chemistry, 2007. **18**(3): p. 989-993.
154. Wängler, C., et al., *Multimerization of cRGD Peptides by Click Chemistry: Synthetic Strategies, Chemical Limitations, and Influence on Biological Properties.* ChemBioChem, 2010. **11**(15): p. 2168-2181.
155. Colombo, M. and A. Bianchi, *Click Chemistry for the Synthesis of RGD-Containing Integrin Ligands.* Molecules, 2010. **15**(1): p. 178-197.
156. Valdivia, A.C., et al., *A fast, simple, and reproducible automated synthesis of [18F]FPyKYNE-c(RGDyK) for αvβ3 receptor positron emission tomography imaging.* Journal of Labelled Compounds and Radiopharmaceuticals, 2008. **55**(2): p. 57-60.

Chapter 2: Aims

2.1 Introduction

The rapid growth of positron emission tomography in nuclear medicine, and the increase of its applications, have stimulated the development of several radiotracers and prosthetic groups as well as novel radiosynthetic strategies appropriate for labeling molecules with different radionuclides.[1, 2]

As previously described (**chap. 1**), the majority of the radiolabelled molecules developed for imaging angiogenesis are peptides derived from the natural binding sequence RGD[3], such as structurally constrained cyclic pentapeptides (i.e. c-[RGDfV], c-[RGDyK] or c-[RGDfK]).[4]

For these reasons, the main proposals of this work are:

- To develop prosthetic groups, which can be conjugated with RGD peptides by the use of azido-alkyne Huisgen's cycloaddition;

- To develop a clinically relevant RGD radioligand for $\alpha_v\beta_3$ integrin receptor;

- To develop a selective, non-peptidic radioligand for $\alpha_5\beta_1$ integrin receptor.

Prosthetic groups

Many synthetic procedures have been investigated for labeling RGD peptides. However since the introduction of the Cu(I)-catalyzed version, the Huisgen's 1,3-dipolar cycloaddition has gained considerable attention in radiochemistry[5] due to its favorable characteristics for the ^{18}F-chemistry.

The prosthetic groups have been designed to be:

- Easily synthesized
- Stable
- Clickable to RGD peptides

The fluorine is directly bound on the aromatic ring in order to avoid the defluorination that often happens *in vivo* with other aliphatic prosthetic groups.

The azido and alkyne moiety for the click chemistry are on the aliphatic chains. The prosthetic groups have different chain lengths in order to investigate whether this can influence the click chemistry.

The 14 molecules designed can be divided in aniline derivatives and benzoic acid derivatives (**figure1**)

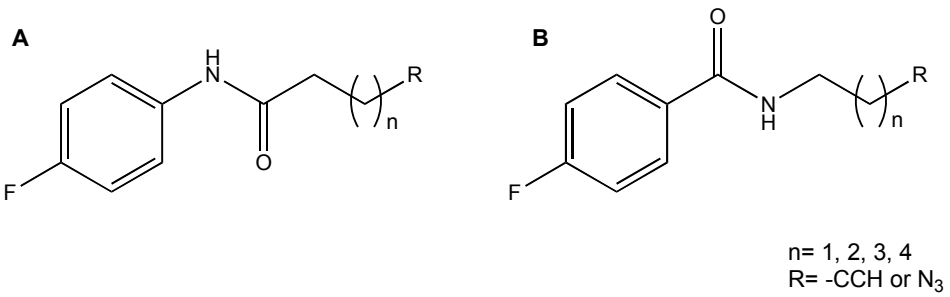

Figure 1| Amidic prosthetic groups
Molecules A and B are the templates of the two groups of this category of prosthetic groups. A is representative of the prosthetic groups synthetized starting from aniline and azide or alkyne acids. Molecules having B as template are synthetized starting from benzoic acid and azide or alkyne amines.

To optimize the conditions for the Huisgen's cycloaddition, we planned to click the prosthetic groups with seven non-natural amino acids having different properties such as polarity, total charge and aliphatic or aromatic moieties.

RGD radioligand

Despite the promising results obtained in preclinical studies with RGD containing peptides, only a limited number has been evaluated in the clinic, and none of them has routinely been applied yet.[6]

The development of appropriate radiochemical synthesis is often the most challenging step to obtain a radiotracer with widespread use in the clinics. Our proposal is to develop a facile and fast radiosynthetic strategy for RGD peptides and for this reason the Huisgen's 1,3-dipolar cycloaddition has been selected for the development of the radiolabeled peptide

Non-peptidic ligand for integrin $\alpha_5\beta_1$

In the last years, several selective antagonists for a number of integrins have been developed thanks to the advancements on the structural characterization of integrin-ligand interaction.[7] Considering that the integrins are expressed in a large number of diseases such as tumor, thrombosis, osteoporosis, autoimmune, inflammatory and

cardiovascular diseases, the possibility to bind a specific kind of integrin allows a selective pharmacological activity, or a selective imaging.

The fundamental role that integrin $\alpha_5\beta_1$ has not only in tumor angiogenesis but also in brain angiogenesis[8] makes it an appealing target not only for tumor monitoring but also for monitoring vascular remodeling after ischemic stroke.

The proposal for this work is to develop a non-peptidic ligand selective for $\alpha_5\beta_1$ integrin receptor. The ligand to synthesize has been identified among several molecules, by homology modeling of the $\alpha_5\beta_1$ integrin receptor. The structure of the selected molecule (**figure 2**) is based on the $\alpha_5\beta_1$ antagonist JSM6427.[9]

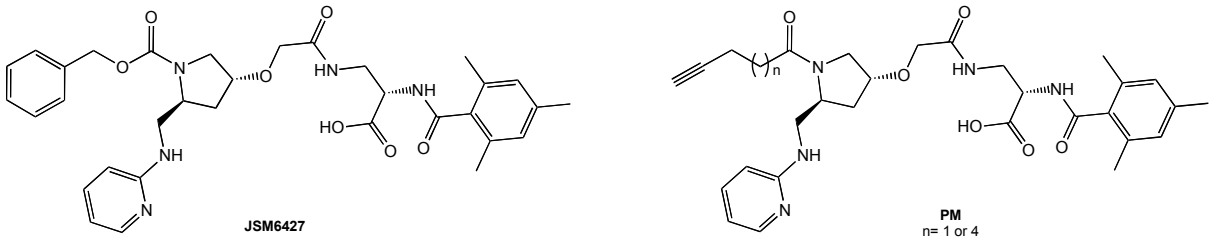

Figure 2| JSM6427 and non-peptidic ligand (PM)

Also in this case, the Huisgen's 1,3-dipolar cycloaddition has been selected for the conjugation of the ligand with the ^{18}F-labeled prosthetic group.

2.2 References

1. Chen, K. and P.S. Conti, *Target-specific delivery of peptide-based probes for PET imaging.* Advanced Drug Delivery Reviews, 2010. **62**(11): p. 1005-1022.
2. Pterze, M., P. Groβe-Gehling, and C. Mamat, *Cross-coupling Reactions as Valuable Tool for the Preparation of PET Radiotracer.* Molecules, 2011. **16**: p. 1129 - 1165.
3. Dijkgraaf, I. and O.C. Boerman, *Radionuclide Imaging of Tumor Angiogenesis.* Cancer Biotherapy & Radiopharmaceuticals, 2009. **24**(6): p. 637 - 647.
4. Chen X, et al., *Micro-PET imaging of alphavbeta3-integrin expression with 18F-labeled dimeric RGD peptide.* Mol. Imaging, 2004. **3**(2): p. 96 - 104.
5. Colombo, M. and A. Bianchi, *Click Chemistry for the Synthesis of RGD-Containing Integrin Ligands.* Molecules, 2010. **15**(1): p. 178-197.
6. Gaertner, F.C., et al., *Radiolabelled RGD peptides for imaging and therapy.* European Journal of Nuclear Medicine and Molecular Imaging, 2012. **39**(1): p. 126-138.
7. Millard, M., Srinivas Odde, and N. Neamati, *Integrin Targeted Therapeutics* Theranostic, 2011. **1**: p. 154-188.
8. Lee, B., et al., *Perlecan domain V is neuroprotective and proangiogenic following ischemic stroke in rodents.* The Journal of Clinical Investigation, 2011. **121**(8): p. 3005-3023.
9. Stragies, R., et al., *Design and Synthesis of a New Class of Selective Integrin α5β1 Antagonists.* Journal of Medicinal Chemistry, 2007. **50**(16): p. 3786-3794.

Chapter 3: Click Chemistry Approach for Modified Amino Acids as Sites for Biomolecules Functionalization

Monaco Alessandra[1,2], Scapozza Leonardo[2] and Seimbille Yann[1,2]

[1]Cyclotron & Radiopharmaceutical Chemistry Unit, Department of Medical Imaging and Information Sciences, University Hospital of Geneva, Geneva, Switzerland; [2]School of Pharmaceutical Sciences, University of Geneva and University of Lausanne, Geneva, Switzerland.

Abstract: Unnatural amino acids are important constituent for the development of radiolabeled peptides used in cancer diagnosis. In this work, we present an optimized strategy to combine functionalized amino acids with fluorinated prosthetic groups by the CuAAC. A variety of clickable UAAs were evaluated as site for the development of radiolabeled peptides.

3.1 Introduction

In living organisms the majority of the functional attributes were dependent on a large number of proteins. For this reason many natural as well as non-natural peptides have been developed for pharmaceutical and biomaterial use.[1]

Because of their versatile application, functionalized peptides were of significant diagnostic and therapeutic interest in tumor targeting and tumor imaging.[2] To make peptides amenable to positron emission tomography imaging, a small radiolabeled molecule, namely a prosthetic group, was usually introduced into peptide substrate by conventional coupling strategies.[3]

Because of its efficiency, selectivity, compatibility with a wide range of functional groups and biocompatible reaction conditions, Cu(I)-catalyzed Huisgen's 1,3-dipolar cycloaddition of organic azide and alkyne has become of high interest in imaging probe development. This click cycloaddition results in 1,4-disubstituted 1,2,3-triazole formed to provide in vivo stability between two chemical entities.[4]

Another high potential of click reaction is due to the easy incorporation of alkyne and azide components into a wide range of substituents.[5]

Since peptides are formed of amino acids, the amino acids modification represents the first step of the process for labeling peptides, and to provide multimodal imaging agents in radiochemistry. Modified amino acids have been then introduced in peptide sequences and used as reagents for the click reaction.[6] As a matter of fact some amino acids like glycine, lysine and valine have already been functionalized on the α-NH_2, side chain or the carboxyl, by the introduction of aliphatic chains, amines or carboxylic acids with terminal azide or alkyne groups.[7],[8]

In this work, we have evaluated the influence of the chemical propriety of the amino acids on the cycloaddition with fluorinated prosthetic groups. For this reason, the amino acids have been selected considering their polarity, total charge and aliphatic or aromatic substituents (**table 1**), and the seven amino acids are functionalized with

an alkynyl moiety on the α-NH_2 position. Subsequently, we designed fluorinated prosthetic groups with an azido function, to be conjugated via Huisgen's cycloaddition with the previously modified amino acids. At a later stage, the fluorine atom on the prosthetic groups could be substituted with ^{18}F-fluorine, a positron emitting radionuclide that is commonly used for PET imaging.

N°	Name	Side Chain (R)	Characteristics	pKa α-COO^-	pKa α-NH_3^+	pKa side chain
1	Gly	-H	nonpolar aliphatic	2.34	9.60	
2	Val	-$CH(CH_3)_2$	nonpolar aliphatic	2.32	9.62	
3	Pro	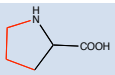	uncharged	1.99	10.60	
4	Phe	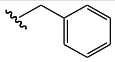	aromatic	1.83	9.13	
5	Tyr	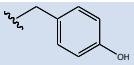	aromatic	2.20	9.11	10.07
6	Glu	-CH_2CH_2COOH	negatively charged	2.19	9.67	4.25
7	Lys	$CH_2CH_2CH_2CH_2NH_2$	positively charged	2.18	8.95	10.79

Table 1 | Amino acids characteristics

3.2 Results and discussion

3.2.1 Chemistry

The modification of the amino acids starts with the protection of the carboxyl group via a formation of the derivative methylesther in methanol using thyonyl chloride,[9] in order to avoid the formation of polymers during the insertion of the alkyne moiety, The methylesters (**8–13**) were obtained as hydrochloric salts due to the production of HCl during the reaction. Thereby, pure crystals (**scheme 1**) were isolated in high yield (82-98%) after a simple filtration. The introduction of alkyne moiety was made by conventional peptide coupling of the previous esterified amino acids with 4-pentynoic acid.[10] *N*-pent-4-ynoyl amino acids (**14-19**) were recovered in high yield (80-98%) after a simple saponification in NaOH in THF.

The free ε-NH_2 in the side chain on lysine makes it not suitable for the synthetic way described in **scheme 1**, another synthetic procedure was then used to introduce the

terminal alkyne on the α-NH_2. Indeed, a selective Fmoc protection of ε-NH_2 of the lysine[11] was obtainedusing region-Cu(II) salts: of a dimeric Cu(II) complex involveing the carboxylic acid and the α-NH_2 functionsof the lysine (**scheme 2**) acts as a temporary non-covalent protective group, and allows the formation of the resulting Fmoc-lysine (**20**) with 80% yield.

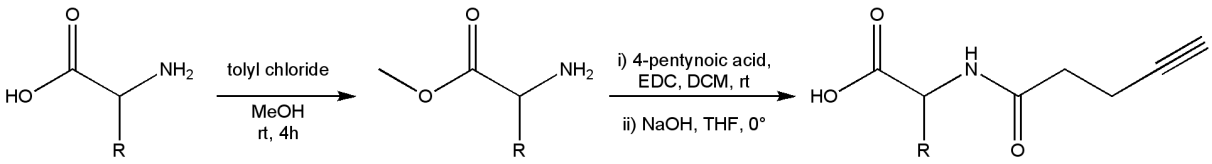

1: **R**= H
2: **R**= $CH(CH_3)_2$
3: **R**= pyrrolydine (cyclization on NH_2)
4: **R**= CH_2-Ph
5: **R**= CH_2-Ph-4-OH
6: **R**= $(CH_2)_2COOH$

8: **R**= H
9: **R**= $CH(CH_3)_2$
10: **R**= pyrrolydine (cyclization on NH_2)
11: **R**= CH_2-Ph
12: **R**= CH_2-Ph-4-OH
13: **R**= $(CH_2)_2COOH$

14: **R**= H
15: **R**= $CH(CH_3)_2$
16: **R**= pyrrolydine (cyclization on NH_2)
17: **R**= CH_2-Ph
18: **R**= CH_2-Ph-4-OH
19: **R**= $(CH_2)_2COOH$

Scheme 1｜ **Synthesis of alkynyl amino acids 14-19**
Reagents and conditions: **a)** Tolyl chloride, methanol, 4h rt; **b)** i) 4-pentynoic acid, EDC, DCM, rt, overnight; ii) NaOH, THF, 0°C, 1h.

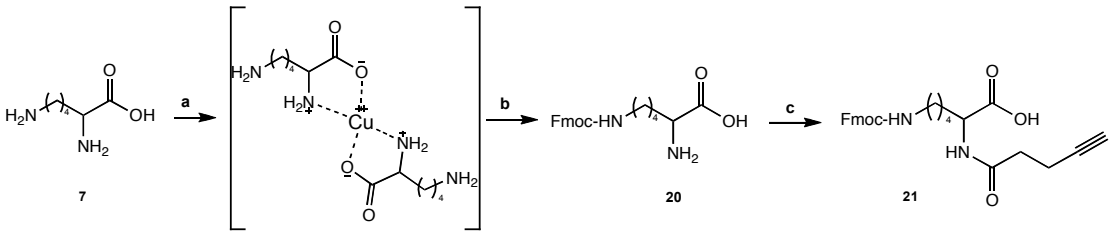

7 20 21

Scheme 2｜ **Synthesis of *N*^{6}-(((9*H*-fluoren-9-yl)methoxy)carbonyl)- *N*^{2}-(pent-4-ynoyl)lysine (21)**
Reagents and conditions: **a)** $CuCO_3$-$Cu(OH)_2$/H_2O, reflux, 30 min; **b)** Fnoc-N_3, MgO, dioxane, 45°C, overnight **c)** **23**, DIPEA, DCM, 3h, rt.

The final alkyne lysine (**21**) was synthesized by the interaction of **20** with freshly prepared succinimidyl activated 4-pentynoic acid (**23**) in a pH=9 set DIPEA solution of DCM **(scheme3**). After 3h of stirring solution at r.t., the reaction was completed and the excess of Fmoc-lysine were eliminated by filtration of the reaction crude to obtain the calcd.compound (**21**) with 81% yield.[12]

The synthesis of precursor **23** occurred in one step using 4-pentynoic acid and *N*-hydroxysuccinimide. In presence of EDC and DMAP as showed in **scheme 3**. The use of the 2,5-dioxopyrrolidin-1-yl pent-4-ynoate (**23**) allows to anchor the alkyne part on the fmoc-lysine, without protecting the carboxyl group remaining.

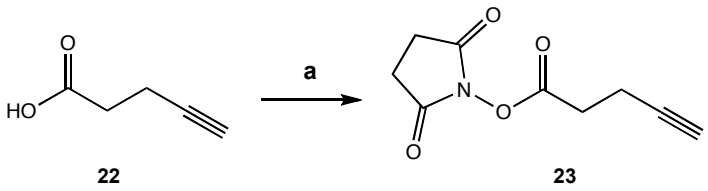

22 **23**

Scheme 3 | Synthesis of 2,5-dioxopyrrolidin-1-yl pent-4-ynoate (23)
Reagents and conditions: **a)** NHS, EDC, DMAP, DCM, overnight, rt.

The azido derivatives 3-azido-*N*-(4-fluorophenyl)propanamide (**27**) and 6-azido-*N*-(4-fluorophenyl) hexanamide (**28**) were synthesized with 60 and 68% yield respectively by peptidic coupling from 4-fluoroaniline (**24**) with azido acids (**25** and **26**) using HOBT and EDC as coupling agents[13] (**scheme 4**).

The access to precursors **25** and **26** was quantitatively yielded after nucleophile substitution of the corresponding bromo compounds (**29** and **30**) by excess of sodium azide. The reaction was carried out in acetone with excess of sodium azide.[14] Thank to the fact that the remaining sodium azide and the sodium bromide formed during the reaction were not soluble in acetone at r.t.; a convenient purification of compounds **25** and **26** was performed (**scheme 5**).

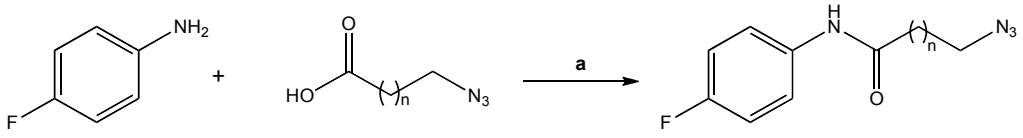

24 **25:** n= 1 **26:** n= 4 **27:** n= 1 **28:** n= 4

Scheme 4 | Synthesis of 3-azido-*N*-(4-fluorophenyl)propanamide (27) and 6-azido-*N*-(4-fluorophenyl) hexanamide (28)
Reagents and conditions: **a)** EDC, HOBT, DCM, rt, overnight.

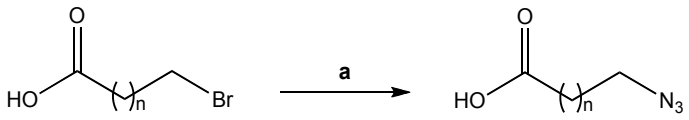

29: n= 1
30: n= 4

25: n= 1
26: n= 4

Scheme 5│ **Synthesis of 3-azidopropanoic acid (25) and 6-azidohexanoic acid (26)**
Reagents and conditions: **a)** CH_3COCH_3, NaN_3, 80°C, overnight.

The modified amino acids (**14-19** and **21**) were conjugated with the azido compounds **27** and **28** by the Huisgen's 1,3-cycloaddition. The reaction was catalysed by Cu(II) and sodium ascorbate was used as reducing agent (**scheme 6**) in a slight excess to prevent the side reaction of alkyne homocupling. The solvent used was water/THF and no additional buffers were added to adjust the pH of the reaction mixture, which ranged between 4.5 and 6.[15]

All the amino acids were conjugated with the azido derivatives **27** and **28** in appreciated short time (1h -3.5h). The clicked products (**31-37a,b**) were isolate after purification in rather good yields (63-92%) (**Table 2**).

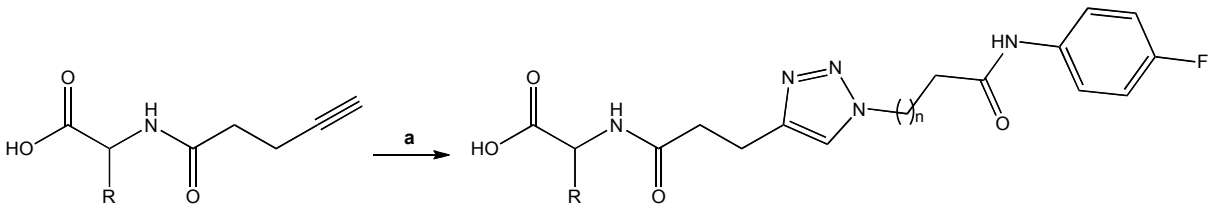

14: R= H
15: R= $CH(CH_3)_2$
16: R= pyrrolydine (cyclization on NH_2)
17: R= CH_2-Ph
18: R= CH_2-Ph-4-OH
19: R= $(CH_2)_2COOH$
21: R= $(CH_2)_4NH$-Fmoc

From **31(a,b)** to **37(a,b)**: **a: n=** 1, **b: n=** 4
31: R= H
32: R= $CH(CH_3)_2$
33: R= pyrrolydine (cyclization on NH_2)
34: R= CH_2-Ph
35: R= CH_2-Ph-4-OH
36: R= $(CH_2)_2COOH$
37: R= $(CH_2)_4NH$-Fmoc

Scheme 7│ **Synthesis of 31(a,b) – 37(a,b)**
Reagent and conditions: **a) 27** (or **28**), $CuSO_4$, sodium ascorbate, H_2O/THF, rt.

Yne a.a.	PG	pH	t	Product	Yield %
14	**27**	5	2 h	31a	90
14	**28**	5	2 h	31b	84
15	**27**	5	1 h	32a	75.7
15	**28**	5	1 h	32b	63.5
16	**27**	5	3.5 h	33a	92.3
16	**28**	5	3.5 h	33b	89.6
17	**27**	5	2 h	34a	87.5
17	**28**	5	2 h	34b	84.8
18	**27**	5	3 h	35a	79.5
18	**28**	5	3 h	35b	64.2
19	**27**	4	3.5 h	36a	78.5
19	**28**	4	3.5 h	36b	91.2
21	**27**	6	2 h	37a	78.6
21	**28**	6	2 h	37b	83.7

Table 2 | Huisgen's Cycloaddition

3.3 Experimental

All reagents and solvents were purchased from Sigma-Aldrich, Fluka or VWR and used without further purification. TLCs were run on silica gel 60 F_{254} pre-coated plastic sheets. The compounds were monitored under UV lamp lighting at 254 nm or by brief immersion in potassium permanganate solution. Flash chromatography columns were performed on silica gel (0.063-0.200 mm). NMRs were taken with a Varian Gemini 2000 NMR Spectrometer (Oxford 300 Nuclear Magnetic Instrument). The samples were dissolved either in $CDCl_3$, Acetone-d6 or DMSO-d6 (Cambridge Isotopes Laboratories Inc.) and the data were processed by MestRe-C software. Chemical shifts were expressed in ppm (δ) relative to the standard and coupling constants (J) in Hz. MS analysis were obtained by an ESI-MS instrument, API 150EX from AB/MDS (Sciex) and HRMS by ESI/nanoESI-IT Esquire 3000 plus (Bruker). All compounds isolated were at least 95% pure.

Gly-OMe HCl (8)

The glycine hydrochloride (2g, 26.64 mmol) was dissolved in dry CH_3OH (20 ml) and thionyl chloride (3.88 ml, 53,28 mmol) was added dropwise at 0°C under an inert atmosphere. The solution was refluxed 4 hours and concentraded *in vacuo* to obtain a hydrochloride salt, which was purified by crystallization in acetone (2.4g, yield 98%). ^{1}H NMR (300 MHz, DMSO-d6): δ 8.57 (2H, s), 3.74 (1H, d, J= 13.8 Hz), 3.37 (3H, s). ^{13}C NMR (300MHz, DMSO-d6): δ 168.01, 52.51, 39.50. MS (ESI) for $C_3H_8NO_2$ $[M+H]^+$: observed m/z 90.3.

***N*-pent-4-ynoyl-Gly (14)**

8 (1.27 g, 10.19 mmol), 4-pentynoic acid (1g, 10.19 mmol) and DMAP (1.86 g, 15.28 mmol) were dissolved in DCM (50 mL). The solution was cooled at 0°C and EDC·HCl (2.15 g, 11.21 mmol) was slowly added. The solution was stirred for 30 min at 0°C and overnight at r.t.. The organic layer was poured into 1M HCl (60 ml) and extracted with DCM (2x50 ml). The two organic layers were combined and washed with a saturated solution of $NaHCO_3$ (2x50 ml) and dried over Na_2SO_4. DCM was removed under reduced pressure. The crude was dissolved in THF (107 ml) and cooled at 0°C, then the ice bath was remouved and the reaction stirred at r.t.. A solution of NaOH (23 ml, 1M) was added dropwise and the reaction was stirred 30 min at 0°C and 30 min at r.t.. The volume of reaction was reduced to 50%, HCl (7.69 ml, 1M) was added and the solution was extracted with DCM (1x20 ml). This organic layer was discarded and the aqueous layer was washed with EtOAc (2x30 ml). The aqueous phase was acidified with HCl (15 ml, 2M) and it was extracted with EtOAc (2x40 ml). The combined EtOAc fractions were washed with $NaHCO_3$ sat. solution (2x25 mL) and dried over Na_2SO_4. The solvent was eliminated under reduced pressure. The residue was purified by flash chromatography (Hexane/EtOAc 1:1) to obtain **14** as white crystals (1.5g, yield: 98%). ^{1}H NMR (300 MHz, DMSO-d6): δ 7.97 (1H, t, J= 5.55 Hz), 3.48 (2H, d, J= 6 Hz), 2.24 (1H, t, J= 1.8 Hz), 2.08 (4H, s). ^{13}C NMR (300MHz, DMSO-d6): δ 171.25, 170.61, 83.66, 71.29, 40.52, 33.81, 14.00. HRMS (ESI) for $C_7H_{10}NO_3$ $[M+H]^+$: calcd. m/z 156.0655, observed m/z 156.0657.

ε-*N*-Fmoc lysine (20)

To a solution of L-Lysine hydrochloride (2.5g, 13.7 mmol) in H_2O (20 ml), basic $CuCO_3$ (2.5g, 22.6 mmol) was added. The mixture was refluxed 30 min, and then

cooled and filtered. The residue washed with H_2O, after cooling at r.t., MgO (0.75 g, 18.6 mmol) was added over the previous solid. A solution of Fmoc-N_3 (5 g, 19.3 mmol) in dioxane (75 ml) was added and the mixture stirred overnight at 45°C. A 2N NaOH solution and AcOH (25ml) were added. The obtained solution was stirred for 1h and then filtered. The solid residue was washed with icey H_2O (3.20 ml) and a white solid was obtained (3.9g, yield 79%). ^{1}H NMR (300 MHz, DMSO-d6): δ 8.41 (2H, bs), 7.88 (2H, d, J= 7.2 Hz), 7.68 (2H, d, J= 7.2 Hz), 7.43-7.30 (5H, m), 4.29-4.18 (3H, m), 3.83 (1H, bs), 3.36 (2H, bs), 2.96 (2H, d, J= 5.4 Hz), 2.08 (1H, d, J= 1.5 Hz), 1.78 (2H, d, J= 6 Hz), 1.40-1.30 (3H, m). ^{13}C NMR (300MHz, DMSO-d6): δ 1174.52, 170.88, 143.86 (2C), 140.62 (2C), 130.15, 127.54 (2C), 126.98 (2C), 125.03 (2C), 120.03 (2C), 65.10, 51.68, 46.63, 29.49, 28.73, 21.54. MS (ESI) for $C_{21}H_{24}N_2O_4$ $[M+H]^+$: 369.3.

N^6-(((9*H*-fluoren-9-yl)methoxy)carbonyl)-N^2-(pent-4-ynoyl)lysine (21)

To a solution of **20** (150 mg, 0.41 mmol) in DCM (2 mL) DIPEA (0.2 ml) was added. Then freshly prepared **23** (40 mg, 0.21 mmol) was introduced and the reaction was stirred 3h at r.t.. The residual **20** was removed by filtration and the organic layer was concentrated under reduced pressure to obtain 149 mg of **21** as yellow oil (81% yield). ^{1}H NMR (300 MHz, Acetone-d6): δ 7.52 (4H, dd, J_d= 7.2, J_d= 36.9 Hz), 7.18 (4H, td, J_t= 8.1 J_d= 24.3 Hz), 6.99 (1H, d, J= 6.9 Hz), 4.20-4.03 (3H, m), 3.47 (3H, t, J= 6.5 Hz), 3.01-2.89 (4H, m) 2.46 (2H. s), 2.31 (2H, s), 1.99 (1H, s), 1.84 (1H, s), 1.70 (1H, bs), 1.56 (1H, bs). ^{13}C NMR (300MHz, $CDCl_3$): δ 176.70, 173.65, 170.92, 156.77, 144.13 (2C), 141.26 (2C), 127.78 (2C), 127.19 (2C), 125.36 (2C), 119.99 (2C), 83.36, 69.32, 66.58, 47.30, 42.26, 53.34, 25.57, 18.04, 15.02, 12.29. HRMS (ESI) for $C_{26}H_{28}N_2O_5$ $[M+H]^+$: calcd. m/z 449.2071, observed m/z 449.2072.

2,5-dioxopyrrolidin-1-yl pent-4-ynoate (23)

To a solution of **22** (500 mg, 9.12 mmol) 15 mL of DCM, were successively added NHS (1 g, 10.19 mmol), DMAP (1.57 g, 10.28 mmol) and EDC.HCl (2.69 g, 14.05 mmol). The mixture was stirred overnight at rt. The solvent was removed under vacuum and the crude was purified by flash chromatography Hexane/EtOAc (3:2), to obtain a white solid (1,55 g, yield 87%). ^{1}H-NMR (300 MHz, DMSO-d6) δ: 2.90-2.83 (6H, m), 2.60 (2H, dt, J_d=2.4, J_t=7.8 Hz), 2.05 (1H, t, J=2.6 Hz). ^{13}C-NMR (300 MHz,

DMSO-d6) δ: 169.11 (2C), 167.18, 81.03, 70.26, 30.46, 25.75 (2C), 14.26. MS (ESI) for $C_9H_9NO_4$ $[M+H_3O^+]^+$: observed *m/z* 214.

3-azidopropanoic acid (25)

To a solution of **29** (2 g, 13.07 mmol) in acetone (15 ml), NaN_3 (2.12 g, 32.68 mmol) was slowly added at rt. The mixture was stirred 72h at 80°C. The insoluble salts were filtered and the solvent was removed under reduced pressure. A brown oil was obtained (1.5g) in quantitative yield. ^{1}H-NMR (300 MHz, $CDCl_3$): δ 10.06 (1H, bs), 3.58 (2H, t, J=6.3 Hz), 2.63 (2H, t, J=6.3 Hz). ^{13}C-NMR (300 MHz, CCl_3): δ 176.85, 47.17, 34.60. No MS observed at *m/z* 115.

3-azido-*N*-(4-fluorophenyl)propanamide (27)

To a solution of **25** (1 g, 8.69mmol) and 4-fluoro aniline (1.21 g, 8.92 mmol) in DCM (30 mL), HOBT (1.76 g, 13.04 mmol) and EDC·HCl (2.05 g, 10.7 mmol) were added. The reaction was stirred overnight at r.t.. The reaction mixture was washed twice with a saturated solution of $NaHCO_3$ (15 mL). The organic layer was dried over Na_2SO_4, filtered and the solvent removed under reduced pressure. The crude was purified on flash chromatography Hexane/Et_2O (3:2) to give the expected compound in form of a white powder (1.1g) with yield of 60%. ^{1}H-NMR (300 MHz, $CDCl_3$): δ 7.70 (1H,bs), 7.47-7.40, (2H, m), 7.02-6.96 (2H, m), 3.68 (2H, t, J=12.6 Hz), 2.57 (2H, t, J=12.6 Hz). ^{13}C-NMR (300 MHz, $CDCl_3$): δ 168.35, 159.52 (d, J= 60.6 Hz), 133.38, 122.22, 115.63 (2C, d, J=22.4 Hz), 47.35, 36.57. HRMS (ESI) for $C_9H_{10}N_4OF$ $[M+H]^+$: calcd. m/z 209.0821, observed m/z 209.2833.

(3-(1-(3-((4-fluorophenyl)amino)-3-oxopropyl)-1*H*-1,2,3-triazol-4-yl)propanoyl) glycine (31a)

Aqueous solutions of $CuSO_4$ (0.1 M, 6.3mL, 0,63 mmol) and sodium ascorbate (0.3 M, 6.3 mL, 1.89 mmol) were added to a solution of **14** (30 mg, 0.175 mmol) and **27** (36 mg, 0.175 mmol) in H_2O/THF (1:1, 50 mL). The mixture was stirred 2.5h at r.t., then THF was removed under reduced pressure and the aqueous phase was extracted with EtOAc (2x30 mL). The organic layer was dried over Na_2SO_4, filtered and concentrated under reduced pressure. The crude was purified on a silica gel flash chromatography with EtOAc to afford **31a** as a light brown solid (71 mg, yield 90%). ^{1}H-NMR (300 MHz, $CDCl_3$): δ 7.50-7.45 (2H, m), 7.32 (1H, bs), 7.03 (2H, t, J=

8.7 Hz), 3.73 (2H, t, J= 6.15 Hz), 2.60 (2H, t J= 6.3 Hz), 1.57 (2H, s), 1.43 (1H, s), 0.90-0.83 (5H, m). ^{13}C-NMR (300 MHz, Acetone-d6): δ 171.98, 170.91 (2C), 153.08, 120.45, 118.28 (2C), 110.32 (2C), 107.35, 89.80, 84.80, 77.25, 76.95, 74.95, 71.38, 63.70. HRMS (ESI) for $C_{16}H_{18}FN_5O_4$ $[M+H]^+$: calcd. m/z 364.1424, observed m/z 364.1416.

3.4 Conclusions

In this work we reported a complete study of an optimized strategy combining functionalized amino acids and the prosthetic groups using click chemistry. Data obtained show that the alkyne moieties can be successfully incorporated in all the selected amino acids with yields ranging between 60 and 90%. Likewise, the click chemistry between the modified amino acids and the prosthetic group gave good yields (54-98%). Furthermore, time of reaction was surprisingly shorter than that published for similar reactions,[7, 8] since the click reaction was completed between 1h and 3,5h instead of 24h.

The range of amino acids selected to evaluate the reactivity of the prosthetic groups suggests that the chemical propriety of the side chain does not influence the cycloaddition, and the same methodology could be then applied to other amino acids. The time of reaction and the yeld obtained suggest that the prosthetic group synthesized are amenable for the developemt of ^{18}F-chemistry, and could be considered for the future development of ^{18}F-labeled peptides.

In conclusion, we demonstrated that the prosthetic groups proposed could be incorporated by the Huisgen's 1,3-cycloaddition to different kind of amino acids, independently to the pH of the reaction with conditions which make this strategy applicable for the development of ^{18}F-labeled peptides.

3.5 References

1. de Graaf, A.J., et al., *Nonnatural Amino Acids for Site-Specific Protein Conjugation.* Bioconjugate Chemistry, 2009. **20**(7): p. 1281-1295.
2. van Berkel, S.S., et al., *Application of Metal-Free Triazole Formation in the Synthesis of Cyclic RGD–DTPA Conjugates.* ChemBioChem, 2008. **9**(11): p. 1805-1815.
3. Hausner, S.H., et al., *In Vivo Positron Emission Tomography (PET) Imaging with an αvβ6 Specific Peptide Radiolabeled using 18F-"Click" Chemistry: Evaluation and Comparison with the Corresponding 4-[18F]Fluorobenzoyl- and 2-[18F]Fluoropropionyl-Peptides.* Journal of Medicinal Chemistry, 2008. **51**(19): p. 5901-5904.
4. Mindt, T.L., et al., *A "Click Chemistry" Approach to the Efficient Synthesis of Multiple Imaging Probes Derived from a Single Precursor.* Bioconjugate Chemistry, 2009. **20**(10): p. 1940-1949.
5. Huisgen, R., *1,3-Dipolar Cycloadditions-Introduction, Survry, Mechanism.* Wiley, ed. I.P.A. editor New York, 1984: p. 1-176.
6. Lu, J., M. Shi, and M.S. Shoichet, *Click Chemistry Functionalized Polymeric Nanoparticles Target Corneal Epithelial Cells through RGD-Cell Surface Receptors.* Bioconjugate Chemistry, 2008. **20**(1): p. 87-94.
7. Mindt, T.L., et al., *A Click Approach to Structurally Diverse Conjugates Containing a Central Di-1,2,3-triazole Metal Chelate.* ChemMedChem, 2009. **4**(4): p. 529-539.
8. Chen, et al., *Bioinspired Modular Synthesis of Elastin-Mimic Polymers To Probe the Mechanism of Elastin Elasticity.* Journal of the American Chemical Society, 2010. **132**(13): p. 4577-4579.
9. Rutjes, F.P.J.T., et al., *Synthesis of Enantiopure Functionalized Pipecolic Acids via Amino Acid Derived N-Acyliminium Ions.* European Journal of Organic Chemistry, 1999. **1999**(5): p. 1127-1135.
10. van Berkel, S.S., et al., *A macrocyclic coumarin-containing tripeptide via CuAAC chemistry.* Chemical Communications, 2009. **0**(28): p. 4272-4274.
11. Albericio, F., et al., *Convenient Syntheses of Fluorenylmethyl-Based Side Chain Derivatives of Glutamic and Aspartic acids, Lysine, and Cysteine.* Synthesis, 1990. **1990**(2): p. 119-122.

12. Galibert, M., P. Dumy, and D. Boturyn, *One-Pot Approach to Well-Defined Biomolecular Assemblies by Orthogonal Chemoselective Ligations.* Angewandte Chemie International Edition, 2009. **48**(14): p. 2576-2579.
13. Bessis, A.S., et al., *Alkynyl derivatives as modulators of metabotropic glutamate receptors*, in *World Intellectual Property Office (WIPO). Patent Collaboration Treaty (PCT) Patents*. 2005.
14. Pirali, T., et al., *Triazole-Modified Histone Deacetylase Inhibitors As a Rapid Route to Drug Discovery.* Journal of Combinatorial Chemistry, 2008. **10**(5): p. 624-627.
15. Glaser, M. and E. Arstad, *"Click Labeling" with 2-[18F]Fluoroethylazide for Positron Emission Tomography.* Bioconjugate Chemistry, 2007. **18**(3): p. 989-993.

3.6 Supporting Information

Chemical characterization data

Esterification

The appropriate amino acid (26.64 mmol) was dissolved in dry CH_3OH (20 ml) and thionyl chloride (3.88 ml, 53,28 mmol) was added dropwise at 0°C under an inert atmosphere. The solution was refluxed 4 hours and concentraded *in vacuo* to obtain a hydrochloride, which was purified by crystallization in acetone

Val-OMe HCl (9): 3g, yield 87%. ^{1}H NMR (300 MHz, $CDCl_3$): δ 8.86 (2H, s), 3.94 (1H, d, J=3.6 Hz), 3.82 (3H, s), 2.47 (1H, s), 1.14 (6H, t, J=6.2 Hz). ^{13}C NMR (300MHz, DMSO-d6): δ 170.16, 57.21, 28.99, 18.20, 17.68 (2C). MS (ESI): observed m/z 132.4 $[M+H]^+$.

Pro-OMe (10): 3.2g, yield 93%. ^{1}H NMR (300 MHz, $CDCl_3$): δ 4.50 (1H, td, J=4.8 Hz), 3.81 (3H, s), 3.63-3.46 (2H, m), 2.47-2.35 (1H, m), 2.20-2.00 (4H, m). ^{13}C NMR (300MHz, $CDCl_3$): δ 169.39, 59.29, 53.54, 46.06, 28.74, 23.66. MS (ESI): observed m/z 130.3 $[M+H]^+$.

Phe-OMe (11): 4.2g, yield 90%. ^{1}H NMR (300 MHz, DMSO-d6): δ 8.76 (2H, bs), 7.35-7.23 (5H, m), 4.23 (1H, t, J=6.6 Hz), 3.64 (3H, s), 3.15 (2H, 2dd, J_d=7.5, J_d=20.9 Hz). ^{13}C NMR (300MHz, DMSO-d6): δ 169.28, 134.64, 129.39 (2C), 128.44 (2C), 127.20, 53.07, 52.57, 35.75. MS (ESI): observed m/z 180.1 $[M+H]^+$.

Tyr-OMe (12): 4.2g, yield 82%. ^{1}H NMR (300 MHz, $CDCl_3$): δ 8.61 (2H, bs), 6.87 (2H, d, J=8.4 Hz), 6.60 (2H, d, J=8.4 Hz), 3.91 (1H, t, J=6 Hz), 3.55 (3H, s), 3.05 (2H, m), 2,67 (1H, s). ^{13}C NMR (300MHz, DMSO-d6): δ 169.98, 157.18, 130.89 (2C), 124.79, 115.92 (2C), 53.92 (2C), 35.59. MS (ESI): observed m/z 196.1 $[M+H]^+$.

Glu-$(OMe)_2$ HCl (13): 4.1g, yield 91%. ^{1}H NMR (300 MHz, $CDCl_3$): δ 8.76 (2H, bs), 4.34 (1H, bs), 3.81 (3H, s), 3.66 (s, 3H), 2.81-2.58 (2H, m), 2.43-2.41 (2H, m). ^{13}C NMR (300MHz, $CDCl_3$): δ 172.82, 169.71, 53.41, 52.66 (2C), 51.97, 29.84, 25.36. MS (ESI): observed m/z 176.3 $[M+H]^+$.

Functionalization

The appropriate methyl ester (10.19 mmol), 4-pentynoic acid (1g, 10.19 mmol) and DMAP (1.86 g, 15.28 mmol) were dissolved in DCM (50 mL). The solution was cooled at 0°C and EDC·HCl (2.15 g, 11.21 mmol) was slowly added. The solution was stirred for 30 min at 0°C and overnight at rt. The organic layer was poured into 1M HCl (60 ml) and extracted with DCM (2x50 ml). The two organic layers were combined and washed with a saturated solution of $NaHCO_3$ (2x50 ml) and dried over Na_2SO_4. DCM was removed under reduced pressure. The crude was dissolved in THF (107 ml) and cooled at 0°C, then the ice bath was remouved and the reaction stirred at rt. A solution of NaOH (23 ml, 1M) was added dropwise and the reaction was stirred 30 min at 0°C and 30 min at rt. The volume of reaction was reduced to 50%, HCl (7.69 ml, 1M) was added and the solution was extracted with DCM (1x20 ml). This organic layer was discarded and the aqueous layer was washed with EtOAc (2x30 ml). The aqueous phase was acidified with HCl (15 ml, 2M) and it was extracted with EtOAc (2x40 ml). The combined EtOAc fractions were washed with $NaHCO_3$ sat. solution (2x25 mL) and dried over Na_2SO_4. The solvent was eliminated under reduced pressure. The residue was purified by flash chromatography (Hexane/EtOAc 1:1).

N-pent-4-ynoyl-Val (15): 1.7g, yield: 87%. ^{1}H NMR (300 MHz, $CDCl_3$): δ 8.78 (1H, bs), 6.61 (1H, d, J=8.1 Hz), 4.51 (1H, q, J=4 Hz), 2.51 (4H, s), 2.26-2.18 (1H, m), 2.02 (1H, s), 0.95 (6H, 2d, J=5.5 Hz). ^{13}C NMR (300MHz, $CDCl_3$): δ 173.01, 170.49, 83.67, 71.22, 56.97, 33.76, 29.80, 19,09, 17.93, 14.19. HRMS (ESI) for $C_{10}H_{16}NO_3$ $[M+H]^+$: calcd. m/z 198.1124, observed m/z 198.1127.

N-pent-4-ynoyl-Pro (16): 2.2g, yield: 82%. ^{1}H-NMR (300 MHz, $CDCl_3$): δ 8.64 (1H, bs), 4.53-4.51 (1H, m), 3.61-3.45 (2H, m), 2.60-2.53 (4H, m), 2.24-1.96 (5H, m). ^{13}C NMR (300MHz, DMSO-d6): δ 173.37, 168.73, 83.95, 71.14, 58.26, 46.24, 32.55, 28.80, 24.22, 13.29. HRMS (ESI) for $C_{10}H_{13}NO_3$ $[M+H]^+$: calcd. m/z 196.0965, observed m/z 196.0968.

N-pent-4-ynoyl-Phe (17): 2.3g, yield: 93%. ^{1}H NMR (300 MHz, $CDCl_3$): δ 10.63 (1H, bs), 7.14-7.06 (3H, m), 7.00-6.98 (2H, m), 6.17 (2H, d, J=7.5 Hz), 4.73 (1H, q, J=6.4 Hz), 3.00 (2H, dd, 2H, J_d=6, J_d=17.6 Hz), 2.27-2.21 (4H, m), 1.77 (1H, t, J=2.3 Hz).

^{13}C NMR (300MHz, DMSO-d6): δ 172.92, 170.19, 137.49, 129.06 (2C), 128.11 (2C), 126.35, 83.56, 71.25, 53.36, 36.76, 33.82, 13.99. HRMS (ESI) for $C_{14}H_{16}NO_3$ $[M+H]^+$: calcd. m/z 246.1124, observed m/z 246.1132

N-pent-4-ynoyl-Tyr (18): 2.4g, yield: 90%. ^{1}H NMR (300 MHz, Acetone-d6): δ 7.03 (2H, d, J=8.4 Hz), 6.75 (2H, d, J=8.7 Hz), 4.64 (1H, q, J=7.2), 3.29 (1H, s), 2.41-2.32 (4H, m), 2.03 (1H, t, J=1.95 Hz). ^{13}C NMR (300MHz, $CDCl_3$): δ 171.78, 170.26, 149.64, 133.47, 130.28 (2C), 121.61 (2C), 69.60 53.07, 37.16, 35.11, 33.44, 14.66. HRMS (ESI) for $C_{14}H_{16}NO_4$ $[M+H]^+$: calcd. m/z 262.1074, observed m/z 262.1074

N-pent-4-ynoyl-Glu (19): 1.8g, yield: 80%. ^{1}H NMR (300 MHz, $CDCl_3$): δ 6.78 (1H, d, J=7.5 Hz), 4.54-4.47 (1H, m), 3.59 (1H, s), 2.47-2.30 (7H, m), 2.21-2.12 (2H, m), 2.00-1.88 (2H, m). ^{13}C NMR (300MHz, DMSO-d6): δ 173.24, 172.59, 170.39, 83.57, 71.18, 51.02, 33.80, 29.81, 26.29, 14.05. HRMS (ESI) for $C_{10}H_{14}NO_5$ $[M+H]^+$: calcd. m/z 228.0866, observed m/z 218.0863

6-azidohexanoic acid (26): To a solution of **30** (2.35 g, 13.07 mmol) in acetone (15 ml), NaN_3 (2.12 g, 32.68 mmol) was added portion wise at rt. The mixture was stirred 72h at 80°C. The insoluble salts were filtered and the solvent was removed under reduced pressure, to obtain a brown oil was obtained in quantitative yield (1.87 g). ^{1}H-NMR (300 MHz, $CDCl_3$): δ 9.78 (1H, bs), 3.27 (2H, t, J=6.8 Hz), 2.36 (2H, t, J=7.2 Hz), 1.70-1.57 (4H, m), 1.47-1.37 (2H, m). ^{13}C-NMR (300 MHz, $CDCl_3$): δ 179.46, 51.08, 28.43 (2C), 26.07, 24.15. No No MS observed at *m/z* 143.

6-azido-*N*-(4-fluorophenyl)hexanamide (28): To a solution of **26** (1.24 g, 8.69mmol) and 4-fluoro aniline (1.21 g, 8.92 mmol) in DCM (30 mL), HOBT (1.76 g, 13.04 mmol) and EDC·HCl (2.05 g, 10.7 mmol) were added. The reaction was stirred overnight at rt. The reaction mixture was washed twice with a saturated solution of $NaHCO_3$ (15 mL). The organic layer was dried over Na_2SO_4, filtered and the solvent removed under reduced pressure. The crude was purified on flash chromatography Hexane/Et_2O (3:2) to give the expected compound as a white powder (3.5g, yield 68%). ^{1}H-NMR (300 MHz, $CDCl_3$): δ 7.48-7.43 (2H, m), 7.19 (1H, bs), 7.00 (2H, t, J=8.6 Hz), 3.28 (2H, t, J=13.2 Hz), 2.36 (2H, t, J=14.7 Hz), 1.81-1.70 (2H, m), 1.69-1.61 (2H, m), 1.59-1.41 (2H, m). ^{13}C-NMR (300 MHz, $CDCl_3$): δ 170.81, 161.08,

121.61 (2C, d, J=8.9 Hz), 115.62 (2C, d, J=22.4 Hz), 97.90, 51.21, 37.26, 28.61, 26.34, 24.94. HRMS (ESI) for $C_{12}H_{15}N_4OFNa$ $[M+Na]^+$: calcd. m/z 273.1110, observed m/z 273.1122.

Huisgen's Cycloaddition

Aqueous solutions of $CuSO_4$ (0.1 M, 6.3mL, 0,63 mmol) and sodium ascorbate (0.3 M, 6.3 mL, 1.89 mmol) were added to a solution of the appropriate alkynyl amino acid (0.175 mmol) and **26** (36 mg, 0.175 mmol) in H_2O/THF (1:1, 50 mL). The mixture was stirred 2.5h at rt, then THF was removed under reduced pressure and the aqueous phase was extracted with EtOAc (2x30 mL). The organic layer was dried over Na2SO_4, filtered and concentrated under reduced pressure. The crude was purified on a silica gel flash chromatography with EtOAc.

(3-(1-(3-((4-fluorophenyl)amino)-3-oxopropyl)-1H-1,2,3-triazol-4-yl)propanoyl) valine (32a): 84 mg, yield 76%. ^{1}H-NMR (300 MHz, CD_3OD): δ 7.57 (1H, bs), 7.32 (2H, td, J=2.35 Hz), 6.83 (2H, t, J=8.85 Hz), 4.51 (2H, t, J=6.6 Hz), 4.10 (1H, d, J=5.4 Hz), 2.80 (4H, t, J=6.45 Hz), 2.43 (2H, t, J=6.6 Hz) 1.97-1.91 (1H, m), 0.72 (6H, d, J=6.9 Hz). ^{13}C-NMR (300 MHz, CD_3OD): δ 190.12, 174.75, 170.30, 1160.73 (d, J=240 Hz), 135.89, 123.11 (2C, d, J=7.8 Hz), 116.29 (2C, d, J=22.5 Hz), 110.46, 47.25, 37.65, 35.98, 31.64, 22.55, 19.67, 18.32 (2C). HRMS (ESI) for $C_{19}H_{25}N_5O_4F$ $[M+H]^+$: calcd. m/z 406.1885, observed m/z 406.1886.

(3-(1-(3-((4-fluorophenyl)amino)-3-oxopropyl)-1H-1,2,3-triazol-4-yl)propanoyl) proline (33a): 76 mg, yield 92%. ^{1}H-NMR (300 MHz, CD_3OD): δ 7.57 (1H, s), 7.33-7.29 (2H, m), 6.83 (2H, t, J=8.9 Hz), 4.51 (2H, t, J=6.5 Hz), 4.19 (1H, dd, J_d=3, J_d=5.4 Hz), 3.39-3.29 (2H, m), 2.82-2.77 (4H, m), 2.52 (2H, t, J=7.2 Hz), 2.06-1.97 (3H, m), 1.80-1.74 (3H, m). ^{13}C-NMR (300 MHz, CD_3OD): δ 175.86, 170.30, 165.67, 162.32, 135.88, 135.39, 124.28, 123.16 (2C, d, J=7.8 Hz), 116.30 (2C, d, J=22.5 Hz), 60.31, 47.28, 37.69, 34.62, 32.31, 30.43, 25.64, 21.61. HRMS (ESI) for $C_{19}H_{23}N_5O_4F$ $[M+H]^+$: calcd. m/z 404.1728, observed m/z 404.1723.

(3-(1-(3-((4-fluorophenyl)amino)-3-oxopropyl)-1H-1,2,3-triazol-4-yl)propanoyl) phenylalanine (34a): 90 mg, yield 88%. ^{1}H-NMR (300 MHz, DMSO-d6): δ 10.13 (1H, s), 8.21 (1H, d, J=8.1 Hz), 7.70 (1H, s), 7.59-7.55 (2H, m), 7.28-7.09 (7H, m), 4.56

(2H, t, J=6.8 Hz), 4.45-4.38 (1H, m), 3.05 (1H, dd, J=6.1 Hz), 3.93 (2H, t, J=6.6 Hz), 2.87-2.79 (1H, m), 2.72 (2H, t, J=7.7 Hz), 2.37 (2H, t, J=7.7 Hz). ^{13}C-NMR (300 MHz, DMSO-d6): δ 189.83, 173.08, 171.02, 167.89, 157.86 (d, J=238.2 Hz), 145.69, 137.69, 128.99 (2C), 128.03 (2C), 126.25, 122.09, 120.78 (2C, d, J=7.7 Hz), 115.19 (2C, d, J=25.9 Hz), 53.41, 45.23, 36.71, 36.18, 34.47, 21.09. HRMS (ESI) for $C_{23}H_{25}N_5O_4F$ $[M+H]^+$: calcd. m/z 454.1885, observed m/z 454.1884

(3-(1-(3-((4-fluorophenyl)amino)-3-oxopropyl)-1H-1,2,3-triazol-4-yl)propanoyl) tyrosine (35a): 103 mg, yield 79.5%. ^{1}H-NMR (300 MHz, CD_3OD): δ 7.52 (1H, s), 7.45-7.40 (2H, m), 6.98-6.91 (4H, m), 6.61 (2H, d, J=4.2 Hz), 4.61 (2H, t, J=6.45 Hz), 4.52-4.48 (1H, m), 3.26-3.24 (2H, m), 3.02-2.71 (6H, m), 2.44 (2H, t, J=7.05 Hz). ^{13}C-NMR (300 MHz, CD_3OD): δ 174.33, 170.31, 162.33, 157.24, 131.31 (2C), 129.37, 124.00, 123.15 (2C, d, J=8 Hz), 116.27 (2C, d, J=22.5 Hz), 121.79, 116.19 (2C), 110.45, 55.68, 54.87, 47.26, 37.77, 37.67, 36.05, 22.37. HRMS (ESI) for $C_{23}H_{25}N_5O_5F$ $[M+H]^+$: calcd. m/z 470.1834, observed m/z 470.1830.

(3-(1-(3-((4-fluorophenyl)amino)-3-oxopropyl)-1H-1,2,3-triazol-4-yl)propanoyl) glutamic acid (36a): 60 mg, yield 79%. ^{1}H-NMR (300 MHz, CD_3OD): δ 7.56 (1H, s), 7.33-7.28 (2H, m), 6.83 (2H, t, J=8.7 Hz), 4.52 (2H, t, J=6.45 Hz), 4.22 (1H, q, J=4.4 Hz), 2.81 (4H, t, J=6,45 Hz), 2.40 (2H, t, J=6.75 Hz), 2.14 (2H, t, J=7.65 Hz), 2.02-1.91 (1H, m), 1.76-1.64 (1H, m). ^{13}C-NMR (300 MHz, CD_3OD): δ 176.06, 174.45, 170.05 (2C), 162.05, 158.84, 135.56, 123.84, 122.86 (2C, d, J=7.8 Hz), 116.01 (2C, d, J=22.5 Hz), 52.84, 47.01, 37.36, 35.76, 30.95, 27.57, 22.09. HRMS (ESI) for $C_{19}H_{23}N_5O_6F$ $[M+H]^+$: calcd. m/z 436.1626, observed m/z 436.1617.

(3-(1-(3-((4-fluorophenyl)amino)-3-oxopropyl)-1H-1,2,3-triazol-4-yl)propanoyl) fmoc-lysine (37a): 90 mg, yield 79%. ^{1}H-NMR (300 MHz, Acetone-d6): δ 7.86-7.60 (6H, m), 7.33 (4H, td, J=11.1 Hz), 7.15 (1H, d, J=41.7 Hz), 7.05 (2H, t, J=8.85 Hz), 4.69-4.64 (2H, m), 4.55-4.31 (10H, m), 4.24-4.18 (3H, m), 3.99-3.91 (5H, m), 3.46 (4H, q, J=7.3 Hz), 1.28 (2H, s). ^{13}C NMR (300MHz, Acetone-d6): δ 193.89, 191.01, 186.43, 184.74, 147.92 (2C), 145.45 (2C), 129.46 (2C), 128.90 (2C), 127.07, 123.12, 122.90, 121.76 (2C), 116.80 (2C), 110.88, 92.67, 86.81 (2C), 77.46, 67.72, 56.76 (2C), 49.08, 47.35, 44.73, 41.66, 27.04, 19.77, 18.39, 14.23. HRMS (ESI) for $C_{35}H_{37}FN_6O_6$ $[M+H]^+$: calcd. m/z 657.2813, observed m/z 657.2831.

(3-(1-(6-((4-fluorophenyl)amino)-6-oxohexyl)-1*H*-1,2,3-triazol-1-yl)propanoyl) glycine (31b): 60 mg, yield 84%. ^{1}H-NMR (300 MHz, $CDCl_3$): δ 7.47 (2H, dd, J=4.4 Hz), 7.18 (1H, bs), 7.01 (2H, d, J=9.2 Hz), 3.29 (2H, t, J=6.8 Hz), 3.37 (2H, t, J=7.5 Hz), 1.82-1.60 (5H, m), 1.52-1.408 (7H, m), 0.85 (2H, t, J=7.1 Hz). ^{13}C NMR (300MHz, Acetone-d6): δ 173.82, 172.96, 172.64, 123.49, 122.75 (2C, d, J=8 Hz), 116.87 (2C, d, J=22.2 Hz), 89.81, 85.66, 77.43, 75.70, 51.20, 42.41, 38.26, 36.81, 27.65, 26.57, 23.22. HRMS (ESI) for $C_{19}H_{24}FN_5O_4$ $[M+H]^+$: calcd. m/z 406.1908, observed m/z 406.1885.

(3-(1-(6-((4-fluorophenyl)amino)-6-oxohexyl)-1*H*-1,2,3-triazol-1-yl)propanoyl) valine (32b): 50 mg, yield 64%. ^{1}H-NMR (300 MHz, CD_3OD): δ 7.58 (1H, bs), 7.34-7.29 (2H, m), 6.82 (2H, t, J=8.7 Hz), 4.16 (3H, t, J=6.8 Hz), 2.78 (2H, bs), 2.44(2H, bs), 2.14 (2H, t, J=7.4 Hz), 1.94 (1H, bs), 1.72 (2H, t, J=7.5 Hz), 1.51 (2H, t, J=7.4 Hz), 1.21-1.08 (3H, m), 0.71 (6H, d, J=6.6 Hz). ^{13}C-NMR (300 MHz, CD_3OD): δ 195.85, 190.31, 185.90, 147.21, 140.42, 140.08, 123.05 (2C), 116.08 (2C, d, J=22.5 Hz), 63.76, 51.02, 37.32, 31.42, 30.78, 26.44(2C), 25.98 (2C), 22.45, 19.48, 18.16 HRMS (ESI) for $C_{22}H_{31}N_5O_4F$ $[M+H]^+$: calcd. m/z 448.2354, observed m/z 448.2341.

(3-(1-(6-((4-fluorophenyl)amino)-6-oxohexyl)-1*H*-1,2,3-triazol-1-yl)propanoyl) proline (33b): 70 mg, yield 90%. ^{1}H-NMR (300 MHz, CD_3OD): δ 8.27 (1H, s), 7.53-7.47 (2H, m), 6.97 (2H, t, J=8.6 Hz), 4.62-4.54 (1H, m), 4.38-4.19 (3H, m), 3.67-3.41 (3H, m), 2.97-2.54 (4H, m), 2.32-2.26 (3H, m), 1.80-1.75 (7H, m), 1.75-1.63 (2H, m). ^{13}C-NMR (300 MHz, CD_3OD): δ 198.73, 194.98, 191.08, 161.96, 135.62, 126.62, 122.85 (2C, d, J=8 Hz), 116.03 (2C, d, J=22.4 Hz), 111.09, 59.98, 50.81, 48.12, 37.23, 34.32, 30.69, 30.11, 26.78, 25.88, 25.41, 21.35. HRMS (ESI) for $C_{22}H_{29}N_5O_4F$ $[M+H]^+$: calcd. m/z 446.2198; observed m/z 446.2199.

(3-(1-(6-((4-fluorophenyl)amino)-6-oxohexyl)-1*H*-1,2,3-triazol-1-yl)propanoyl) phenylalanine (34b): 74 mg, yield 85%. ^{1}H-NMR (300 MHz, CD_3OD): δ 7.42 (1H, s), 7.34 (2H, dd, J=4.7 Hz), 7.09-6.99 (5H, m), 6.84 (2H, t, J=8.9 Hz), 4.46 (1H, q, J=4,6 Hz), 4.14 (2H, t, J=6.9 Hz), 3.01 (1H, dd, J=4.8 Hz), 2.77-2.68 (3H, m), 2.31 (2H, t, J=6.9 Hz), 2.15 (2H, t, J=7.5 Hz), 1.76-1.66 (2H, m), 1.56-1.46 (2H, m), 1.20-1.10 (2H, m). ^{13}C-NMR (300 MHz, CD_3OD): δ 173.01, 172.99, 172.81, 153.61, 137.26,

134.71, 130.41, 128.89 (2C), 128.05 (2C), 126.38, 124.56, 121.72 (2C, d, J=7.8 Hz), 114.85 (2C, d, J=22.4 Hz), 53.83, 49.70, 37.09, 36.10, 34.64, 29.54, 25.63, 24.74, 21.02. HRMS (ESI) for $C_{26}H_3FN_5O_4$ $[M+H]^+$: calcd. m/z 496.2351; observed m/z 496.2355.

(3-(1-(6-((4-fluorophenyl)amino)-6-oxohexyl)-1*H*-1,2,3-triazol-1-yl)propanoyl) tyrosine (35b): 57 mg, yield 64%. ^{1}H-NMR (300 MHz, CD_3OD): δ 7.46-7.42 (3H, m), 6.97-6.91 (3H, m), 6.60 (2H, d, J=8.4 Hz), 4.51-4.47 (1H, m), 4.23 (2H, t, J=7.1 Hz) 3.24-3.21 (1H, m), 3.01 (1H, dd, J=6.1 Hz), 2.84-2.70 (3H, m), 2.43 (2H, t, J=7.1 Hz), 2.25 (2H, t, J=7.4 Hz), 1.85-1.75 (2H, m), 1.66-1.53 (2H, m), 1.29-1.66 (2H, m). ^{13}C-NMR (300 MHz, CD_3OD): δ 175.37, 174.33, 174.24, 157.26, 131.30 (2C), 129.36, 123.54, 123.12 (2C, d, J=7.8 Hz), 116.24 (2C, d, J=22.4 Hz), 116.19 (2C), 55.68, 51.08, 37.76, 37.5, 36.08, 30.94, 27.01, 26.14, 22.42. HRMS (ESI) for $C_{23}H_{25}N_5O_5F$ $[M+H]^+$: calcd. m/z 512.2303; observed m/z 512.2303.

(3-(1-(6-((4-fluorophenyl)amino)-6-oxohexyl)-1*H*-1,2,3-triazol-1-yl)propanoyl) glutamic acid (36b): 76 mg, yield 91%. ^{1}H-NMR (300 MHz, CD_3OD): δ 7.56 (1H, s), 7.36-7.31 (2H, m), 6.84 (2H, t, J=10.5 Hz), 4.26-4.16 (3H, m), 3.13-3.11 (2H, m), 2.08 (2H, t, J=7.2 Hz), 2.41 (2H, t, J=7.4 Hz), 2.15 (4H, td, J=10.5 Hz), 2.03-1.91 (1H, m), 1.79-1.77 (2H, m), 1.69-1.67 (2H, m), 1.22-1.10 (2H, m). ^{13}C-NMR (300 MHz, CD_3OD): δ 176.33, 175.05, 175.05, 174.71, 167.04, 145.36, 134.79, 123.67, 123.13 (2C, d, J=8 Hz), 116.25 (2C, d, J=22.5 Hz), 53.22, 51.14, 37.51, 36.10, 31.25, 30.95, 27.93, 27.06, 26.16, 22.40. HRMS (ESI) for $C_{22}H_{29}N_5O_6F$ $[M+H]^+$: calcd. m/z 478.2096; observed m/z 478.2099.

(3-(1-(6-((4-fluorophenyl)amino)-6-oxohexyl)-1*H*-1,2,3-triazol-1-yl)propanoyl) lysine (37b): 102 mg, yield 84%. ^{1}H-NMR (300 MHz, Acetone-d6): δ 9.24 (1H, bs), 7.77 (6H, dd, J=44.4 Hz), 7.42-7.29 (4H, m), 7.05 (2H, t, J=8.1 Hz), 4.53-3.87 (16H, m), 3.37 (2H, d, J=5.4 Hz), 3.15 (2H, bs), 2.35 (2H, bs), 1.97 (2H, bs), 1.68 (2H, bs), 0.87 (1H, bs). ^{13}C NMR (300MHz, Acetone-d6): δ 175.03, 173.64, 173.05, 172.51, 146.15 (2C), 143.05 (2C), 129.36 (2C), 128.93 (2C), 127.16 (2C), 123.59, 122.86, 121.8 (2C), 116.85 (2C, d, J=23.6 Hz), 107.64, 93.38, 89.81 (2C), 77.39, 75.73 (2C), 67.73, 56.42, 53.93, 51.24, 44.12, 27.65, 27.04, 26.58, 24.58, 23.28, 13.96. HRMS (ESI) for $C_{38}H_{41}FN_6O_6$ $[M+H]^+$: calcd. m/z 699.3304, observed m/z 699.3301.

Chapter 3:
Click Chemistry Approach for Modified Amino Acids as Sites for Biomolecules Functionalization

Chapter 4: Synthesis and *in Vitro* Evaluation of a Novel Radioligand for $\alpha_v\beta_3$ Integrin Receptor Imaging: [^{18}F]FPPA-c[RGDfK]*

Alessandra Monaco[a,b], Vincent Zoete[c], Gian Carlo Alghisi[d], Curzio Rüegg[d,e], Olivier Michelin[c], John Prior[f], Leonardo Scapozza[b] and Yann Seimbille[a,b*]

[a]Cyclotron Unit, University Hospital of Geneva, Rue Gabrielle Perrte-Gentil 4, Geneva 1211, Switzerland.; [b]School of Pharmaceutical Sciences, University of Geneva and University of Lausanne, Quai Ernest Ansermet 30, Geneva 12 11, Switzerland; [c]Swiss Institute of Bioinformatics, University of Lausanne, Quartier Sorge, Lausanne 1015, Switzerland ; [d]University of Lausanne, Division of Experimental Oncology, Multidisciplinairy Oncology Canter, Chemin des Boveresses 155, Lausanne 1066, Switzerland; [e]University of Fribourg, Faculty of Science, Department of Medicine, Rue Albert Gockel 1, Fribourg 1700, Switzerland; [f]CHUV, Department of nuclear Medicine, Rue du Bugnon 46, Lausanne 1011, Switzerland

*A. Monaco et al. *Bioorganic and Medicinal Chemistry Letters* **2013**, 23, 6068–6072

Abstract: The development of RGD-based antagonist of αvβ3 integrin receptor has enhanced the interest in PET probes to image this receptor for the early detection of cancer, to monitor the disease progression and the response to therapy. In this work, a novel prosthetic group (*N*-(4-fluorophenyl)pent-4-ynamide or FPPA) for the ^{18}F-labeling of an αvβ3 selective RGD-peptide was successfully prepared. [^{18}F]FPPA was obtained in three steps with a radiochemical yield of 44% (decay corrected). Conjugation to c(RGDfK(N_3)) by the Cu(II) catalyzed Huisgen azido alkyne cycloaddition provided the [^{18}F]FPPA-c(RGDfK) with a radiochemical yield of 29% (decay corrected), in an overall synthesis time of 140 min.

Keywords: αvβ3 integrin; c(RGDfK); click chemistry; [^{18}F]-labeling; positron emission tomography

4.1 Introduction

Angiogenesis is an important process for tumor growth, invasion and metastasis. **[1]** Integrins, which are cell-surface heterodimers formed by the noncovalent association of two subunits (α and β play an important role in the formation of new blood vessels.[2] The αvβ3 integrin is the most promiscuous of all integrins and is up-regulated in angiogenic endothelial cells during wound healing and cancer. In addition, αvβ3 overexpression is associated with increased metastatic potential and, as result, αvβ3 has been chosen as therapeutic targets.[3] The arginine-glycine-aspartate (RGD) motif is the natural ligand sequence recognized by several integrins, including αvβ3 and RGD-based soluble peptides have been developed as antagonistic compounds (such as cilengitide) to selectively inhibit αvβ3 integrin. Such peptides are currently tested in clinical trials for their antiangiogenic and anti-tumoral activities.[4-6]

Ligands for molecular imaging based on RGD peptides have already been radiolabeled with ^{99m}Tc, ^{111}In and ^{123}I for single photon emission computed tomography (SPECT) imaging, while ^{68}Ga, ^{64}Cu and ^{18}F ($t_{1/2}$ = 109.8 min, 97% β^+, E_{max} = 0.64 MeV) have been widely investigated to radiolabel RGD peptides for positron emission tomography (PET).[7-10] All those radiotracers have been evaluated in animal models and recently the FDA has approved first trial with [^{18}F]FPP(RGD)$_2$ (IND104150).[11] The specificity of this probe against αvβ3 integrin has been

*A. Monaco et al. *Bioorganic and Medicinal Chemistry Letters* **2013**, 23, 6068–6072

demonstrated *in vivo* and on tissue sections with competition with unlabeled peptides or irrelevant peptides. However, some concerns were raised since the fixation was not solely restricted to endothelial cells. Moreover, the preparation of this ^{18}F-labeled RGD dimer is challenging, which may considerably hamper its applications in patients.[12] Thus, there is a need for a more accessible probe to provide noninvasive quantitative imaging of αvβ3 integrin expression for the evaluation and optimization of novel antiangiogenic therapeutic compounds, as well as for the appropriate selection of cancer patients entering clinical trials with such therapeutic drugs.

Labeling of biomolecules with fluorine-18 is usually accomplished through the conjugation of a targeting entity with a radioactive prosthetic group.[13] In the present study, we aimed at labeling c(RGDfK), a cyclic peptide known to bind with high affinity and selectivity to αvβ3 integrin, with a radiolabeled prosthetic group *N*-(4-[^{18}F]fluorophenyl)pent-4-ynamide ([^{18}F]**3** or [^{18}F]FPPA).

4.2 Results and discussion

4.2.1 Design of a peptide sequence for $\alpha_v\beta_3$ imaging

In silico molecular docking was initially performed to check whether the presence of the prosthetic group (FPPA) into this structurally constrained cyclic pentapeptide might influence the binding with the receptor. The minor contact with the protein surface of the valine residue of cilengitide suggests that it could be easily replaced by a lysine to provide an anchor point to generate multivalent ligands or to conjugate drugs or radiolabeled moieties. Suggestion of a sequence modification of the cyclic pentapeptide allowing the addition of FPPA without compromising the binding affinity towards αvβ3 integrin was made by the calculation of the binding free energy contributions made by each residue of c(RGDfV) (cilengitide), in complex with αvβ3 integrin (PDB ID 1L5G).[14] We chose to convert the primary amine on the side chain of the lysine residue into an azide to facilitate the addition of the prosthetic group to the RGD peptide by using the Huisgen's click reaction. This reaction was selected due to its high selectivity and efficiency, the rapid formation of the triazole in presence of copper catalyst, and the ease of purification of the final product.[15] All those advantages are of crucial importance while we perform labeling with trace amount of a short half-life radionuclide, such as fluorine-18. Several cyclic peptides

*A. Monaco et al. *Bioorganic and Medicinal Chemistry Lett*ers **2013**, 23, 6068–6072

coupled to the prosthetic group were docked to the surface of αvβ3 using the EADock program.[16, 17] The results demonstrated that the binding mode of the RGDf fragment of the peptide, which is responsible for the major part of the interaction between the ligand and the binding domain of αvβ3, is conserved. The prosthetic group is oriented towards solvent and remains at the surface of the integrin receptor. Thus, the modification on the lysine residue and the incorporation our radiolabeled prosthetic group does not affect the binding of the pentapeptide (**Figure 1**).

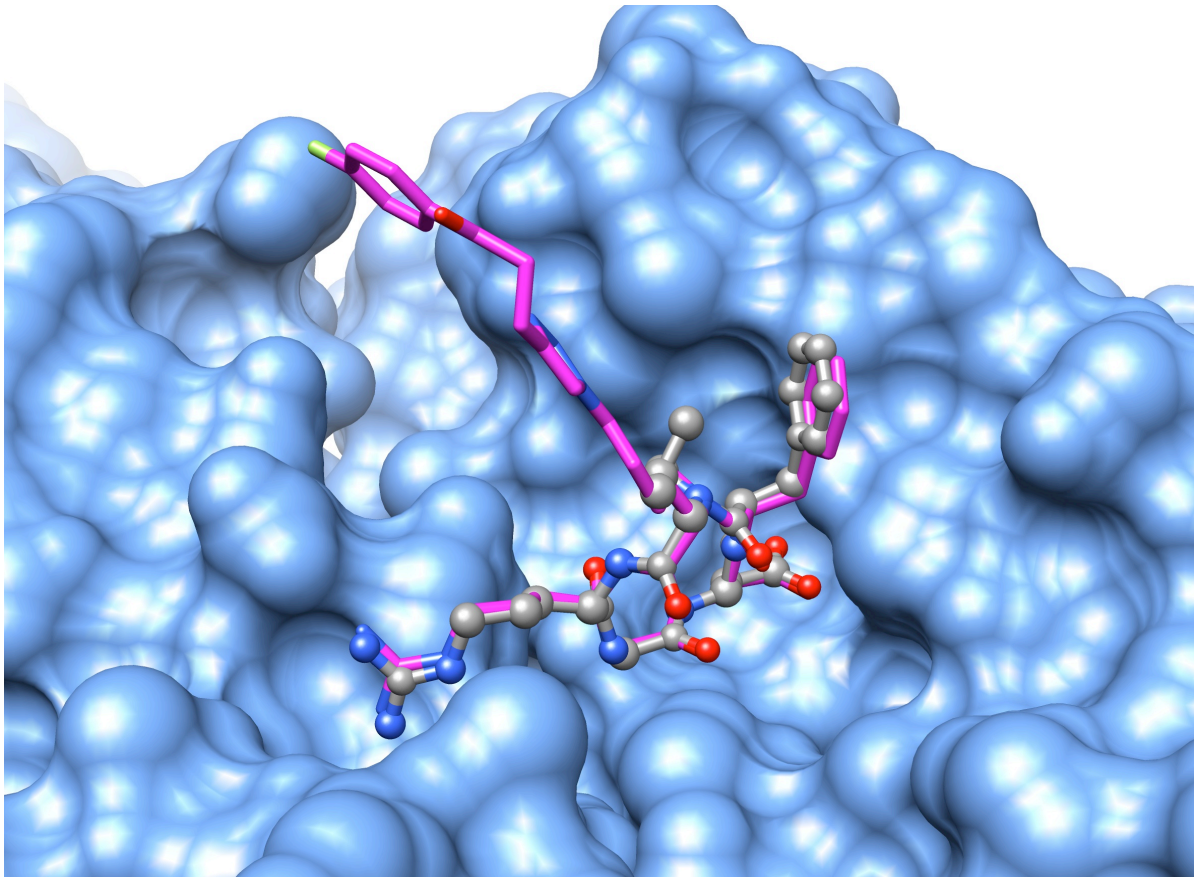

Figure 1| Binding mode of cilengitide and FPPA-c[RGDfK]
Binding mode of cilengitide and FPPA-c(RGDfK)**.** The experimental binding mode of cilengitide (ball and stick model colored according to the atom types) on the αvβ3 surface (in cornflower blue), compared to the calculated binding mode of FPPA-c(RGDfK) (thick lines, with carbon atoms in magenta).

*A. Monaco et al. *Bioorganic and Medicinal Chemistry Letters* **2013**, 23, 6068–6072

4.2.2 Chemistry and radiochemistry

FPPA (**scheme 1**) has been specially designed to bear a fluorine atom and to possess a terminal alkynyl function. The fluorine atom was implemented at the 4-position of the phenyl ring of FPPA to provide better in vivo stability. Indeed, although incorporation of fluorine-18 into prosthetic groups via substitution reactions usually proceeds better with aliphatic substrates than aromatic compounds, defluorination of aliphatic C-F bond is often observed and leads to bone uptake and artifacts on the PET images.[18-20] Then, a terminal alkynyl group was introduced to the prosthetic group to allow attachment of FPPA to the peptide according to the Huisgen's click reaction.[21] FPPA was synthesized in one step in 91% yield starting from commercially available 4-fluoroaniline (**1**) and 4-pentynoic acid (**2**) (**Scheme 1**).[22] The reaction was performed in dichloromethane in presence of the standard coupling agents 1-ethyl-3-(3-dimethylaminopropyl)carbodiimide (EDC) and 1-hydroxybenzotriazole (HOBt). Then, FPPA was conjugated to c(RGDfK(N_3)) by Huisgen's 1,3-dipolar cycloaddition. The peptide has been synthesized according to a reported method.[23] The reaction occurred in water/THF and was catalyzed by Cu(II) in presence of sodium ascorbate. The latter was used as reducing agent in slight excess (**Scheme 1**).[24] Following the click reaction, the salts were removed by filtration and the final product was purified by HPLC. Identity of FPPA-c(RGDfK) (**5**) was confirmed by MALDI-TOF. Subsequently, **5** has been used as non-radioactive standard for purification and quality control of its radiolabeled analog [^{18}F]-**5** and to confirm binding and selectivity of this RGD peptide to αvβ3 integrin.

*A. Monaco et al. *Bioorganic and Medicinal Chemistry Lett*ers **2013**, 23, 6068–6072

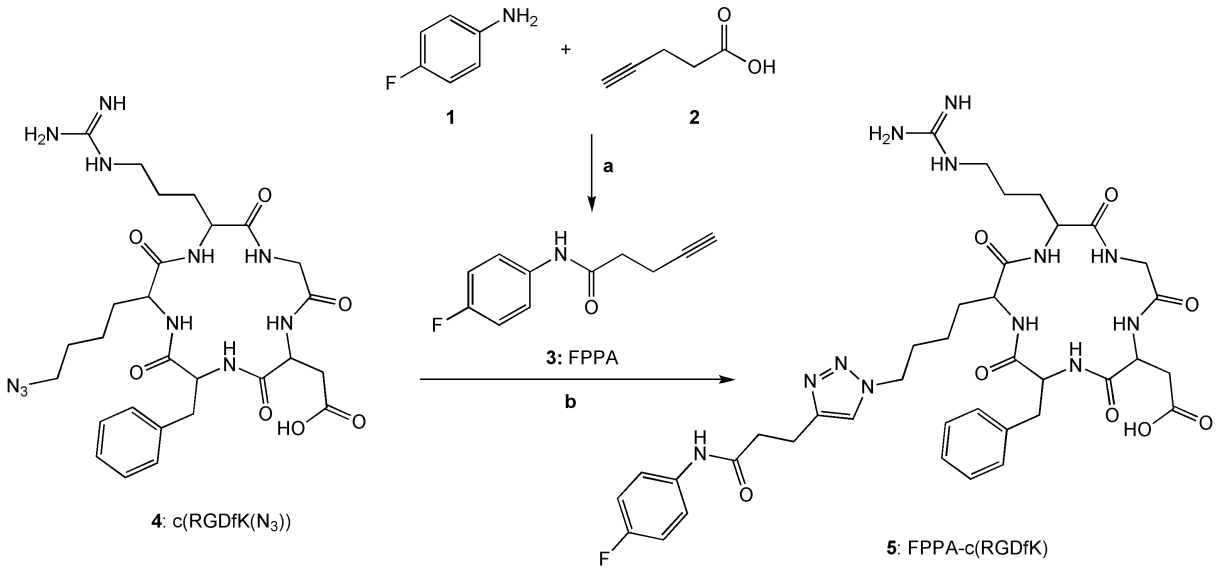

Scheme 1| Synthesis of FPPA-c(RGDfK) (**5**). Reagents and conditions: (a) EDC, HOBt, DCM, rt, overnight, 91%; (b) water/THF, $CuSO_4$ (0.1 M), sodium ascorbate (0.3 M), rt, 1h, 86%.

Considering that fluoride is a poor nucleophile and the low activation of the 4-position on the phenyl ring of FPPA, due to the lack of adjacent electron withdrawing groups, we decided to investigate two radiochemical routes for the preparation of [^{18}F]FPPA ([^{18}F]-**3**) (**Scheme 2**). Trimethylammonium salts were synthesized as precursors for the ^{18}F-fluorination reaction. *N*-(4-(trimethylammonium)phenyl)pent-4-ynamide trifluoromethanesulfonate (**8**) and *N*-(4-trimethylammonium)nitrobenzene trifluoromethanesulfonate (**11**) were obtained in two steps from 4-(dimethylamino)aniline (**6**) (**Scheme 2A**) and 4-nitroaniline (**9**) (**Scheme 2B**), respectively. Treatment of **6** with 4-pentynoic acid gave *N*-(4-(dimethylamino)phenyl)pent-4-ynamide (**7**) in 90% yield, while dimethylation of **9** with iodomethane yielded *N,N*-dimethyl-4-nitroaniline (**10**). Finally, methylation of the dimethylamino intermediates **7** and **10** with methyl trifluoromethanesulfonate afforded the trimethylammonium precursors **8** and **11** in 66% and 68% yield, respectively.

*A. Monaco et al. *Bioorganic and Medicinal Chemistry Let*ters **2013**, 23, 6068–6072

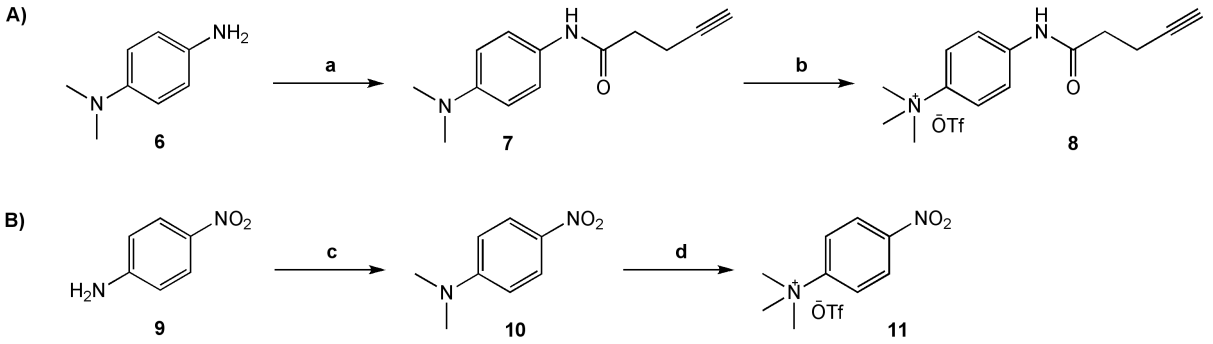

Scheme 2| Synthesis of the trimethylammonium trifluoromethanesulfonate precursors (**8**) (A) and (**11**) (B). Reagents and conditions: (a) **2**, EDC, HOBt, DCM, rt, overnight, 90%; (b) methyl trifluoromethanesulfonate, DCM, 2h, 0°C, 66%; (c) i) NaH, THF, 5 min, rt; ii) MeI, THF, 24h, 73%; (d) methyl trifluoromethanesulfonate, DCM, 0°C, 68%.

The radiolabeled RGD peptide [^{18}F]-**5** or [^{18}F]FPPA-c(RGDfK) was prepared starting with the standard kryptofix-K_2CO_3-mediated nucleophilic ^{18}F-exchange reaction with the trimethylammonium triflate precursors **8** or **11** (**Scheme 3**). Introduction of the fluorine-18 using a no-carrier-added nucleophilic substitution with K[^{18}F]F$^-$/K_{222} was initially conducted with precursor **8** in acetonitrile at 60^{o}C for 10 min, but low radiochemical yield (0.4% decay non corrected) was observed. Therefore, we investigated whether we could improve the nucleophilic incorporation of [^{18}F]fluoride into this trimethylammonium triflate salt by changing the reaction conditions (temperature, time, and solvent). We obtained our best radiochemical yield of 4.9% (decay non-corrected) with respect to initial [^{18}F]fluoride when the reaction was performed in DMSO at 165°C for 12 min. The lack of electron withdrawing groups on the aromatic ring that would favor the fluorination at the 4-position considerably limited the efficacy of this reaction. Therefore, although this one step approach would obviate the need of sophisticated radiochemical route to prepare [^{18}F]FPPA, we considered that it would not provide quantities which are practical for use as PET radiopharmaceuticals. Consequently, a three steps radiochemical route has been established. The first radiochemical step (**Scheme 3B**), which consisted of the ^{18}F-fluorination of our second activated trimethylammonium precursor **11** resulted in [^{18}F]fluoro-nitrobenzene (**12**), with radiochemical yield of 69% (decay non-corrected) when the reaction mixture was heated at 95^{o}C for 10 min in acetonitrile. Then, reduction of the nitro group of [^{18}F]fluoro-nitrobenzene (**12**) with sodium borohydride,

*A. Monaco et al. *Bioorganic and Medicinal Chemistry Lett*ers **2013**, 23, 6068–6072

in presence of palladium on activated carbon, gave 4-[^{18}F]fluoroaniline ([^{18}F]-**1**) as an hydrochloric salt after quenching the reaction with either 1M HCl or 12M HCl, with a radiochemical yields of 45% and 53% (decay corrected) respectively.[25] Identity of [^{18}F]-**1** was confirmed by HPLC analysis by co-elution with authentic unlabeled 4-fluoroaniline (**Figure 1-SD**). Subsequent coupling of 4-[^{18}F]fluoroaniline with the 2,5-dioxopyrrolidin-1-yl pent-4-ynoate (**13**)[26] in dichloromethane in presence of triethylamine afforded the ^{18}F-labeled prosthetic group [^{18}F]-**3** in 44% radiochemical yield (decay corrected) within 40 min (**Figure 2-SD)**.

Finally, [^{18}F]-**3** was conjugated with c(RGDfK(N_3)) following the same procedure used for the preparation of the non-radioactive conjugate (**5**), to obtain the ^{18}F-labeled peptide [^{18}F]-**5** with 66% yield (decay corrected) (**Scheme 3**). [^{18}F]FPPA-c(RGDfK) was then obtained in about 140 min with a total radiochemical yield of 29% (decay corrected). Identity of the new radiopharmaceutical was confirmed by comparing its HPLC mobility with the retention time of the non-radioactive analogue (**Figure 3-SD**).

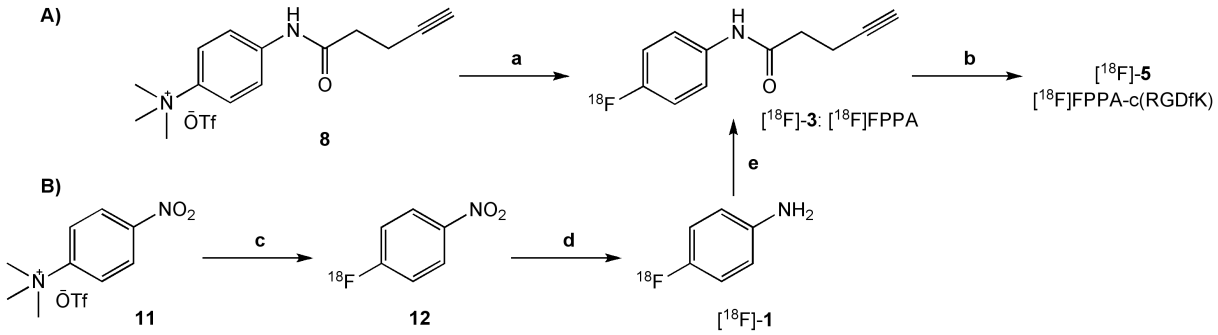

Scheme 3| Synthesis [^{18}F]FPPA ([^{18}F]-**3**). Reagents and conditions: (a) [^{18}F]F^-, K_{222}/K_2CO_3, CH_3CN or DMSO, 60-165°C, 10-15 min, 0.4-5%; (b) **4**, water/THF, $CuSO_4$ (0.3 M), sodium ascorbate (0.7 M), rt, 15 min, 66%; (c) [^{18}F]F^-, K_{222}/K_2CO_3, CH_3CN, 10 min, 95°C, 69%; (d) i) $NaBH_4$, MeOH, Pd/C, rt, 2 min; ii) 12M HCl, rt, 53%; (e) **13**, Et_3N, DCM, 75°C, rt, 10 min, 44%.

4.2.3 Biological results

The affinity of the fluorinated c-(RGDfK) was then experimentally tested with an ELISA *in vitro* assay using recombinant soluble integrins binding to their immobilized natural ligands in the absence or presence of gradual amounts of the test peptide.

*A. Monaco et al. *Bioorganic and Medicinal Chemistry Let*ters **2013**, 23, 6068–6072

Soluble recombinant αvβ3 and α5β1 integrins were expressed in HEK293T cells transfected with cDNA encoding for the α and β subunits of the integrins of interest.[27] All cDNAs encoded for truncated integrins (*i.e.* all integrin subunits lacked their respective transmembrane and C-terminal domains) and were tagged with either a His-tag or fused with a human IgG-Fc-fragment. As a result expressed integrins were secreted in the culture medium ('conditioned medium'). Soluble truncated αvβ3 and α5β1 (α5β1 was used for specificity control) are assumed to adopt a rod-like shape conformation associated with high affinity ligand-binding for their substrate.[27] Then, IC_{50} values were obtained by challenging binding of the integrins to the surface-immobilized matrix protein in the presence of increasing amounts of peptide **5**. A cyclic peptide c(RGDfV), which is the equivalent structure of the cilengitide, was used as control peptide to validate the method. An IC_{50} of 0.51 nM was obtained for c(RGDfV) (**Figure 4-SD**), which is in accordance with what has been previously reported in the literature (IC_{50} ranging from 0.13 to 1.89 nM).[28] For FPPA-c(RGDfK) (**5**), IC_{50} values of 10.6 nM and 3.6 μM were obtained for αvβ3 and α5β1, respectively (**Figure 2**). The difference of binding affinity of **5** between the two integrins tested clearly demonstrates the high specificity of FPPA-c(RGDfK) for αvβ3 integrin. To further characterize the properties of FPPA-c(RGDfK), we performed flow-cytometry analysis on HUVEC (Human Umbilical Vascular Endothelial) cells, which are known to highly express αvβ3 integrin. When bound to integrins, high affinity ligands activate the receptor.[27] The presence of activated αvβ3 integrin can then be detected with a specific antibody LIBS-1 (Ligand Induced Binding Site), which solely recognizes the activated form (ligand bound) of the β3 integrin subunit. To validate that our peptide (**5**) retains the same activity of c(RGDfV) on αvβ3 integrin after binding, cells were incubated with either media (negative control), 1 mM of Mn^{2+} or 10 μM of c(RGDfV) (both are positive controls for activation), or with FPPA-c(RGDfK). The activation of the receptor was observed in cells treated with Mn^{2+}, c(RGDfV) and FPPA-c(RGDfK) (**Figure 5-SD**). This confirms that the cyclic pentapeptide is active towards its receptor, and the presence of the FPPA moderately affects the interaction.

*A. Monaco et al. *Bioorganic and Medicinal Chemistry Letters* **2013**, 23, 6068–6072

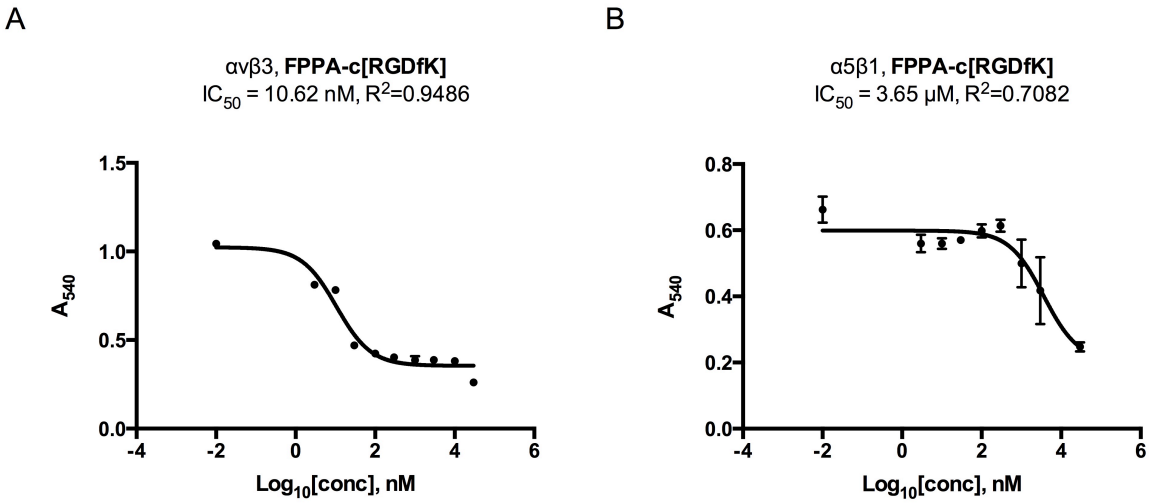

Figure 2| IC_{50} determination of the new peptide for soluble αvβ3 and α5β1 integrins. (**A**) Results of the IC_{50} determination test for the new peptide towards the αvβ3 integrin showing a 10.6 nM value. (**B**) Corresponding IC_{50} value for the α5β1 is proximally 300 times lower than the affinity for αvβ3. The data are the results of experiments done in triplicate, and the standard deviations have been reported as vertical bars.

4.3 Conclusions

In summary, a novel prosthetic group *N*-(4-fluorophenyl)pent-4-ynamide (FPPA) for labeling of biomolecule via click reaction has been proposed. Docking studies confirmed that the presence of FPPA on c(RGDfK) doesn't have a negative influence on the interaction with the αvβ3 integrin receptor. Modeling predictions were correlated with the in vitro measurements of the affinity and the activation of integrin αvβ3 by FPPA-c(RGDfK). [^{18}F]FPPA ([^{18}F]-**3**) was synthetized from *N*-(4-(trimethylammonium)phenyl)pent-4-ynamide trifluoromethanesulfonate (**8**) by direct [^{18}F]fluorination in position 4, or from *N*-(4-trimethylammonium)nitrobenzene trifluoromethanesulfonate (**11**) by a nucleophilic aromatic fluorination, a reduction of the nitro group and a conjugation with the alkynyl chain. The three steps strategy gave a better radiochemical yield (44% decay corrected). The Cu(II)-catalyzed azido-alkyne Huisgen's cycloaddition has been adopted to attach our prosthetic group with the RGD-based peptide. This strategy yielded the final radiopharmaceutical [^{18}F]FPPA-c(RGDfK) in 140 min total synthesis with a radiochemical yield of 29% (decay corrected).

*A. Monaco et al. *Bioorganic and Medicinal Chemistry Let*ters **2013**, 23, 6068–6072

4.4 References

1. Desgrosellier, J.S. and D.A. Cheresh, *Integrins in cancer: biological implications and therapeutic opportunities.* Nat Rev Cancer, 2010. **10**(1): p. 9-22.
2. Alghisi, G.C. and C. Ruegg, *Vascular integrins in tumor angiogenesis: Mediators and therapeutic targets.* Endothelium-Journal of Endothelial Cell Research, 2006. **13**(2): p. 113-135.
3. Nip, J., et al., *Human-Melanoma Cells Derived from Lymphatic Metastases Use Integrin Alpha-V-Beta-3 to Adhere to Lymph-Node Vitronectin.* Journal of Clinical Investigation, 1992. **90**(4): p. 1406-1413.
4. Stupp, R. and C. Ruegg, *Integrin inhibitors reaching the clinic.* Journal of Clinical Oncology, 2007. **25**(13): p. 1637-1638.
5. *Cilengitide (EMD 121974) in Treating Patients With Advanced Solid Tumors or Lymphoma*. 2013 [cited 2013.
6. *Cilengitide in Treating Children With Refractory Primary Brain Tumors*. 2013 [cited 2013.
7. Dumont, R.A., et al., *Novel 64Cu- and 68Ga-Labeled RGD Conjugates Show Improved PET Imaging of αvβ3 Integrin Expression and Facile Radiosynthesis.* Journal of Nuclear Medicine, 2011. **52**(8): p. 1276-1284.
8. Hao, G., et al., *Cyclization of RGD peptide sequences via the macrocyclic chelator DOTA for integrin imaging.* Dalton Transactions, 2012. **41**(46): p. 14051-14054.
9. Paeng, J., et al., *Feasibility and kinetic characteristics of 68Ga-NOTA-RGD PET for in vivo atherosclerosis imaging.* Annals of Nuclear Medicine, 2013: p. 1-8.
10. Inkster, J.A.H., et al., *Radiosynthesis and bioconjugation of [18F]FPy5yne, a prosthetic group for the 18F labeling of bioactive peptides.* Journal of Labelled Compounds and Radiopharmaceuticals, 2008. **51**(14): p. 444-452.
11. Liu, S., et al., *18F-labeled galacto and PEGylated RGD dimers for PET imaging of alphavbeta3 integrin expression.* Mol Imaging Biol, 2010. **12**(5): p. 530-8.
12. Chen X, et al., *Micro-PET imaging of alphavbeta3-integrin expression with 18F-labeled dimeric RGD peptide.* Mol. Imaging, 2004. **3**(2): p. 96 - 104.

13. Li, Z. and P.S. Conti, *Radiopharmaceutical chemistry for positron emission tomography.* Adv Drug Deliv Rev, 2010. **62**(11): p. 1031-51.
14. Wu, Y., W. Cai, and X. Chen, *Near-infrared fluorescence imaging of tumor integrin alpha v beta 3 expression with Cy7-labeled RGD multimers.* Mol Imaging Biol, 2006. **8**(4): p. 226-36.
15. Gill, H.S. and J. Marik, *Preparation of 18F-labeled peptides using the copper(I)-catalyzed azide-alkyne 1,3-dipolar cycloaddition.* Nat Protoc, 2011. **6**(11): p. 1718-25.
16. Grosdidier, V. Zoete, and O. Michielin, *EADock: docking of small molecules into protein active sites with a multiobjective evolutionary*

optimization. Proteins, 2007. **67**: p. 1010-1025.

17. Grosdidier, A., V. Zoete, and O. Michielin, *Blind docking of 260 protein–ligand complexes with EADock 2.0.* Journal of Computational Chemistry, 2009. **30**(13): p. 2021-2030.
18. Poethko, T., et al., *Two-Step Methodology for High-Yield Routine Radiohalogenation of Peptides: 18F-Labeled RGD and Octreotide Analogs.* Journal of Nuclear Medicine, 2004. **45**(5): p. 892-902.
19. Tipre, D.N., et al., *PET Imaging of Brain 5-HT1A Receptors in Rat In Vivo with 18F-FCWAY and Improvement by Successful Inhibition of Radioligand Defluorination with Miconazole.* Journal of Nuclear Medicine, 2006. **47**(2): p. 345-353.
20. Jahan, M., et al., *Decreased defluorination using the novel beta-cell imaging agent [18F]FE-DTBZ-d4 in pigs examined by PET.* EJNMMI Research, 2011. **1**(1): p. 33.
21. Kolb, H.C. and K.B. Sharpless, *The growing impact of click chemistry on drug discovery.* Drug Discov Today, 2003. **8**(24): p. 1128-37.
22. Bessis, A.-S., et al., *Alkynyl derivatives as modulators of metabotropic glutamate receptors*, in *World Intellectual Property Office (WIPO). Patent Collaboration Treaty (PCT) Patents*. 2005.
23. van Berkel, S.S., et al., *Application of metal-free triazole formation in the synthesis of cyclic RGD-DTPA conjugates.* Chembiochem, 2008. **9**(11): p. 1805-15.

24. Li, Z.-B., et al., *Click Chemistry for 18F-Labeling of RGD Peptides and microPET Imaging of Tumor Integrin αvβ3 Expression.* Bioconjugate Chemistry, 2007. **18**(6): p. 1987-1994.
25. Seimbille, Y., et al., *Fluorine-18 labeling of 6,7-disubstituted anilinoquinazoline derivatives for positron emission tomography (PET) imaging of tyrosine kinase receptors: synthesis of 18F-Iressa and related molecular probes.* Journal of Labelled Compounds and Radiopharmaceuticals, 2005. **48**(11): p. 829-843.
26. Funder, E.D., et al., *Synthesis of Dopamine and Serotonin Derivatives for Immobilization on a Solid Support.* The Journal of Organic Chemistry, 2012. **77**(7): p. 3134-3142.
27. Alghisi, G.C., L. Ponsonnet, and C. Rüegg, *The Integrin Antagonist Cilengitide Activates αVβ3, Disrupts VE-Cadherin Localization at Cell Junctions and Enhances Permeability in Endothelial Cells.* PLoS ONE, 2009. **4**(2): p. e4449.
28. Tentori, L., et al., *The integrin antagonist cilengitide increases the antitumor activity of temozolomide against malignant melanoma.* Oncology Reports, 2008. **19**(4): p. 1039-1043.

4.5 Supporting Data

4.5.1 General

Chemicals, TLC and flash chromatography

All the reagents and solvents were purchased from Sigma-Aldrich, Fluka or VWR and were used without further purification. TLCs were run on VWR silica gel 60 F_{254} pre-coated plastic sheets. The compounds were localized by UV lamp at 254 nm or by brief immersion in potassium permanganate solution. Radioactive spots on TLC were detected with a Cyclone Phosphoimager (Perkin-Elmer). Flash chromatography columns were conducted on silica gel (0.063-0.200 mm).

HPLC

HPLC were performed with an Ultimate 3000 RS from Dionex with a Gemini C18 column (250 x 4.6 mm, 5 µm) from Phenomenex operated at a flow rate of 1 mL/min with a linear gradient over 20 minutes from 10 to 100% CH_3CN in water. UV detector was set at four different wavelengths: 215 nm, 220 nm, 254 nm and 280 nm. Radioactivity was detected by connecting the outlet of the UV-photometer to a NaI detector. The data were processed by Chromeleon 6.8 software package from Dionex.

Spectrometry: NMR and MS

^{1}H NMR and ^{13}C NMR were recorded on a Varian Gemini 2000 NMR Spectrometer, Oxford 300 Nuclear Magnetic Instrument. The samples were dissolved in $CDCl_3$ or DMSO-d_6 (Cambridge Isotopes Laboratories Inc.) and the data were processed by MestRe-C software. Chemical shifts are expressed in ppm (δ) relative to the standard and coupling constants (J) in Hz. MS analyses were obtained with an API 150EX ESI-MS instrument from AB/MDS (Sciex) whereas HRMS were acquired on an ESI/nanoESI-IT Esquire 3000 plus from Bruker.

Antibodies, peptides and proteins

The anti-β3 ligand-induced binding site mAb LIBS-1 was kindly provided by Dr. M. Ginsberg, University of California San Diego (La Jolla, CA.)**.** The equivalent structure of cilengitide c(RGDfV) was purchased from Bachem, and c-(RGDfK(N_3)) was synthesized at the Institute of Biochemistry of the University of Lausanne according

to the procedure reported by van Berkel et al.[1] Human plasma fibronectin and human fibrinogen were purchase from Sigma.

Soluble recombinant integrins

cDNA for the expression of the soluble recombinant $\alpha_v\beta_3$ (human Fc fagged) $\alpha_{iib}\beta_3$ and $\alpha_5\beta_1$ (6-HIS tagged) were obtained from Urs Greber (University of Zürich and Timothy Springer, Center for Blood research, Boston, MA) or from the mammalian gene collection (Source Biosciences, UK). Paired plasmids encoding the α and β subunits of interest were co-transfected into HEK 293T cells by lipofectamin (Life Technologies). Conditioned supernatants (Opti-MEM medium) were collected 3 days after transfection and stored at 4°C for immediate use or -20°C for long-term storage.[2]

4.5.2 Chemistry

*N-(4-fluorophenyl)pent–4-ynamide (*FPPA, ***3****)*

To a solution of 4-fluoro aniline (**1**) (1.21 g, 8.92 mmol) in DCM (30 mL) 4-pentynoic acid (**2**) (1 g, 8.89mmol), HOBT (1.18 g, 13.38 mmol) and EDC·HCl (2.05 g, 10.7 mmol) were added. The reaction was stirred overnight at room temperature. Then it was quenched with water and the organic layer was washed with 1 M $NaHCO_3$, dried over Na_2SO_4, filtered and the solvent was removed under reduced pressure. The crude product was purified by flash chromatography Hexane:Et_2O (3:2), 1.55g of a white solid were obtained, yield 91%. ^{1}H-NMR (300 MHz, $CDCl_3$) δ: 7.49-7.44 (3H, m), 7.01 (2H, dt, J_d=2.1, J_t=17.1 Hz), 2.61–2.58 (4H, m,), 2.07 (1H, t, J=4.5 Hz) ppm. ^{13}C-NMR (300 MHz, $CDCl_3$) δ: 197.03, 161.04, 121.83, 115.66 (2C, d, J= Hz), 115.93 (2C, d, J= 22.5 Hz), 69.81, 38.24, 36.13, 14.78 ppm. HRMS (ESI) for $C_{11}H_{11}FON$ $[M+H]^+$: expected m/z 192.0825, observed m/z 192.0824.

*Synthesis of FPPA-c(RGDfK) (****5****)*

c(RGDfK) (1 mg) and **3** (7 mg) were dissolved in water/THF (400 µL). $CuSO_4$ (100 µL, 0.1 M) and sodium ascorbate (100 µL, 0.3 M) were added. The reaction mixture was stirred for 1h at room temperature. The crude was filtered and purified by HPLC to obtain a white powder with 86% yield. MS (MALDI-TOF) for $C_{38}H_{50}FN_{12}O$ $[M+H]^+$: expected *m/z* 821.8771, observed *m/z* 822.1848.

*A. Monaco et al. *Bioorganic and Medicinal Chemistry Lett*ers **2013**, 23, 6068–6072

*N-(4-(dimethylamino)phenyl)pent-4-ynamide (**7**)*

To a solution of 4-dimethylamino aniline (**6**) (1.01 g, 9.12 mmol) in DCM (30 mL) 4-pentynoic acid (**2**) (1 g, 10.19 mmol), HOBt (1.57 g, 10.28 mmol) and EDC·HCl (2.69 g, 14.05 mmol) were added. The reaction was stirred overnight at rt, then quenched with water and the organic layer was washed with 1 M $NaHCO_3$, dried over Na_2SO_4, then filtered. Solvent was removed by reduced pressure and the crude product was purified by flash chromatography with Hexane/Et_2O (3:2) to obtain 1.8 g of grey crystals, 90% yield. ^{1}H-NMR (300 MHz, DMSO-d6) δ: 9.66 (1H, s), 7.39 (2H, d, J=9 Hz), 6.66 (2H, d, J=9 Hz), 2.83 (6H, s), 2.79 (1H, sb), 2.44 (4H, s) ppm. ^{13}C-NMR (300 MHz, DMSO-d6) δ: 168.28, 146.86, 128.96, 120.37 (2C), 112.57 (2C), 83.70, 71.36, 40.44 (2C), 34.94, 14.12 ppm ppm. MS (ESI): m/z 217.3 $[M+H]^+$.

N-(4-(trimethylammonium)phenyl)pent-4-ynamide trifluoromethanesulfonate (**8**)

7 (200 mg, 0.9 mmol) was dissolved in 2.5 mL of DCM at 0°C in inert atmosphere. Methyl trifluoromethanesulfonate (0.16 mL, 1.8 mmol) was slowly added. After 16 hours overnight light brown crystals formed, and were filtered off and recrystallized in acetone/Et_2O to obtain 150 mg of white crystals, yield 66%.^{1}H-NMR (300 MHz, DMSO-d6) δ: 10.07 (1H, s), 7.56 (2H, d, J=8.7 Hz), 7.45 (2H, d, J=8.7 Hz), 3.24 (9H, s), 2.23-2.14 (5H, m) ppm. ^{13}C-NMR (300 MHz, DMSO-d6) δ: 169.89, 141.65, 140.09, 121.08 (2C), 119.38 (2C), 83.37, 71.56, 56.55 (3C), 35.13, 13.98 ppm. HRMS (ESI) for $C_{14}H_{19}N_2O^+$ $[M]^+$: expected m/z 231.1503, observed m/z 231.1492

*N,N-dimethyl-4-nitroaniline (**10**)*

NaH (0.7 g, 28 mmol) was dissolved in anhydrous THF (15 mL) and **9** (1.12 g, 8.18 mmol) was slowly added. The reaction was stirred for 5 minutes at room temperature and a solution of MeI (2.84 g, 41.76 mmol) in anhydrous THF (5 mL) was added. The reaction mixture was stirred at room temperature for 24h. Water (30 ml) was added and the solution extracted twice with EtOAc. The organic layer was dried over Na_2SO_4, filtered and the solvent removed under reduced pressure. The crude product was purified by flash chromatography with hexane:Et_2O (3:2) to obtain 1 g of a yellow powder, yield 73%. ^{1}H-NMR (300 MHz, $CDCl_3$) δ: 8.11 (2H, d, J=9.6 Hz), 6.60 (2H, d, J=9.3 Hz), 3.11 (6H, s) ppm. ^{13}C-NMR (300 MHz, $CDCl_3$) δ: 154.09, 136.96, 126.06 (2C), 110.30 (2C), 40.28 (2C). MS (ESI): m/z 167.4 $[M+H]^+$.

*A. Monaco et al. *Bioorganic and Medicinal Chemistry Letters* **2013**, 23, 6068–6072

*4-trimethylammonium-nitrobenzene trifluoromethanesulfonate (**11**)*

10 (350 mg, 2.1 mmol) was dissolved in anhydrous DCM (4 mL) and cooled at 0°C. Methyl trifluoromethanesulfonate (630 mg, 4.2 mmol) was slowly added and white crystals were slowly forming. After 2h, the crystals were filtered and washed with ice-cooled DCM. They were obtained with 68% yield (260 mg). ^{1}H-NMR (300 MHz, DMSO-d6) δ: 8.47 (2H, d, J=9.6 Hz), 8.27 (2H, d, J=9.6 Hz), 3.67 (9H, s) ppm. ^{13}C-NMR (300 MHz, DMSO-d6) δ: 151.29, 147.82, 125.12 (2C), 122.73 (2C), 56.28 (3C) ppm. HRMS (ESI) for $C_9H_{13}N_2O_2^+$ $[M]^+$: expected m/z 181.0968, observed m/z 181.0971.

*2,5-dioxopyrrolidin-1-yl pent-4-ynoate (**13**)*

2 (500 mg, 9.12 mmol) was dissolved in 15 mL of DCM. *N*-hydroxysuccinimide (1 g, 10.19 mmol), DMAP (1.57 g, 10.28 mmol) and EDC·HCl (2.69 g, 14.05 mmol) were added and the reaction was stirred overnight at rt. The solvent was removed under reduced pressure and the crude product purified by flash chromatography using hexane:EtOAc (3:2). 1.55 g of a white solid were obtained, yield 87%. ^{1}H-NMR (300 MHz, DMSO-d6) δ: 2.90-2.83 (6H, m), 2.60 (2H, dt, J_d=2.4, J_t=7.8 Hz), 2.05 (1H, t, J=2.6 Hz). ^{13}C-NMR (300 MHz, DMSO-d6) δ: 169.11 (2C), 167.18, 81.03, 70.26, 30.46, 25.75 (2C), 14.26. MS (ESI) $[M+H_3O^+]^+$: observed *m/z* 214

4.5.3 Radiochemistry

No-carrier-added fluorine-18 was produced by the irradiation (10 min at 10 μA) of 2 ml of ^{18}O-enriched water (>97% pure) by a proton beam generated by a Cyclone-18/9 cyclotron (IBA). The produced carrier-free [^{18}F]fluoride was trapped on a single use anion-exchange column to remove the excess of [^{18}O]water which was recovered in a separate vial. The trapped [^{18}F]fluoride was eluted from the column with an aqueous solution of potassium carbonate and Kryptofix 222 in acetonitrile, and transferred into the reactor. This solution was warmed at 85°C and then the temperature was increased to 110°C to allow complete evaporation of the solvent. After cooling down the reactor to 40°C, a solution of **8** or **11** dissolved in DMSO or CH_3CN (1 mL) was added to the reactor containing the dry K[^{18}F]F-K_{222} complex, and the mixture was stirred for 10 to 25 min at 30 to 165°C. The reactor was cooled to

*A. Monaco et al. *Bioorganic and Medicinal Chemistry Letters* **2013**, 23, 6068–6072

room temperature; water (8 mL) was added and the solution transferred onto a C18 Sep-Pak. The cartridge was rinsed with 5 ml of water and dried with a flow of argon. The fluorinated intermediates [^{18}F]-**3** and **12** were eluted with MeOH (1.5 ml). The amount of precursor, reaction conditions and radiochemical yields are indicated in Table 1. The radiochemical yields were determined by TLC analysis, while product identities were confirmed by comparing their HPLC retention time with those of the non-radioactive analogues.

The solution of **12** was transferred in a second reactor containing $NaBH_4$ (7 mg) and Pd/C (1 mg). After 2 min at room temperature, concentrated HCl (100 µL) was added and the mixture was filtered. Typically, the ^{18}F-labeled aniline [^{18}F]-**1** was obtained with an overall radiochemical yield of 53% (decay corrected). After evaporation of the solvent, a solution of **13** (10 mg) in DCM (1 ml) and Et_3N (150 µL) was added. The reaction mixture was stirred at 75°C for 10 min and then the solvent was removed. The product was recovered in 6 mL of diethyl ether/hexane (1:2) and passed through a silica Sep-Pak. [^{18}F]FPPA was eluted from the column with 10 mL of diethyl ether/hexane (1:1). After evaporation, [^{18}F]FPPA was obtained within 40 minutes in 44% radiochemical yield (decay corrected).

c(RGDfK(N_3)) (1 mg) in H_2O/THF (0.5 ml) followed by $CuSO_4$ (300 µL, 0.1 M) and sodium ascorbate (300 µL, 0.3 M) were added to the reactor containing [^{18}F]FPPA. The mixture was stirred at room temperature for 15 min and analyzed by HPLC. The final [^{18}F]FPPA-c(RGDfK) was obtained with a radiochemical yield of 29% (decay corrected). Specific activity, determined by using on-line measurements of radioactivity and UV absorption, was > 0.4 GBq/µmol.

*A. Monaco et al. *Bioorganic and Medicinal Chemistry Let*ters **2013**, 23, 6068–6072

Reagent	Amount (mg)	Solvent	Temp (°C)	Time (min)	Product	Yield (% dnc)
8	4	CH_3CN	60	10	[^{18}F]-**3**	0.4
8	3.8	CH_3CN	95	15	[^{18}F]-**3**	0,9
8	4.1	DMSO	120	12	[^{18}F]-**3**	2.1
8	6	DMSO	140	12	[^{18}F]-**3**	2.5
8	5	DMSO	150	12	[^{18}F]-**3**	2.1
8	3.9	DMSO	165	12	[^{18}F]-**3**	4.9
11	4	CH_3CN	30	25	**12**	9.3
11	3.8	CH_3CN	85	25	**12**	48
11	4.1	CH_3CN	95	10	**12**	69

Table 1| Assessment of reaction conditions on ^{18}F-fluorination yields. All the reactions were analyzed by radioactive TLC, and the formation of products [^{18}F]-**3** and **12** were confirmed by HPLC analysis.

HPLC chromatograms

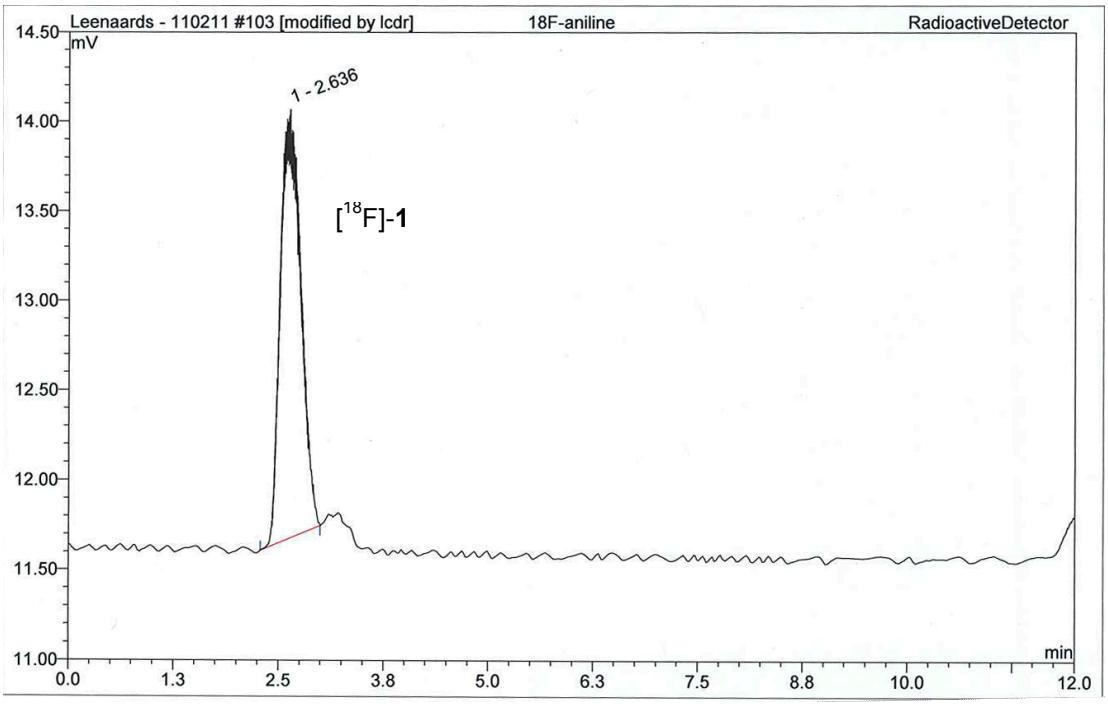

Figure 1-SD. HPLC radiochromatogram of 4-[^{18}F]fluoroaniline ([^{18}F]-**1**). Phenomenex C18 Luna (250 x 10 mm, 5 μm), CH_3CN/H_2O/TFA (50:49.5:0.5), 1 mL/min.

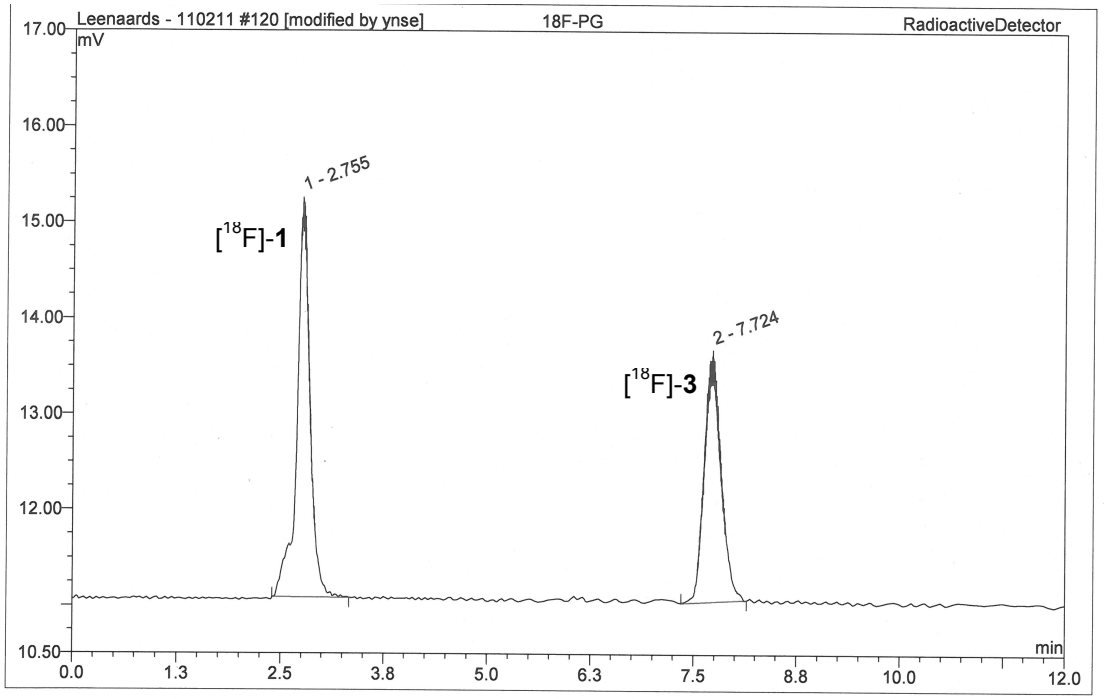

Figure 2-SD. HPLC radiochromatogram of [^{18}F]FPPA ([^{18}F]-**3**). Phenomenex C18 Luna (250 x 10 mm, 5 μm), CH_3CN/H_2O/TFA (50:49.5:0.5), 1 mL/min.

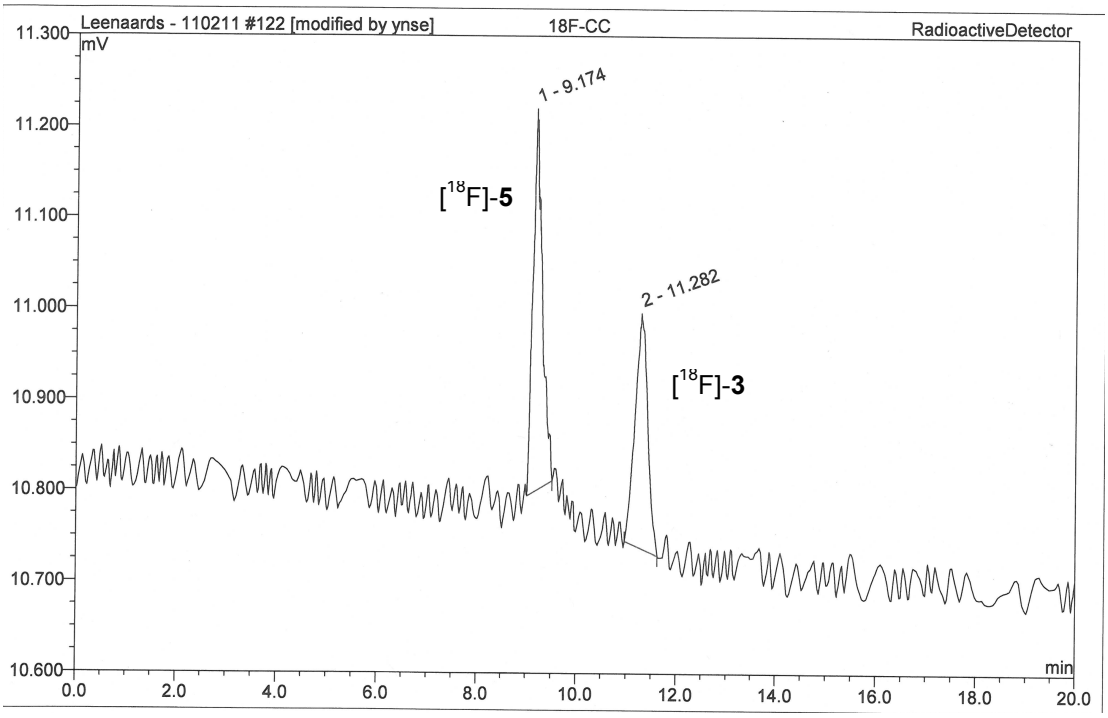

Figure 3-SD. HPLC radiochromatogram of [^{18}F]FPPA-c(RGDfK) ([^{18}F]-**5**). Phenomenex C18 Luna (250 x 10 mm, 5 μm), t=0 CH_3CN/H_2O (1:9) - t=20 CH_3CN, 1 mL/min. Peak at 9.2 min corresponds to [^{18}F]FPPA-c(RGDfK) and peak at 11.3 min corresponds to [^{18}F]-**3**. No traces of [^{18}F]fluoride, **12** or [^{18}F]-**1** (retention time of 2.8 min, 15.5 min and 5.1 min, respectively) were found.

*A. Monaco et al. *Bioorganic and Medicinal Chemistry Lett*ers **2013**, 23, 6068–6072

4.5.4 Competition ELISA

For protein coating, Maxisorp 96 wells ELISA plates (NUNC) were incubated with 0.5 µg/well (50ul) of human plasma fibronectin or human fibrinogen for 16 hours at 4°C in carbonate buffer (pH 8). Wells were washed with PBS, blocked with 2% BSA (200 ul/well) (Sigma) for 2 hours at 37°C. After washing with PBS (3 times 200 µl), recombinant soluble integrins were added to the wells (10 µl conditioned medium in 100 µl final volume) in Opti-MEM medium, in the presence or absence of various amounts of the inhibitors, and incubated for 2 hours at room temperature. Wells were washed again 3 times with PBS, and a goat-anti-human IgG-HRP conjugated polyclonal antibody (Jackson Labs, West Greove, PA) (100 µl / well at 1:8000 dilutions) or a mouse-anti-His6-HRP monoclonal antibody (Roche, Basel, Switzerland) (100 µl / well at 1:500 dilutions) were added and plates incubated for 1 hour at room temperature. After a final wash (4 times with PBS) substrate TMB substrate was added in citrate/phosphate buffer (100 µl/well). After 10-30 minutes reaction was stopped with 50 µl/well sulphuric acid and absorption was measured at 450 nm with reference at 620 nm (Perkin Elmer). Curves were generated by Sigma plot.

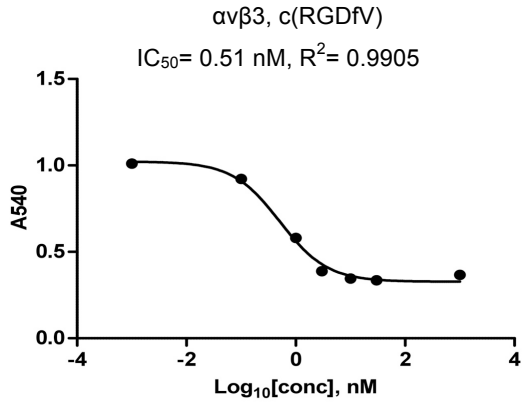

Figure 4-SD. IC_{50} of c(RGDfV). To validate our assay, the IC_{50} of the known peptide c(RGDfV) was measured (0.51 nM) and corresponds with published data.

*A. Monaco et al. *Bioorganic and Medicinal Chemistry Lett*ers **2013**, 23, 6068–6072

4.5.5 FACS analysis

HUVEC were collected by trypsinization, washed twice in PBS/5% FCS and incubated with LIBS-1 primary antibodies for 30 min at 4°C. After washing in cold PBS, cells were incubated with a secondary PE-labeled antibody for 30 min at 4°C. Cells were washed and analyzed with a FACScan II® and Cell Quest® software (Becton Dickinson, Mountain View, California).

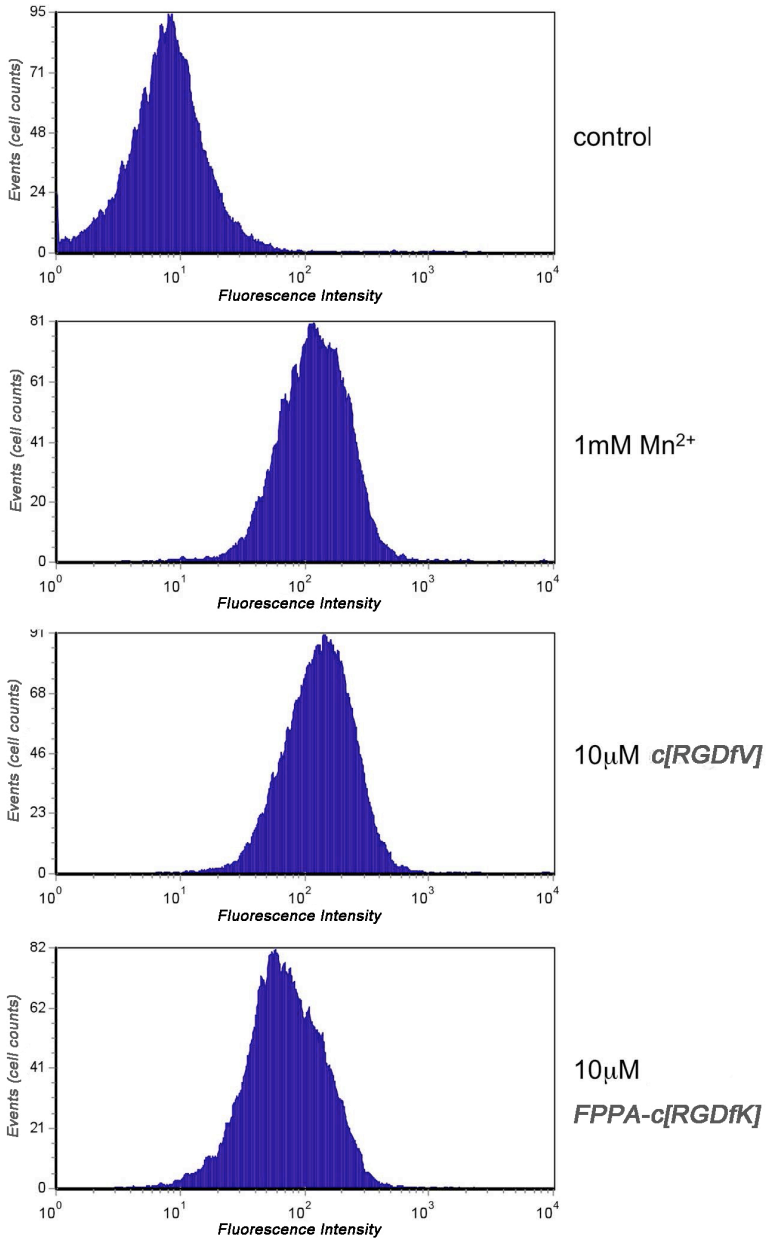

Figure 5-SD. Flow cytometry analysis performed with of FPPA-c(RGDfK) (**5**). The activated $\alpha_v\beta_3$ integrin is detected with the LIBS-1 antibody. Top panel: no compound added (negative control); 2nd and 3rd panels: Mn^{2+} and c(RGDfV), respectively (positive controls); Bottom panel: peptide developed in our study.

*A. Monaco et al. *Bioorganic and Medicinal Chemistry Letters* **2013**, 23, 6068–6072

4.5.6 References (SD)

1. van Berkel, S.S., et al., *Application of Metal-Free Triazole Formation in the Synthesis of Cyclic RGD–DTPA Conjugates.* ChemBioChem, 2008. **9**(11): p. 1805-1815.
2. Alghisi, G.C., L. Ponsonnet, and C. Rüegg, *The Integrin Antagonist Cilengitide Activates αVβ3, Disrupts VE-Cadherin Localization at Cell Junctions and Enhances Permeability in Endothelial Cells.* PLoS ONE, 2009. **4**(2): p. e4449.
Ponsonnet and C. Rüegg, PLoS ONE, 2009, 4, e4449.

Chapter 5: Synthesis of a Novel Non-Peptidic PET Tracer for α5β1 Integrin Receptor*

A. Monaco[1,2], V. Zoete[3], O. Michelin[3], John Prior[3], C. Rüegg[4], L. Scapozza[2] and Y. Seimbille[1,2]

[1]Cyclotron & Radiopharmaceutical Chemistry Unit, Department of Medical Imaging and Information Sciences, University Hospital of Geneva, Geneva, Switzerland; [2]School of Pharmaceutical Sciences, University of Geneva and University of Lausanne, Geneva, Switzerland; [3]CHUV, Department of Nuclear Medicine, Lausanne, Switzerland; [4] University of Fribourg, Department of Medicine, Fribourg, Switzerland.

*A. Monaco et al, *Journal of Labelled Compounds and Radiopharmaceuticals* **2014**, 57, 365-370

Abstract: RGD-containing peptides have been traditionally used as PET probes to non-invasively image angiogenesis, but recently small selective molecules for $\alpha_5\beta_1$ integrin receptor have been developed with promising results. 61 antagonists were screened, and tert-butyl (S)-3-(2-((3R,5S)-1-(3-(1-(2-fluoroethyl)-1H-1,2,3-triazol-4-yl)propanoyl)-5-((pyridin-2-ylamino)methyl)pyrrolidin-3-yloxy)acetamido)-2-(2,4,6-trimethylbenzamido)propanoate (FPMt) was selected for the development of a PET tracer to image the expression of $\alpha_5\beta_1$ integrin receptors. An alkynyl precursor (PMt) was initially synthesized in 6 steps, and its radiolabeling was performed according to the azide-alkyne copper(II) catalyzed Huisgen's cycloaddition by using 1-azido-2-[^{18}F]fluoroethane ([^{18}F]**12**). Different reaction conditions between PMt and [^{18}F]**12** were investigated, but all of them afforded [^{18}F]FPMt in 15 minutes with similar radiochemical yields (80-83%, decay corrected). Overall, the final radiopharmaceutical ([^{18}F]FPMt) was obtained after a synthesis time of 60-70 min in 42-44% decay corrected radiochemical yield.

Keywords: $\alpha_5\beta_1$ integrin receptor; PET, 1-azide-2-[^{18}F]fluoroethane; click chemistry; peptido-mimetic.

5.1 Introduction

Integrins are an extensive group of transmembrane cell adhesion receptors, composed by non covalently linked α and β subunits.[1] They mediate cell migration and cell proliferation by the connection of the extracellular matrix (ECM) with the intracellular cytoskeleton.[2] Activation of the integrins by ligand binding promotes cell proliferation, migration and survival, but unligated or antagonized integrins may activate "integrin-mediated-death".[3] Integrins are of crucial support for the formation of capillaries and angiogenesis in physiological and pathological processes,[4] and three of them ($\alpha_v\beta_3$, $\alpha_v\beta_5$ and $\alpha_5\beta_1$) have a prominent role for the development of new vascular system.[5, 6]
The involvement of these integrins in many diseases such as tumor, thrombosis, cardiovascular and inflammatory diseases, makes them an appealing target for the development of anti-angiogenic therapies.[7, 8] Of

*A. Monaco et al, Journal of Labelled Compounds and Radiopharmaceuticals, in press, January 2014.

them, $\alpha_v\beta_3$ is the most targeted integrin, and several antagonists such as monoclonal antibodies[9, 10] and RGD-based peptides[11] are currently in clinical trials.[7, 12, 13] Moreover radiolabeled analogs of the RGD peptides have been evaluated in preclinical and clinical studies, as tracers, to visualize angiogenesis in growing tumors. [14, 15]

In the last years, integrin $\alpha_5\beta_1$ has gained great interest, not only because of its involvement in tumor angiogenesis but also for its fundamental role in brain angiogenesis.[16] Recently several small molecules have been developed to selectively antagonize this integrin receptor.[17-19] The promising biological results obtained have enhanced the interest in non-α_v integrins as target for new therapies and for imaging to monitor tumor angiogenesis and neurovascular remodeling after ischemic stroke.[16, 20]

In this manuscript, we advance a novel non-peptidic PET tracer designed to image the $\alpha_5\beta_1$ integrin receptor. We report herein a reliable and reproducible procedure to radiolabel this pyrrolidine derivative that relies on: i) the preparation and purification of a widely used radiolabeled synthon 1-azido-2-[^{18}F]fluoroethane, and ii) its subsequent conjugation to our alkynyl precursor (PMt) via the Huisgen's 1,3-dipolar cycloaddition. .

5.2 Experimental

Reagents and instrumentation

All the solvents and reagents were purchased from Sigma-Aldrich and Fluka (Basel, Switzerland) or VWR (Nyon, Switzerland) and were used without further purification. Flash chromatography columns were performed on VWR silica gel (0.063-0.200 mm). Thin layer chromatography (TLC) was performed on pre-coated silica gel 60 F_{254} plastic sheets from VWR. The compounds were monitored under UV at 254 nm or by brief immersion in potassium permanganate solution. Radioactive spots were detected with a Cyclone Phosphoimager from Perkin-Elmer (Waltham, Massachussetts). The radiochemical yields were determined by TLC analysis of reaction mixture samples taken at specified times. High-performance liquid chromatography (HPLC) was performed on an UltiMate 3000 Rapid Separation LC system (Dionex, Basel, Switzerland) with Chromeleon 6.8 software package. The UV

*A. Monaco et al, Journal of Labelled Compounds and Radiopharmaceuticals, in press, January 2014.

detector was set at four different wavelengths (215 nm, 220 nm, 254 nm and 280 nm). Radioactivity was detected with a NaI scintillation detector (Nuclear Interface, Munich, Germany) connected on the outflow of the UV detector. The HPLC column used for the purification of the product and the characterization of radioactive compounds against standards was a Phenomenex Gemini 5µ C18 110Å (250 x 4.60 mm) column operated at a flow rate of 1 mL/min using a gradient of 5% acetonitrile in water containing 0.1% TFA to CH_3CN/TFA (99.9:0.1) over 20 minutes. The radiochemical purities were determined by HPLC analyses. NMR data were recorded with a Varian Gemini 2000 NMR Spectrometer, Oxford 300 Nuclear Magnetic Instrument (Oxfordshire, UK). The samples were dissolved either in $CDCl_3$ or in acetone-d_6 (Cambridge Isotopes Laboratories Inc., Burgdorf, Switzerland) and the data were processed by MestRe-C 4.8 software. Chemical shifts (δ) are expressed in ppm relative to the signals of the solvents and coupling constants (J) in Hz. MS analyses were performed using an ESI-MS instrument, API 150EX from AB/MDS (Sciex, Framingham, Massachussetts) or ES TQ-detector Aquti™ (Waters, Baden-Dättwil, Switzerland). HRMS spectra were recorded by ESI/nanoESI-IT Esquire 3000 plus (Bruker, Faellanden, Switzerland).

5.3 Chemistry

*Methyl (2S,4R)-4-hydroxy-1-(pent-4-ynoyl)pyrrolidine-2-carboxylate (**2**)*

Methyl-(2S,4R)-4-hydroxypyrrolidie-2-carboxylate (**1**) (1.00 g, 5.48 mmol), 4-pentynoic acid (0.54 g, 5.48 mmol), EDC (1.26 g, 6.57 mmol) and DMAP (1.00 g, 8.21 mmol) were dissolved in 20 mL of DCM. Et_3N (0.20 ml) was added dropwise and the reaction mixture was stirred at room temperature overnight. Then the mixture was extracted with EtOAc (3 x 30 mL). The organic layer was dried over Na_2SO_4, filtered and concentrated under reduced pressure. The crude product was purified by chromatography on silica gel hexane/EtOAc (1:1) to obtain a colorless oil. Yield: 90%. ^{1}H-NMR (300 MHz, $CDCl_3$) δ: 4.42 (1H, d, J= 10.2 Hz), 4.39 (2H, t, J= 7.7 Hz), 4.21 (1H, bs), 3.66-3.59 (4H, m), 2.48-2.35 (4H, m), 2.16 (1H, t, J= 10.65 Hz), 1.95-1.86

*A. Monaco et al, Journal of Labelled Compounds and Radiopharmaceuticals, in press, January 2014.

(2H, m). ^{13}C-NMR (300MHz, $CDCl_3$) δ: 172.75, 170.35, 83.44, 70.53, 69.03, 57.77, 55.16, 52.59, 38.02, 33.69, 14.17. MS (ESI): m/z 226.4 $[M+H]^+$.

*Methyl (2S,4R)-4-(2-tert-butoxy)-2-oxoethoxy)-1-(pent-4-ynoyl)pyrrolidine-2-carboxylate (**3**)*

NaH 60% in paraffin oil (0.31 g, 7.75 mmol), *tert*-butylbromoacetate (2.00 mL, 13.67 mmol), and *n*-$Bu_4N^+I^-$ (1.44 g, 3.90 mmol) were suspended under argon in 28 mL of dry THF. Then, **2** (1.10 g, 4.88 mmol) was dissolved in 2 mL of dry THF, slowly added to the reaction mixture and stirred overnight. The solvent was removed under reduced pressure. The crude product was purified by chromatography on silica gel using EtOAc/hexane (2:3) to obtain a light yellow oil. Yield: 75%. ^{1}H-NMR (300 MHz, $CDCl_3$) δ: 4.53 (1H, t, J= 7.65 Hz), 4.28 (1H, q, J= 4.3 Hz), 3.96 (2H, d, J= 2.1 Hz), 3.77 (1H, s), 3.72 (2H, s), 3.65 (1H, dd, J_d= 1, J_d= 3 Hz), 2.57-2.50 (4H, m), 2.41-2.22 (1H, m), 2.16-2.03 (1H, m), 1.96 (1H, t, J= 2.4 Hz), 1.68 (1H, s), 1.47 (9H, s). ^{13}C-NMR (300MHz, $CDCl_3$) δ: 172.64, 169.77, 169.09, 83,24, 82.13, 78.35, 68.84, 68.56, 67.06, 57.51, 52.25, 34.66, 33.45, 28.09 (3C), 13.85. MS (ESI): m/z 340.3 $[M+H]^+$.

*Tert-butyl 2-((3R,5S)-5-(hydroxymethyl)-1-(pent-4-ynoyl)pyrrolidin-3-yloxy)acetate (**4**)*

To a cooled solution of **3** (1.15 g, 3.39 mmol) in anhydrous THF/EtOH (65:35, 26 mL) at 0°C, LiCl (0.80 g, 18,87 mmol) and $NaBH_4$ (0.30 g, 7.93 mmol) were added. After 1 h, the ice bath was removed and the reaction mixture was stirred overnight. Then the reaction mixture was concentrated, and 20 mL of water was added. The aqueous layer was extracted with ethyl acetate (3 x 30 mL). The organic layer was dried over Na_2SO_4, filtered and concentrated under vacuum. The crude product was purified by chromatography on silica gel using EtOAc/hexane (1:1) to obtain a light yellow oil. Yield: 88%. ^{1}H-NMR (300 MHz, $CDCl_3$) δ: 4.96 (1H, d, J= 8.1 Hz), 4.30 (1H, q, J= 8.5 Hz), 4.20 (1H, t, J= 1,8 Hz), 3.95 (2H, d, J= 5.4 Hz), 3.76-3.5 (4H, m), 2.62-2.47 (4H, m), 2.26-2.18 (1H, m), 1.73-1.64 (2H, m), 1.46 (9H, s). ^{13}C-NMR (300MHz, $CDCl_3$) δ: 172.07, 169.25, 82.08, 77.42, 77.21, 69.00, 68.70, 66.68, 60.13, 53.61, 34.12, 33.86, 28.07 (3C), 14.86. MS (ESI): m/z 312.1 $[M+H]^+$.

*A. Monaco et al, Journal of Labelled Compounds and Radiopharmaceuticals, in press, January 2014.

*Tert-butyl 2-((3R,5S)-5-((tert-butyldimethylsilyl)oxy)methyl)-1-(pent-4-ynoyl)pyrrolidin-3-yl)oxy)acetate (**5**)*

4 (0.80 g, 2.57 mmol), imidazole (0.44 g, 6.42 mmol), and *tert*-butyldimethylsilyl chloride (0.43 g, 2.83 mmol) were dissolved in 15 mL of DMF and stirred for 3 h at room temperature. The solvent was removed by evaporation and 20 ml of EtOAc were added and extracted with water, saturated $NaHCO_3$, and dried over Na_2SO_4, then filtered. The solvent was removed by evaporation and the product was purified by chromatography on silica gel using EtOAc to obtain a colorless oil. Yield: 82%. ^{1}H-NMR (300 MHz, $CDCl_3$) δ: 4.37-4.24 (2H, m), 3.96-3.89 (3H, m), 3.68-3.63 (1H, dd, J_d= 4.2 J_d= 6 Hz), 3.58-3.51 (2H, m), 2.59-2.41 (4H, m), 2.26-2.17 (1H, m), 2.07-1.95 (2H, m), 1.47 (9H, s), 0.85 (9H, s), 0.04-0.01 (6H, m). ^{13}C-NMR (300MHz, $CDCl_3$) δ: 169.40, 156.50, 81.88, 78.43, 78.35, 68.60, 67.08 (2C), 63.11, 57.73, 52.91, 33.91, 33.27, 28.21 (3C), 25.85 (3C), 14.06, -5.50 (2C). MS (ESI): m/z 426.5 $[M+H]^+$.

*Tert-butyl (S)-3-(2-((3R,5S)-5-(hydroxymethyl)-1-(pent-4-ynoyl)pyrrolidin-3-yloxy)acetamido)-2-(2,4,6-trimethylbenzamido)propanoate (**6**)*

5 (0.10 g, 2.35 mmol) was dissolved in 25 mL of MeOH, and LiOH*H_2O (0.23 g, 9.40 mmol) was added. After stirring 4 h at room temperature, NH_4Cl was added and the solution was stirred for 10 min. The solid was filtered, the solvent was removed under vacuum and then 30 ml of EtOAc were added and extracted with water (2 x 30 mL). The organic layer was dried over Na_2SO_4, filtered and the solvent was removed under reduced pressure. The crude was dissolved in 2 mL of DMF, **9** (0.92 g, 2.99 mmol), EDC (0.54 g, 2.82 mmol) and DMAP (0.43 g, 3.53 mmol) were added and the solution was stirred overnight at room temperature. The solvent was then removed under reduced pressure, 20 mL of ethyl acetate were added and the organic layer was washed with saturated $NaHCO_3$ (2 x 20 mL), and brine (20 mL). The organic layer was dried with Na_2SO_4, filtered and the solvent removed under reduced pressure. The product was purified by column chromatography on silica gel using EtOAc/hexane (2:3) to obtain a light brown oil. Yield: 40%. ^{1}H-NMR (300 MHz, $CDCl_3$) δ: 7.39 (1H, td, J= 31.2 Hz), 6.79 (3H, s), 4.78-4.71 (1H, m) 4.20-4.09 (2H, m), 3.95-3.81 (8H, m), 2.57-2.31 (4H, m), 2.23-2.22

*A. Monaco et al, Journal of Labelled Compounds and Radiopharmaceuticals, in press, January 2014.

(9H, m), 2.14 (3H, s), 1.76-1.65 (1H, m), 1.45, (9H, m). ^{13}C-NMR (300MHz, $CDCl_3$) δ: 171.68, 171.24, 169.56, 168.60, 138.63, 133.88 (2C), 133.66, 128.15 (2C), 83.27, 77.90, 77.68, 68.76, 68.52, 67.91, 65.55, 59.48, 52.97, 42.26, 33.83, 33.36, 27.81 (3C), 20.94, 18.88 (2C), 13.86. MS (ESI): m/z 544.7 $[M+H]^+$.

*Tert-butyl (S)-3-(2-((3R,5S)-1-pent-4-ynoyl-5-((pyridin-2-ylamino)methyl) pyrrolidin-3-yloxy)acetamido)-2-(2,4,6-trimethylbenzamido)propanoate (PMt, **7**)*

6 (0.11 g, 0.22 mmol) and Et_3N (0.46 mL) were dissolved in 4.6 mL of DCM/DMSO (75:25) and cooled at 0°C. SO_3-pyridine complex (0.43 g, 2.67 mmol) was added and the reaction mixture was stirred for 2 h. The DCM fraction was removed under reduced pressure. The remaining DMSO fraction was diluted in 30 mL of ethyl acetate. The organic layer was washed with H_2O (30 ml), and saturated $NaHCO_3$ solution (2 x 20 ml). The organic layer was dried over Na_2SO_4, filtered and the solvent was removed under reduced pressure. The crude obtained (0.14 mg, 0.26 mmol), 2-aminopyridine (0.24 g, 2.58 mmol), and $Ti(OiPr)_4$ (0.96 mL, 4.96 mmol) were dissolved in 1.8 mL of DCE. After stirring overnight at room temperature, $NaBH(OAc)_3$ (1.5 g, 0.71 mmol) was added and the reaction was stirred 4 additional hours. Saturated $NaHCO_3$ solution (2.70 mL) was added, and the mixture was stirred for 1 h. It was then extracted with DCM, dried with Na_2SO_4 and the solvent removed by evaporation. A light brown oil was obtained in 67% yield. ^{1}H-NMR (300 MHz, $CDCl_3$) δ: 8.09-8.02 (2H, m), 7.40 (1H, dd, J_d= 1.8, J_d= 8.1 Hz) 7.35-7.30 (2H, t, J= 7.8 Hz), 6.80 (1H, s), 6.63-6.53 (2H, m), 6.44 (2H, td, J_t= 8.4, J_d= 16.5 Hz), 6.01 (1H, bs), 5.09-4.99 (1H, m), 4.90-4.78 (1H, m), 4.71-4.52 (2H, m), 4.28 (1H, t, J= 4.5 Hz), 4.05-3.58 (5H, m), 2.49-1.94 (13H, m), 1.47 (2H, s), 1.28-1.19 (6H, m), 0.87 (1H, bs). ^{13}C-NMR (300MHz, $CDCl_3$) δ: 172.14, 171.10, 169.57, 168.78, 158.28, 157.79, 157.44, 147.79, 137.64, 133.96 (2C), 128.15 (2C), 113.79, 108.53, 83.27, 83.09, 78.12, 77.34, 68.76, 68.17, 62.95, 60.57, 52.79, 42.09, 33.64, 30.79, 27.82 (3C), 20.95, 18.95 (2C), 13.96. HRMS (ESI) for $C_{34}H_{43}N_5O_6$ $[M+H]^+$: calculated m/z 618.3286, found m/z 618.3282.

*A. Monaco et al, Journal of Labelled Compounds and Radiopharmaceuticals, in press, January 2014.

*Tert-butyl (S)-3-(2-((3R,5S)-1-(3-(1-(2-fluoroethyl)-1H-1,2,3-triazol-4-yl)propanoyl)-5-((pyridin-2-ylamino)methyl)pyrrolidin-3-yloxy)acetamido)-2-(2,4,6-trimethylbenzamido)propanoate (FPMt, **8**)*

7 (10 mg, 0.16 mmol) was dissolved in 1 mL of water/THF and **12** (62% m/m in DMF, 20 µL, 7.60 mmol) was added. Sodium ascorbate (0.5 mL, 2.1 M) and $CuSO_4$ (0.5 mL, 0.7 M) were slowly added and the reaction was stirred at room temperature for 2 h. The crude was filtered and the product was purified by C-18 chromatography to obtain a light brown solid. Yield: 45%. ^{1}H-NMR (300MHz, $CDCl_3$) δ: 9.33 (1H, d. J= 3.9 Hz), 7.75-7.63 (3H, m), 6.82 (2H, s), 4.92 (1H, t, J= 4.7 Hz), 4.76-4.68 (4H, m), 4.64-4.21 (2H, m), 4.01-3.59 (7H, m), 2.96-2.70 (7H, m), 2.24 (9H, d, J= 5.7 Hz), 1.48 (9H, s), 0.88 (2H, t, J= 5.6 Hz). ^{13}C-NMR (300MHz, $CDCl_3$) δ: 171.35, 169.75, 169.41, 168.76, 161.61, 155.39, 149.30, 146.83, 138.85, 134.06 (2C), 133.42, 128.30 (2C), 126.55, 116.39, 102.89, 83.52, 81.51 (d, J= 171.3 Hz), 80.39, 78.82, 68.24, 62.86, 52.94, 52.64, 50.26, 42.55, 33.06, 31.23, 29.68, 27.95 (3C), 21.07, 19.04 (2C). MS (APPI$^+$) for $C_{36}H_{47}FN_8O_6$: m/z 707.00 $[M+H]^+$.

*2-Fluoroethyl 4-methylbenzenesulfonate (**11**)*

Fluoroethanol (**10**) (1.00 mL, 30.25 mmol) was stirred overnight with p-toluensulfonyl chloride (4.80 g, 51.20 mmol) and 7 ml of Et_3N in 15 ml of DCM. The solvent was removed under reduced pressure. Then 20 mL of EtOAc were added and the mixture extracted with saturated solution of $NaHCO_3$ (2 x 20 mL). The organic layer was dried over Na_2SO_4, filtered and the solvent removed under reduced pressure. The crude obtained was purified by column chromatography on silica gel using ethyl acetate/hexane (1:5). A brown oil was obtained with a yield of 78%. ^{1}H-NMR (300 MHz, $CDCl_3$) δ: 7.79 (2H, d, J= 8.1 Hz), 7.35 (2H, dd, J_d= 3.9, J_d= 8.4 Hz), 4.13 (2H, td. J_t= 2, J_d= 5.1 Hz), 3.46 (2H, t. J= 4.95 Hz), 2.43 (3H, s). ^{13}C-NMR (300MHz, $CDCl_3$) δ: 145.19, 132.32, 129.89 (2C), 127.81 (2C), 68.07, 49.43, 21.56. MS (ES$^+$): m/z 219 $[M+H]^+$.

*1-Azido-2-fluoroethane (**12**)*

11 (1.52 g, 7.09 mmol) was dissolved in 3.5 mL of DMF and NaN_3 (1.34 g, 20.60 mmol) was added. The mixture was stirred overnight at 80°C. The

*A. Monaco et al, Journal of Labelled Compounds and Radiopharmaceuticals, in press, January 2014.

product was purified by azeotropic distillation giving a DMF solution of **12** (62% m/m). ^{1}H-NMR (300 MHz, $CDCl_3$, in DMF solution) δ: 4.56 (2H, dt, J_t= 4.2, J_d= 38.1 Hz), 3.49 (2H, d, J= 27.9 Hz). ^{13}C-NMR (300MHz, $CDCl_3$, extrapolated form a DMF solution) δ: 99.90, 82.14 (d, J= 170 Hz). HRMS (ESI): m/z 90.0462 $[M+H]^+$.

5.4 Radiochemistry

^{18}F-Fluoride production

No-carrier-added fluorine-18 was produced according to the nuclear reaction $^{18}O(p,n)^{18}F$ by irradiation (10 min at 10 μA) of 2 ml of highly enriched (>97%) [^{18}O]water (Marshall isotopes, Tel-Aviv, Israel) by a proton beam using a Cyclone-18/9 cyclotron (IBA, Louvain-la-Neuve, Belgium). The initial radioactivity of [^{18}F]fluoride was estimated to be around 5 GBq.

*1-Azido-2-[^{18}F]fluoroethane ([^{18}F]**12**)*

The produced carrier-free [^{18}F]fluoride was trapped on a single use light-QMA anion-exchange column (Waters, Baden-Dättwil, Switzerland) and the excess of [^{18}O]water was removed. Trapped [^{18}F]fluoride was eluted from the column with 2.5 mL of a CH_3CN/H_2O solution (6:1) of K_2CO_3 (3.5 mg, 25 μmol) and Kryptofix [2.2.2] (K_{222}; 20 mg, 53 μmol), and transferred into the reactor. This solution was then dried by consecutive heating at 85°C and 110°C under a stream of argon. After cooling the reactor to 40°C, a solution of 2-azidoethyl-4-methylbenzenesulfonate (**13**) (2 mg, 9 μmol) in CH_3CN (350 μL) was added to the dry K[^{18}F]F^-/K_{222} complex and the reaction mixture was stirred at 80°C for 15 min. Then, 1-azido-2-[^{18}F]fluoroethane ([^{18}F]**12**) was purified by distillation at 130°C for 5 min and collected into a vial containing 150 μL of CH_3CN. The radiochemical purity of this intermediate was estimated to be above 98% (Figure 1) and the radiochemical yield was 64% (decay corrected).

*A. Monaco et al, Journal of Labelled Compounds and Radiopharmaceuticals, in press, January 2014.

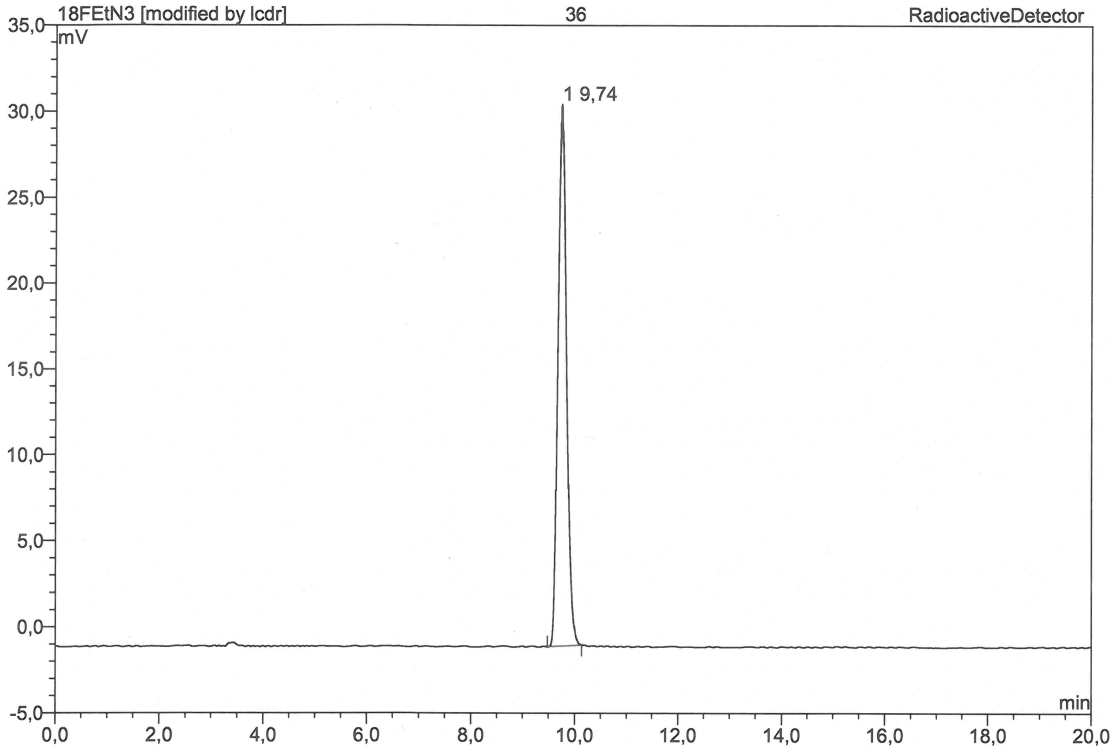

Figure 1| HPLC radiochromatogram of [^{18}F]**12**: retention time of [^{18}F]**12** is 9.7 min.

*Tert-butyl (S)-3-(2-((3R,5S)-1-(3-(1-(2-[^{18}F]fluoroethyl)-1H-1,2,3-triazol-4-yl)propanoyl)-5-((pyridin-2-ylamino)methyl)pyrrolidin-3-yloxy)acetamido)-2-(2,4,6-trimethylbenzamido)propanoate ([^{18}F]FPMt, [^{18}F]**8**)*

Aliquots (50 µL) of the previous solution of 1-azido-2-[^{18}F]fluoroethane ([^{18}F]**12**) were treated with tert-butyl (S)-3-(2-((3R,5S)-1-pent-4-ynoyl-5-((pyridin-2-ylamino)methyl)pyrrolidin-3-yloxy)acetamido)-2-(2,4,6-trimethylbenzamido)propanoate (**7**) (3 mg, 4.85 µmol or 6 mg, 9.70 µmol), $CuSO_4$ (50 µL, 0.35 M or 1.05 M) and sodium ascorbate (50 µL, 0.7 M or 2.1 M) in a mixture of CH_3CN/H_2O (1:1, v/v). The reaction mixtures were stirred for 15 min at room temperature, filtered and then [^{18}F]**8** was purified by HPLC under the conditions previously described (Figure 2). Radiochemical yields between 80% and 83% (decay corrected) were obtained for the click chemistry reactions. Typically, [^{18}F]**8** was prepared in 60–70 min from the end of bombardment and the radiochemical yield was estimated to 42-44% (decay corrected). Identity of the final product was confirmed by comparing its HPLC mobility with the retention time of the non-radioactive standard under the

*A. Monaco et al, Journal of Labelled Compounds and Radiopharmaceuticals, in press, January 2014.

same analytical conditions used to characterize [^{18}F]**12**. [^{18}F]**8** and **8** had similar retention time of 13.2 and 13.1 min, respectively, versus 9.7 and 11.3 min for the starting materials [^{18}F]**12** and **7** under the same elution conditions. The radiochemical purity of [^{18}F]**8** was estimated to be above 95%, and its specific activity, determined by using on-line measurements of radioactivity and UV absorption, was > 1.3 GBq/μmol.

5.5 Results and discussion

5.5.1 Chemistry

Based on docking studies, a pyrrolidine pharmacophore has been reported to yield selective ligands for integrin $\alpha_5\beta_1$. Indeed, the 2-amino pyridine and a 2,4,6-trimethyl benzoic acid moieties divided by an appropriate linker determines the selectivity for $\alpha_5\beta_1$ integrin receptor.[21, 22] The 2-aminopyridine interacts with the (α_5)-Phe 187 on the (α_5)β-propeller domain, while the mesitylene group enables π-π interaction with (β_1)-Tyr 127 placed in a pocket on the β_1 subunit, which is not available on the $\alpha_v\beta_3$ surface.[21] *Tert*-butyl (S)-3-(2-((3R,5S)-1-(3-(1-(2-fluoroethyl)-1H-1,2,3-triazol-4-yl)propanoyl)-5-((pyridin-2-ylamino)methyl)pyrrolidin-3-yloxy)acetamido)-2-(2,4,6-trimethylbenzamido)propanoate (FPMt, **8**) has been identified among 61 $\alpha_5\beta_1$ antagonists, as the most appropriate molecule for the development of a ^{18}F-labeled $\alpha_5\beta_1$ radioligand. FPMt has a structure closely related to the selective $\alpha_5\beta_1$ antagonist JSM6427.[17] A fluorinated substituent is incorporated on the pyrrolidine nitrogen in order to not interfere with the binding of this peptidomimetic molecule with $\alpha_5\beta_1$ integrin receptor. Synthesis of **7** (Scheme 1) was adapted from the synthesis of JSM6427, as reported by Stragies et al.

*A. Monaco et al, Journal of Labelled Compounds and Radiopharmaceuticals, in press, January 2014.

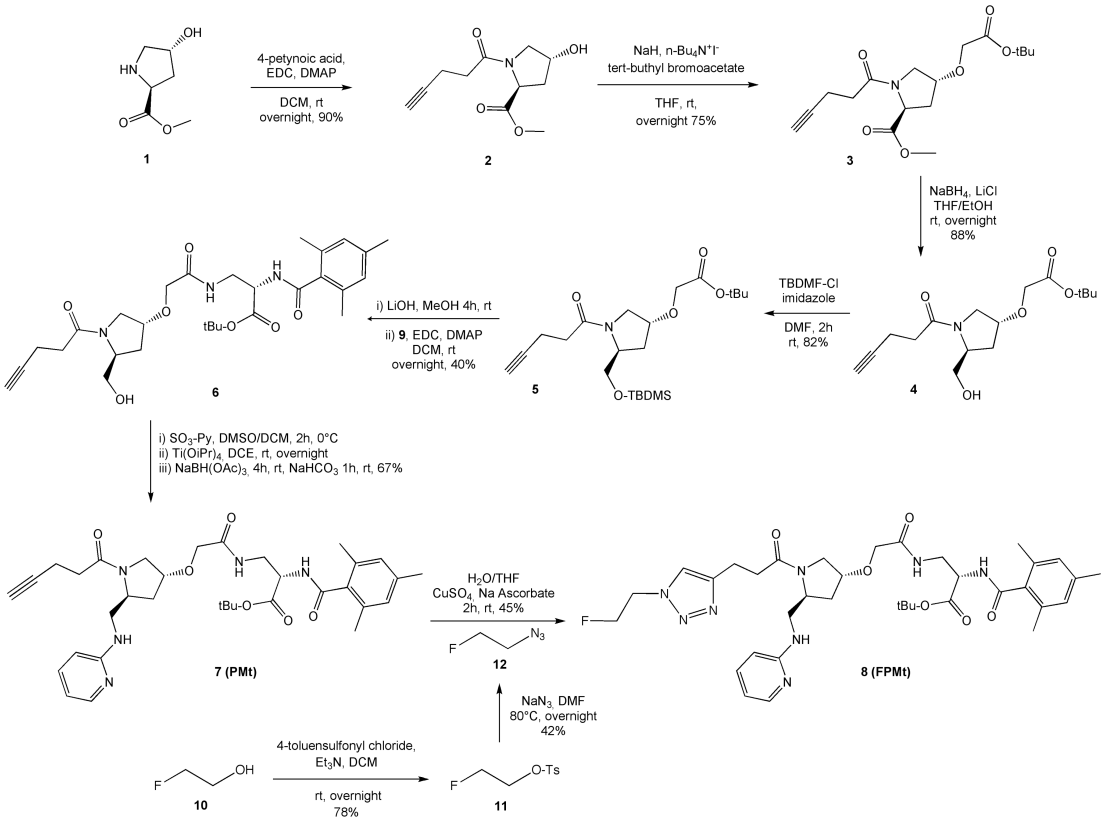

Scheme 1| Synthesis of FPMt (**8**)

An alkynyl function was introduced into compound **2** by coupling of 4-pentynoic acid to the 4-hydroxyproline methyl ester (**1**) to allow subsequent attachment of the radiolabeled azido synthon to the alkynyl precursor **7** by the the copper(II) catalyzed Huisgen's cycloaddition. Conversion of the secondary alcohol into alcoholate and Williamson ether synthesis with *tert*-butyl bromoacetate provided intermediate **3** in 60% yield. Deprotection and concomitant reduction of the methyl ester in position 2 with sodium borohydride in presence of lithium chloride yielded intermediate **4**. Protection of the primary alcohol of **4** as *tert*-butyldimethylsilyl ether afforded compound **5** in 82% yield. The *tert*-butyl group was then selectively removed with lithium hydroxide in methanol, and the resulting carboxylic acid underwent an amidation by treatment with *tert*-butyl (S)-3-amino-2-(2,4,6-trimethylbenzamido)propanoate (**9**) in presence of 4-dimethylaminopyridine and the coupling reagent 1-ethyl-3-(3-dimethylaminopropyl)carbodiimide. Deprotection in position 2 occurred simultaneously to afford the primary

*A. Monaco et al, Journal of Labelled Compounds and Radiopharmaceuticals, in press, January 2014.

alcohol **6** in 40% yield. Compound **9** was synthesized in two steps starting from commercially available asparagine *tert*-butyl ester as previously described.[17] Treatment of **6** with SO_3-pyridine complex to oxidize the primary alcohol into aldehyde, followed by the reductive amidation of the aldehyde with 2-aminopyridine in presence of $Ti(OiPr)_4$ and $NaBH(OAc)_3$ gave the alkynyl precursor **7** in 67% yield. Our optimized synthetic approach allowed us to obtain the alkynyl pyrrolidine derivative **7** in seven steps, whereas the strategy described by Stragies provided similar analogs in nine steps. Moreover, **7** was obtained with an overall satisfactory yield of 45%.

1-azido-2-fluoroetanol (**12**) was synthetized in two steps. Activation of the hydroxyl group of 2-fluoroethanol (**10**) by a tosylation, followed by a nucleophilic substitution with NaN_3 afforded **12**, which was recovered by distillation and obtained as DMF solution (62% m/m of **12**) in 42% yield. [23, 24] Finally, the Cu(II) catalyzed Huisgen's 1,3-dipolar cycloaddition between **7** and the azido synthon **12** gave the final peptidomimetic molecule **8** (FPMt) in only 2h with 45% yield.[25] The time of reaction and the yield obtained suggested that this strategy could be applied for the development of a ^{18}F-labeled analog.

5.5.2 Radiochemistry

Nucleophilic ^{18}F-fluorination of 2-azidoethyl-4-methylbenzenesulfonate (**13**) was carried out in anhydrous CH_3CN with standard K[^{18}F]F^-/Kryptofix complex. The reaction was conducted in 15 min at 80°C, and 1-azido-2-[^{18}F]fluoroethane ([^{18}F]**12**) was isolated by distillation at 130°C into a vial containing anhydrous CH_3CN (Scheme 2).[24] [^{18}F]**12** was obtained in 30 min from the end of bombardment (EOB) with a radiochemical yield of 64% (decay corrected) in accordance with the data reported in literature[24, 26] (Figure 1). The copper(II) catalyzed Huisgen's cycloaddition with the alkynyl pyrrolidine **7** was performed at room temperature in CH_3CN/H_2O in presence of $CuSO_4$ and sodium ascorbate (Scheme 2). The catalytic effect on the kinetic of the click reaction was studied on aliquot of [^{18}F]**12** by modulating the concentrations of **7**, $CuSO_4$ and sodium ascorbate. Good radiochemical yields between 80 and 83% (decay corrected) were obtained and [^{18}F]**12** was completely consumed

*A. Monaco et al, Journal of Labelled Compounds and Radiopharmaceuticals, in press, January 2014.

during the reaction (Figure 2). No influence of the concentration of the reagents was observed on the reaction yield. The radiolabeling method was reproducible, robust, and provided the final ^{18}F-labeled putative $\alpha_5\beta_1$ ligand ([^{18}F]**8)** in two steps with an overall synthesis time of 60–70 min from EOB and 42-44% radiochemical yield (decay corrected).

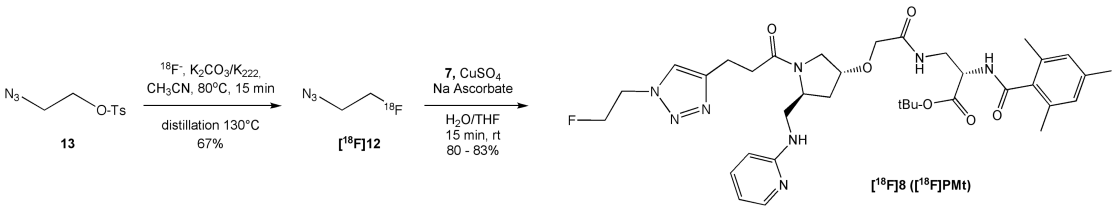

Scheme 2| Radiosynthesis of [^{18}F]FPMt ([^{18}F]**8**)

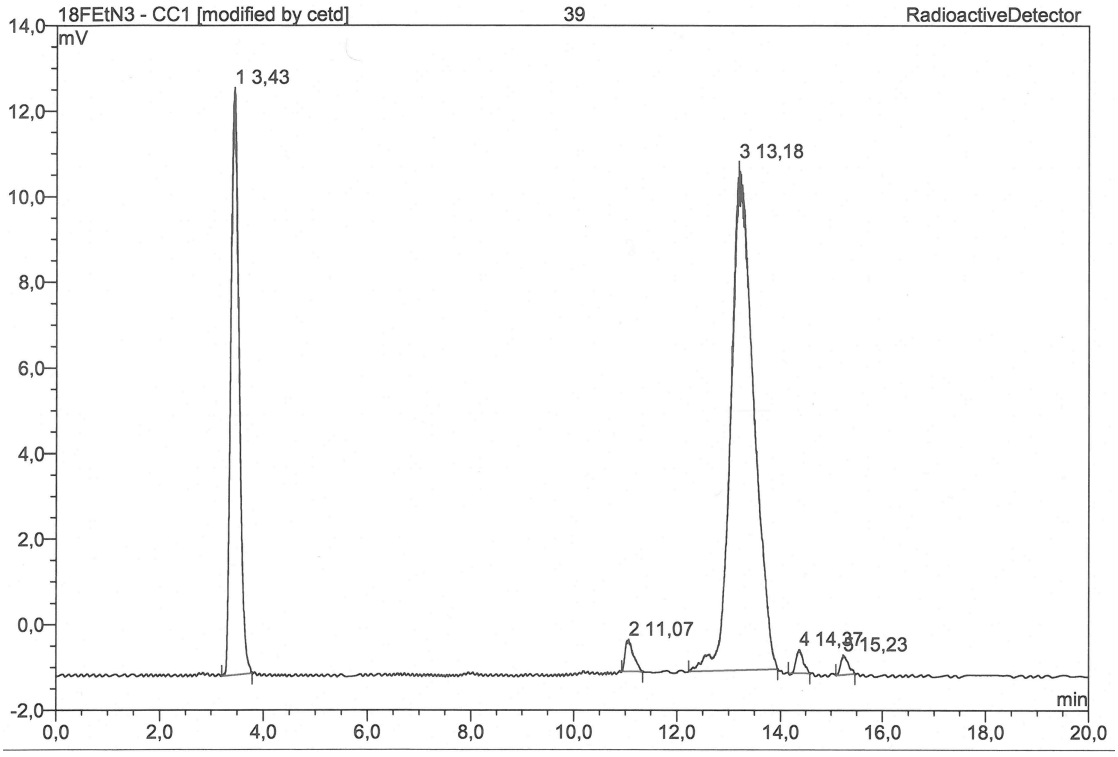

Figure 2| HPLC radiochromatogram of [^{18}F]FPMt **(**[^{18}F]**8**): retention time of [^{18}F]**8** is 13.2 min. No traces of [^{18}F]**12** were found. The peak at 3.4 min corresponds to an unidentified impurity.

*A. Monaco et al, Journal of Labelled Compounds and Radiopharmaceuticals, in press, January 2014.

5.6 Conclusions

Herein, we report the synthesis of [^{18}F]FPMt ([^{18}F]**8**), a non-peptidic radiopharmaceutical for PET imaging with a structure derived from a selective antagonist of $\alpha_5\beta_1$ integrin receptor.[17] Our alkynyl precursor **7** was successfully synthesized and all the steps were optimized to provide good yields. 1-azido-2-fluoroethane (**12**) was chosen as synthon for the development of the PET tracer and it was clicked to **7** following the standard CuAA click reaction. Future studies will be aimed at determining the affinity and specificity of [^{18}F]FPMt for integrin $\alpha_5\beta_1$ and to demonstrate how useful this imaging agent may be in assessing angiogenesis in tumors and monitoring therapy.

*A. Monaco et al, Journal of Labelled Compounds and Radiopharmaceuticals, in press, January 2014.

5.7 References

1. Humphries, J.D., A. Byron, and M.J. Humphries, *Integrin ligands at a glance.* Journal of Cell Science, 2006. **119**(19): p. 3901-3903.
2. Takagi, J., et al., *Global Conformational Rearrangements in Integrin Extracellular Domains in Outside-In and Inside-Out Signaling.* Cell, 2002. **110**(5): p. 599-611.
3. Stupack, D.G., et al., *Apoptosis of adherent cells by recruitment of caspase-8 to unligated integrins.* The Journal of Cell Biology, 2001. **155**(3): p. 459-470.
4. Stupack, D.G. and D.A. Cheresh, *Apoptotic cues from the extracellular matrix: regulators of angiogenesis.* Oncogene, 2003. **22**(56): p. 9022-9029.
5. Luscinskas, F.W. and J. Lawler, *Integrins as dynamic regulators of vascular function.* The FASEB Journal, 1994. **8**(12): p. 929-38.
6. Albelda, S.M. and C.A. Buck, *Integrins and other cell adhesion molecules.* The FASEB Journal, 1990. **4**(11): p. 2868-80.
7. Huveneers, S., H. Truong, and E.H.J. Danen, *Integrins: Signaling, disease, and therapy.* International Journal of Radiation Biology, 2007. **83**(11-12): p. 743-751.
8. Cox, D., M. Brennan, and N. Moran, *Integrins as therapeutic targets: lessons and opportunities.* Nat Rev Drug Discov, 2008. **9**(10): p. 804-820.
9. Tae Jin Kim, et al., *Combined anti-angiogenic therapy against VEGF and integrin aVb3 in an orthotopic model of ovarian cancer.* Cancer Biology & Therapy, 2009. **8**(23): p. 2261-2270.
10. Gordon, C.R., et al., *A Review on Bevacizumab and Surgical Wound Healing: An Important Warning to All Surgeons.* Annals of Plastic Surgery, 2009. **62**(6): p. 707-9.
11. Mas-Moruno C., Florian Rechenmacher, and H. Kessler*, *Cilengitide: The First Anti-Angiogenic Small Molecule Drug Candidate. Design, Synthesis and Clinical Evaluation.* Anticancer Agents Med. Chem., 2010. **10**(10): p. 753-768.

*A. Monaco et al, Journal of Labelled Compounds and Radiopharmaceuticals, in press, January 2014.

12. *Cilengitide (EMD 121974) in Treating Patients With Advanced Solid Tumors or Lymphoma*. 2013.
13. *Cilengitide in Treating Children With Refractory Primary Brain Tumors*. 2013.
14. Dijkgraaf, I. and O.C. Boerman, *Radionuclide Imaging of Tumor Angiogenesis.* Cancer Biotherapy & Radiopharmaceuticals, 2009. **24**(6): p. 637 - 647.
15. Gaertner, F., et al., *Radiolabelled RGD peptides for imaging and therapy.* European Journal of Nuclear Medicine and Molecular Imaging, 2012. **39**(0): p. 126-138.
16. Lee, B., et al., *Perlecan domain V is neuroprotective and proangiogenic following ischemic stroke in rodents.* The Journal of Clinical Investigation, 2011. **121**(8): p. 3005-3023.
17. Stragies, R., et al., *Design and Synthesis of a New Class of Selective Integrin α5β1 Antagonists.* Journal of Medicinal Chemistry, 2007. **50**(16): p. 3786-3794.
18. Cue, D., et al., *A nonpetide integrin antagonist can inhibit epithelial cell ingestion of Streptococcus pyogenes by blocking formation of integrin α5β1-fibronectin-M1 protein complexes.* Proc Natl Acad Sci U S A, 2000. **97**(6): p. 2858–2863.
19. Martinkova, E., et al., *α5β1 integrin antagonists reduce chemotherapy-induced premature senescence and facilitate apoptosis in human glioblastoma cells.* International Journal of Cancer, 2010. **127**(5): p. 1240-1248.
20. Boroujerdi, A., et al., *Chronic cerebral hypoxia promotes arteriogenic remodeling events that can be identified by reduced endoglin (CD105) expression and a switch in [beta]1 integrins.* J Cereb Blood Flow Metab, 2012. **32**(9): p. 1820-1830.
21. Heckmann, D., et al., *Rational Design of Highly Active and Selective Ligands for the α5β1 Integrin Receptor.* ChemBioChem, 2008. **9**(9): p. 1397-1407.
22. Heckmann, D., et al., *Probing Integrin Selectivity: Rational Design of Highly Active and Selective Ligands for the α5β1 and αvβ3 Integrin*

*A. Monaco et al, Journal of Labelled Compounds and Radiopharmaceuticals, in press, January 2014.

Receptor. Angewandte Chemie International Edition, 2007. **46**(19): p. 3571-3574.

23. Pirali, T., et al., *Triazole-Modified Histone Deacetylase Inhibitors As a Rapid Route to Drug Discovery.* Journal of Combinatorial Chemistry, 2008. **10**(5): p. 624-627.
24. Glaser, M. and E. Arstad, *"Click Labeling" with 2-[18F]Fluoroethylazide for Positron Emission Tomography.* Bioconjugate Chemistry, 2007. **18**(3): p. 989-993.
25. Li, Z.-B., et al., *Click Chemistry for 18F-Labeling of RGD Peptides and microPET Imaging of Tumor Integrin αvβ3 Expression.* Bioconjugate Chemistry, 2007. **18**(6): p. 1987-1994.
26. Gaeta, A., et al., *Use of 2-[18F]fluoroethylazide for the Staudinger ligation – Preparation and characterisation of GABAA receptor binding 4-quinolones.* Bioorganic & Medicinal Chemistry Letters, 2010. **20**(15): p. 4649-4652.

*A. Monaco et al, Journal of Labelled Compounds and Radiopharmaceuticals, in press, January 2014.

*A. Monaco et al, Journal of Labelled Compounds and Radiopharmaceuticals, in press, January 2014.

Chapter 6: Conclusions and Outlook

The main purposes of this thesis were: 1) to develop prosthetic groups conjugable by the click chemistry to peptides; 2) to develop a clinical relevant RGD radioligand for $\alpha_v\beta_3$ integrin receptor; 3) to develop a selective non-peptidic radioligand for $\alpha_5\beta_1$ integrin receptor.

1. Prosthetic Groups (chap 3 and 7)

14 prosthetic groups have been synthesized for labeling RGD peptides. All of them have been designed to be stable, suitable for click chemistry and obtained with a simple synthesis. They can be divided in aniline derivatives and benzoic acid derivatives and each group presents an alkyne or azide terminal function (**chap. 7**).
The prosthetic groups obtained starting from aniline were synthesized with a yield between 53 and 90% and benzoic acid derivatives have a yield ranging 58 – 78%.
The aniline derivatives showed higher stability in solution and in acid conditions than the benzoic acid prosthetic groups.
Two prosthetic groups (3-azido-N-(4-fluorophenyl)propanamide and 6-azido-N-(4-fluorophenyl)hexanamide) have been selected to test the click chemistry with seven non-natural amino acids (**chap. 3**). The amino acids selected (glycine, valine, proline, phenylalanine. tyrosine, glutamic acid and lysine) have different proprieties such as polarity, total charge and the presence of aliphatic or aromatic residues. To make them suitable for the click chemistry, an alkynyl substituent was introduced by the coupling of 4-pentynoic acid on the α-NH_2. All the amino acids were easily modified and the alkynyl amino acids were obtained with yields between 60 and 90%.
The Huisgen's cycloaddition between the prosthetic groups and the alkynyl-amino acids was carried out in water/THF with $CuSO_4$ as catalyst and sodium ascorbate as reducing agent. No buffers were used to adjust the pH, which ranged between 4.5 and 6, without any influence on the reactions and the products were obtained in yields between 54 and 98%. The time of reaction was between 1h and 3.5h, which is significantly shorter than similar reactions reported in the literature, it suggests that the click reaction can be applied to the development of ^{18}F-radiosynthetic strategies.
With this selection of amino acids we wanted to demonstrate that the click cycloaddition could be adapted to a wide range of chemical structures, and as consequence can be considered a universal approach to label peptides.

These prosthetic groups could then be considered as good candidates for the development of ^{18}F-labeled peptides for clinical applications.

2. [^{18}F]FPPA-c[RGDfK] (Chap. 4)

The conditions of reaction tested with the alkynyl amino acids were then translated for the development of a c[RGDfK] radioligand. The binding sites for the prosthetic group, as well as the binding energy for $\alpha_v\beta_3$ integrin receptor were established by docking of the peptide on the receptor surface.

The prosthetic group (*N*–(4-fluorophenyl)pent–4-ynamide, FPPA, **3**) has been introduced by the Huisgen's cycloaddition on the -N_3 modified lysine residue of the c[RGDfK] peptide. The click reaction was fast, under mild conditions, with a simple work-up, reproducible and adaptable to ^{18}F-chemistry. Considering the good results obtained with the cold prosthetic group, we investigated the radiochemical strategy. The first precursor evaluated for the fluorination was the *N*-(4-trimethylammonium-benzene) pentynamide trifluoromethanesulfonate (**11**), to obtain the ^{18}F-prosthetic group in one step. Several conditions for the fluorination have been tested but the best yield obtained was around 5% (decay non-corrected). Considering that, a second radiochemical strategy was evaluated having 4-nitroaniline as precursor. In this case the ^{18}F-prosthetic group was synthesized in three steps (90 min) with 44% yield (decay corrected). A fourth later step is needed to conjugated the **[^{18}F]3** with the c[RGDfK] peptide. The final compound was obtained with a radiochemical yield of 29% (decay corrected) with a total synthesis of in 140 min.

The selectivity of **FPPA-c[RGDfK]** for integrin receptor $\alpha_v\beta_3$, and the negligible effect of the prosthetic groups on the affinity of the ligand to its receptor were confirmed by a new validated ELISA protocol, as well as the FACS analysis confirmed the bonding of the **FPPA-c[RGDfK]** to the receptor. The IC_{50} value observed for $\alpha_v\beta_3$ is approximately 300 times lower than the value observed for $\alpha_5\beta_1$.

In conclusion the synthesized peptide, with a close structure to the integrin $\alpha_v\beta_3$ inhibitor cilengitide, binds with high affinity to $\alpha_v\beta_3$ even in the presence of a prosthetic group. However considering the complexity of the radiosynthesis the automation of the process is challenging which would hamper potential clinical application of this biomarker.

To simplify the radiosynthesis some modification of the process can be considered. The first option is to click an activated 4-pentynoic acid to the RGD peptide and then to couple it with the ^{18}F-aniline. The disadvantage of this approach is due to the harsh condition of reaction that might be needed for the coupling and the non-selectivity of the reaction. A second option could be the ^{18}F-labeling of the prosthetic group by electrophilic fluorination or the modification of the prosthetic group to have the fluorine in a less activated position (meta) to directly introduce the ^{18}F-fluoride and obtain the **[^{18}F]FPPA-c[RGDfK]** in two steps with an automated process.

3. Non-peptidic ligand (Chap. 5)

A new non-peptidic ligand for $\alpha_5\beta_1$ integrin receptor was identified by homology modeling among 61 antagonists. This molecule was successfully synthesized in seven steps, and all the steps were optimized to provide good yields.

Two different prosthetic groups have been evaluated for the development of the ^{18}F synthetic strategy. The fluorination of 3-(5-azidopentyloxy)-2-nitropyridine (**25**) gave the **[^{18}F]22** in 15 min with 95% radiochemical yield (non-decay corrected). Unfortunately, the conjugation with the ligand did not end up in the final product.

A second prosthetic group was then considered: 1-azido-2-fluoroethane (**11**) and 2-azidoethyl 4-methylbenzenesulfonate (**16**) as precursor for the radiochemistry. Both of them were synthesized with good yield (42 and 86% respectively). The Huisgen's cycloaddition was made first with 4PM (**17**) following two different procedure. With the classical Cu(II) catalyzed cycloaddition, any product was formed and a fragmentation of **17** was observed. The reaction was then carried out in PBS with TBTA and CuBr, in that case although the product formed could be characterized it was unstable and completely decomposed within 20-30 minutes. Therefore 4PMt (**7**) was considered for the click reaction. The standard CuAA Huisgen's cycloaddition gave a stable product (**18**) with 45% yield, and **7** was then chosen for the development of the radiosynthetic strategy.

The fluorination of 2-azidoethyl 4-methylbenzenesulfonate gave the 1-azido-2-[^{18}F]fluoroethane (**[^{18}F]11**) in 25 min with 52% yield (non-decay corrected). The **[^{18}F]11** was divided in 5 aliquots and different reaction conditions were investigated to perform the click reaction. In all the test reactions the ^{18}F-labeled $\alpha_5\beta_1$ antagonist was formed in 15 min with a radiochemical yield of 47% (non-decay corrected). This

data suggest that the concentration of the $CuSO_4$ and sodium ascorbate did not influence the reaction at the time considered. We cannot exclude that at higher concentrations the product is formed in shorter time than lower concentrations.

In conclusion, this PET imaging agent of $\alpha_5\beta_1$ expression can be synthesize in 60 – 70 min with a radiochemical yield of 20 – 25% (decay corrected).

Chapter 7: Annex

Annex

7.1 Prosthetic groups characterization

7.1.1 Prosthetic groups from aniline

General procedure: To a solution of 4-fluoro aniline (1.21 g, 8.92 mmol) in DCM (30 mL) 4-pentynoic acid is added (1 g, 8.89mmol), HOBT (1.18 g, 8.73 mmol) and EDC·HCL (2.05 g, 10.7 mmol). The reaction is stirred overnight at rt, then quenched with water and the organic layer is washed with 1 M $NaHCO_3$, dryed over Na_2SO_4 and the solvent is removed by reduced pressure. The crude product is purified by flash chromatography Hexane:Et_2O (3:2).

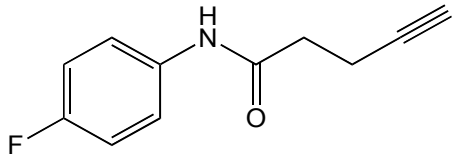

N–(4-fluorophenyl)pent–4-ynamide (1): yield 90%. ^{1}H-NMR (300 MHz, $CDCl_3$) δ ppm: 7.49-7.41 (3H, m), 7.01 (2H, t, J=17.1 Hz), 2.62–2.57 (4H, m,), 2.06 (1H, t, J=4.5 Hz) ppm. ^{13}C-NMR (300 MHz, $CDCl_3$) δ ppm: 122.18, 122.10, 121., 116.08, 70.10, 70.05, 36.40, 15.05, 14.98 ppm. HRMS (ESI) clacd. for $C_{11}H_{10}FON$ $[M+H]^+$: expected m/z 192.0825, observed m/z 192.0824.

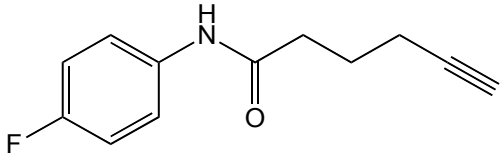

***N*-(4-fluorophenyl)hex-5-ynamide (2):** yield 57%. ^{1}H-NMR (300 MHz, $CDCl_3$) δ ppm: 7.72 (1H, sb), 7.49-7.44 (2H, m), 7.04-7.96 (1H, m), 2.50 (2H, t, J=14.7 Hz), 2.31 (2H, td, J=16.2 Hz), 2.02 (1H, t, J=5.1), 1.99-1.89 (2H, m) ppm.^{13}C-NMR (300 MHz, $CDCl_3$) δ ppm: 121.96, 121.86, 116.21, 115.72, 69.72, 36.04, 24.12, 18.01 ppm. HRMS (ESI) clacd. for $C_{12}H_{12}FON$ $[M+H]^+$: expected m/z 206.0973, observed m/z 206.0975.

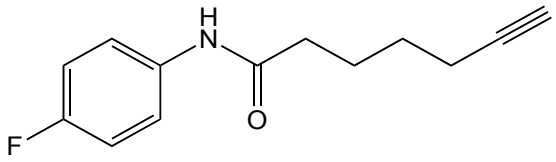

***N*-(4-fluorophenyl)hept-6-ynamide (3):** yield 67%. ^{1}H-NMR (300 MHz, $CDCl_3$) δ ppm: 7.48-7.43 (2H, m), 7.00 (2H, t, J=17.1 Hz), 2.37 (2H, t, J=15 Hz), 2.24 (2H, td, J=16.5 Hz), 1.97 (1H, T, J=5.4 Hz), 1.90-1.80 (2H, m) ppm. ^{13}C-NMR (300 MHz, $CDCl_3$) δ ppm: 171.09, 121.98, 121.89, 116.01, 115.71, 84.23, 69.00, 37.15, 28.06, 24.82, 18.43 ppm. HRMS (ESI) clacd. for $C_{13}H_{14}FON$ $[M+H]^+$: expected m/z 220.1147, observed m/z 220.1132.

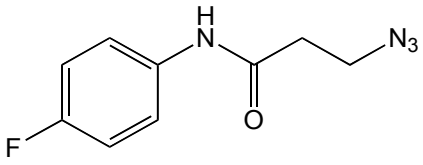

3-azido-*N*-(4-fluorophenyl)propanamide (4): yield 60%. ^{1}H-NMR (300 MHz, $CDCl_3$) δ ppm: 7.70 (1H,sb), 7.47-7.40, (2H, m), 7.02-6.96 (2H, m), 3.68 (2H, t, J=12.6 Hz), 2.57 (2H, t, J=12.6 Hz) ppm. ^{13}C-NMR (300 MHz, $CDCl_3$) δ ppm: 133.67, 122.64, 122.34, 116.07, 115.77, 47.64, 36.86 ppm. HRMS (ESI) clacd. for $C_9H_{10}N_4OF$ $[M+H]^+$: expected m/z 209.0821, observed m/z 209.2833.

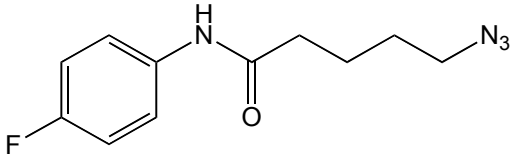

5-azido-*N*-(4-fluorophenyl)pentanamide (5): yield 53%. ^{1}H-NMR (300 MHz, $CDCl_3$) δ ppm: 7.48-7.43 (2H, m), 7.18 (1H, sb), 7.04-6.98 (2H, m), 3.34 (2H, t, J=13.2 Hz), 2.39 (2H, t, J=14.4 Hz), 1.87-1.77 (2H, m), 1.73-1.66 (2H, m) ppm. ^{13}C-NMR (300 MHz, $CDCl_3$) δ ppm: 122.03, 122.01, 121.97, 121.81, 116.05, 115.75, 51.44, 36.99, 28.57, 22.917 ppm. HRMS (ESI) clacd. for $C_9H_{10}N_4OF$ $[M+H]^+$: expected m/z 259.0957, observed m/z 259.0965.

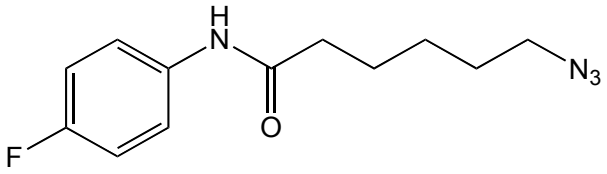

6-azido-*N*-(4-fluorophenyl)hexanamide (6): yield 68%; ^{1}H-NMR (300 MHz, $CDCl_3$) δ ppm: 7.48-7.43 (2H, m), 7.19 (1H, sb), 7.00 (1H, t, J=17.1 Hz), 3.28 (2H, t, J=13.2 Hz), 2.36 (2H, t, J=14.7), 1.81-1.70 (2H, m), 1.69-1.61 (2H, m), 1.59-1.41 (2H, m) ppm. ^{13}C-NMR (300 MHz, $CDCl_3$) δ ppm: 171.21, 122.00, 121.94, 121.825, 116.02, 115.728, 51.46, 51.38, 37.44, 28.86, 26.59, 25.20 ppm. HRMS (ESI) clacd. for $C_{12}H_{15}N_4OFNa$ $[M+Na]^+$: expected m/z 273.1110, observed m/z 273.1122.

7.1.2 Prosthetic gropus from benzoic acid

General procedure: To a solution of 4-fluoro benzoic acid (1 g, 7.14 mmol) and but-3-yn-1-amine (500 mg, 7.23 mmol) in DCM (25 mL), HOBT (960 mg, 10.71 mmol) and EDC·HCL (2 g, 8.57 mmol). The reaction is stirred overnight at rt, then quenched with water and the organic layer is washed with 1 M $NaHCO_3$, dryed over Na_2SO_4 and the solvent is removed by reduced pressure. The crude product is purified by flash chromatography Hexane:Et_2O (3:2).

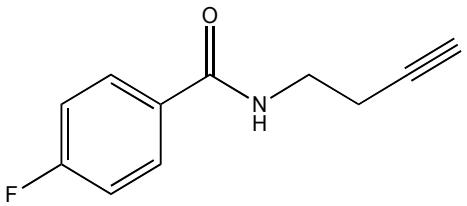

4-fluoro-*N*-(but-3-ynyl)benzamide (7): yield 78%. ^{1}H-NMR (300 MHz, $CDCl_3$) δ ppm: 7.81-7.76 (2H, m), 7.11 (2H, t, J= 17.1 Hz), 6.42 (1H, sb), 3.64 – 3.58 (2H, m,), 2.53 (2H, td, J=15.3 Hz), 2.05 (1H, t, J=5.4 Hz) ppm; ^{13}C-NMR (300 MHz, $CDCl_3$) δ ppm: 129.14, 129.02, 115.65, 115.36, 70.15, 38.25, 30.22, 19.33ppm. HRMS (ESI) clacd. for $C_{11}H_{11}ONF$ $[M+H]^+$: expected m/z 192.0822, observed m/z 192.0819.

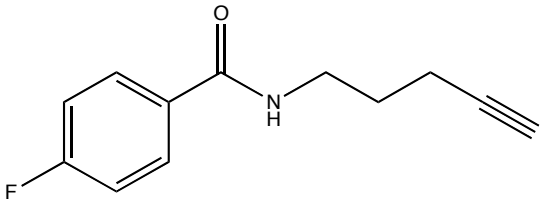

4-fluoro-*N*-(pent-4-ynyl)benzamide (8): yield 78%. ^{1}H-NMR (300 MHz, $CDCl_3$) δ ppm: 7.79-7.75 (2H, m), 7.13-7.07 (2H, m), 6.39 (1H, sb), 3.61-3.55 (2H, m), 2.31 (2H, td, J=16.5 Hz), 2.02 (1H, t, J=5.1 Hz), 1.90-1.81 (2H, m) ppm. ^{13}C-NMR (300 MHz, $CDCl_3$) δ ppm: 129.19, 129.07, 115.72, 115.44, 69.38, 39.40, 27.90, 16.29 ppm. HRMS (ESI) clacd. for $C_{12}H_{15}N_4OFNa$ $[M+Na]^+$: expected m/z 206.0984, observed m/z 206.0975.

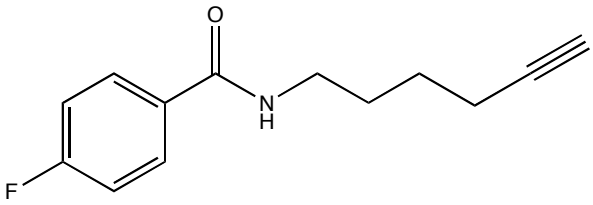

4-fluoro-*N*-(hex-5-ynyl)benzamide (9): yield 70%. ^{1}H-NMR (300 MHz, $CDCl_3$) δ ppm: 7.91-7.44 (2H, m), 7.13-7.03 (2H, m), 6.52 (1H, sb), 3.47-3.40 (2H, m), 2.22 (2H, td, J=16.2 Hz), 1.95 (2H, t, J=5.4 Hz), 1.77-1.67 (2H. m) 1.63-1.54 (2H, m) ppm. ^{13}C-NMR (300 MHz, $CDCl_3$) δ ppm: 129.23, 129.11, 115.60, 115.31, 68.77, 39.569, 28.528, 25.66, 18.02 ppm. HRMS (ESI) clacd. for $C_{12}H_{15}N_4OFNa$ $[M+Na]^+$: expected m/z 220.1140, observed m/z 220.1132.

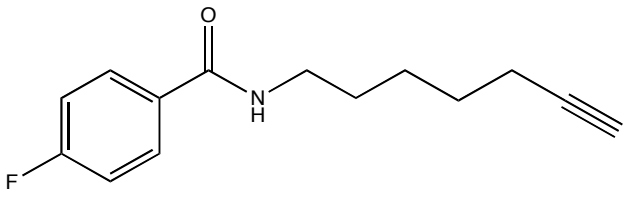

4-fluoro-*N*-(hept-6-ynyl)benzamide (10): yield 72%. ^{1}H-NMR (300 MHz, $CDCl_3$) δ ppm: 7.79-7.74 (2H, m), 7.12-7.06 (2H, m), 6.16 (2H, sb), 3.48-3.41 (2H, m), 2.10 (2H, td, J=15.9 Hz), 1.94 (2H, t, J=5.1 Hz), 1.68-1.46 (6H. m) ppm. ^{13}C-NMR (300 MHz, $CDCl_3$) δ ppm: 129.43, 129.31, 115.95, 115.66, 68.73, 40.21, 29.36 28.19,

26.18, 18.51 ppm. HRMS (ESI) clacd. for $C_{14}H_{16}ONFNa$ $[M+Na]^+$: expected m/z 256.1115, observed m/z 256.1108.

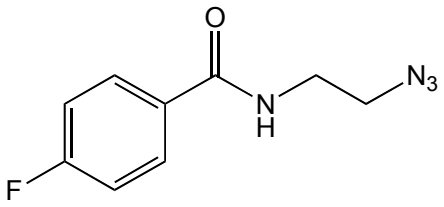

3-azido-*N*-(4-fluorophenyl)propanamide (11): yield 74%. ^{1}H-NMR (300 MHz, $CDCl_3$) δ ppm: 7.70 (1H,sb), 7.47-7.40, (2H, m), 7.02-6.96 (2H, m), 3.68 (2H, t, J=12.6 Hz), 2.57 (2H, t, J=12.6 Hz) ppm. ^{13}C-NMR (300 MHz, $CDCl_3$) δ ppm: 133.67, 122.64, 122.34, 116.07, 115.77, 47.64, 36.86 ppm $C_9H_{10}N_4OF$ $[M+H]^-$: expected m/z 207.0676, observed m/z 207.0674.

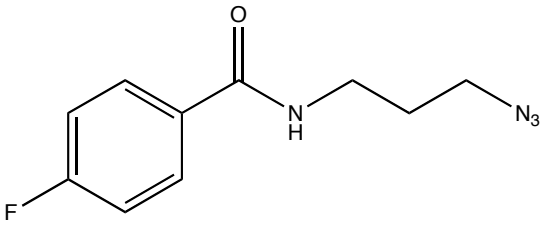

***N*-(3-azidopropyl)-4-fluorobenzamide (12):** yield 58%. ^{1}H-NMR (300 MHz, $CDCl_3$) δ ppm: 7.79-7.74 (2H, m), 7.10-7.05 (2H, m), 6.65 (1H, sb), 3.55-3.48 (2H, m), 3.42 (2H, t, J=13.2 Hz), 1.93-1.48 (2H, m) ppm. ^{13}C-NMR (300 MHz, $CDCl_3$) δ ppm: 129.23, 129.11, 115.68, 115.39, 49.54, 37.84, 28.66 ppm. . HRMS (ESI) clacd. for $C_{10}H_{11}N_4OF$ $[M+H]^+$: any result was observed at *m/z* 222.2

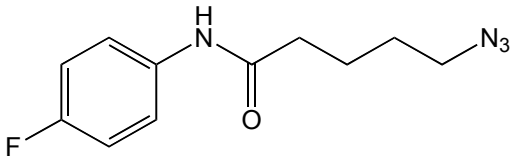

5-azido-*N*-(4-fluorophenyl)pentanamide (13): yield 65%. ^{1}H-NMR (300 MHz, $CDCl_3$) δ ppm: 7.48-7.43 (2H, m), 7.18 (1H, sb), 7.04-6.98 (2H, m), 3.34 (2H, t, J=13.2 Hz), 2.39 (2H, t, J=14.4 Hz), 1.87-1.77 (2H, m), 1.73-1.66 (2H, m) ppm.^{13}C-NMR (300 MHz, $CDCl_3$) δ ppm: 122.03, 122.01, 121.97, 121.81, 116.05, 115.75,

51.44, 36.99, 28.57, 22.917 ppm. HRMS (ESI) clacd. for $C_{11}H_{13}N_4OF$ $[M+H]^+$: any result was observed at m/z 236.3

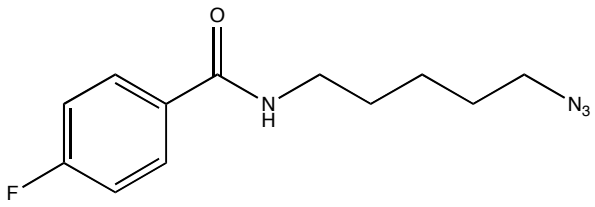

6-azido-*N*-(4-fluorophenyl)hexanamide (14): yield 73%. ^{1}H-NMR (300 MHz, $CDCl_3$) δ ppm: 7.48-7.43 (2H, m), 7.19 (1H, sb), 7.00 (1H, t, J=17.1 Hz), 3.28 (2H, t, J=13.2 Hz), 2.36 (2H, t, J=14.7 Hz), 1.81-1.70 (2H, m), 1.69-1.61 (2H, m), 1.59-1.41 (2H, m) ppm; ^{13}C-NMR (300 MHz, $CDCl_3$) δ ppm: 171.21, 122.00, 121.94, 121.825, 116.02, 115.728, 51.46, 51.38, 37.44, 28.86, 26.59, 25.20 ppm; HRMS (ESI) clacd. for $C_{14}H_{16}ONFNa$ $[M+Na]^+$: expected m/z 273.1115, observed m/z 273.1122.